CRANFIELD UNIVERSITY

YERBOL SARBASSOV

Formation of SO_3 under oxy-fired fluidised beds

School of Energy, Environment & Agrifood

PhD

Academic Year: 2015 - 2016

Principal supervisor: Prof. Edward J. Anthony
Associate-supervisor: Dr Kumar Patchigolla

October 2016

CRANFIELD UNIVERSITY

School of Energy, Environment & Agrifood
Centre for Combustion, Carbon Capture & Storage

Doctor of Philosophy

Academic Year 2015 - 2016

YERBOL SARBASSOV

Formation of SO_3 under oxy-fired fluidised beds

Supervisor: Professor Edward J. Anthony
Co-Supervisor: Dr Kumar Patchigolla

October 2016

This thesis is submitted in partial fulfilment of the requirements for the degree of Doctor of Philosophy

© Cranfield University 2016. All rights reserved. No part of this publication may be reproduced without the written permission of the copyright owner.

ABSTRACT

In oxy-fuel combustion, fuel is burned in the presence of higher concentrations of oxygen diluted with the recycled flue gas (RFG). The nitrogen fraction in the air is replaced by the recycled flue gas to moderate the combustion temperature in the furnace. Nitrogen is removed from the mainstream by the air separation unit (ASU) to provide nearly pure oxygen. However, combustion environment of fuel with RFG differs significantly from conventional air combustion due to the high heating capacity of CO_2. In typical air combustion process, sulfur in fuel is converted to sulfur dioxide (SO_2), while a smaller fraction is converted to the sulfur trioxide (SO_3). However, during the oxy-fuel combustion with RFG tends to increase the SO_2 concentrations in the combustion furnace. Thus, higher concentrations of SO_3 along with SO_2 and steam may increase risks associated with the corrosion of metal surfaces in the boiler. This occurs as the fraction of SO_3 reacts with steam to form sulfuric acid at low temperatures.

The aim of this PhD thesis is to evaluate the formation of SO_3 concentrations during the oxy-fuel combustion. Thus, SO_3 concentrations were measured experimentally under air and oxy-fuel environments. To reach the goals of this work, bench-scale bubbling fluidised bed and fixed bed rigs were used to measure SO_3 concentrations. At a larger scale, a pilot-scale 50 kW circulating fluidised bed rig (CFB) was employed. The PhD thesis provides a literature survey on SO_3 formation in air and oxy-fuel combustion environments, the development of SO_3 sampling train and an experimental description of the tests. Finally, the results obtained from each rig have been discussed. As supporting case, fly ashes were analysed in TGA to investigate the amount of unburnt carbon content. The collected fly ash after the tests was scanned by using X-ray fluorescence (XRF) to evaluate the change of metal oxides.

Keywords:

Oxy-fuel combustion, fluidised bed, sulfur dioxide, sulfur trioxide;

ACKNOWLEDGEMENTS

I would like to express my sincere gratitude to my supervisor Professor Edward J. Anthony for his exceptional support and guidance to conduct research at Cranfield University. Working with him has inspired me to pursue high-quality research. You always took a time to discuss issues related to my project, from which I gained useful skills.

I also would thank my co-supervisor Dr Kumar Patchigolla and Dr Lunbo Duan, for their strong support during my experimental work and discussions. In particular, I would like to thank Dr Lunbo Duan for hosting me at Southeast University in China and facilitating my stay and research. I would also like to thank Professor Vasilije Manovic for his useful discussions and valuable guidance during my research project. I also wish to thank all technicians, especially Martin Roskilly at the Centre of Combustion and CCS for their help and facilitating my setup.

I wish to thank Dr Nelia Jurado and Dr Michal Jeremias for their useful advices on the FTIR instrument and analytical chemistry techniques. My deep appreciation goes to Sam Skears who provided me with an enormous administrative support during the course of my research. All people mentioned above have supported me and I will miss them all in future.

Finally, I would like to express my heartfelt gratitude to my wife Ainur for being with me and providing a continuous support and encouragement throughout this difficult time. I also wish to thank my father for his support.

The financial support of PhD program from Nazarbayev University (Kazakhstan) and Cranfield University (UK) is gratefully acknowledged.

TABLE OF CONTENTS

ABSTRACT i
ACKNOWLEDGEMENTS ii
LIST OF FIGURES vi
LIST OF TABLES viii
LIST OF EQUATIONS ix
LIST OF ABBREVIATIONS x
1 INTRODUCTION 1
1.1 Influence of sulfur compounds in combustion systems 2
1.2 Formation of SO_3 during the combustion 3
1.3 Aims and scope 5
1.4 Dissemination of PhD project 6
1.5 Content of the thesis 7
2 LITERATURE REVIEW 9
2.1 Oxy-fuel combustion technology 9
2.2 Flue gas recirculation concept 13
2.3 Fundamental studies of the oxy-fuel combustion 15
2.3.1 SO_2 emissions 15
2.3.2 NO_x emissions 18
2.3.3 Ash and deposit formation 19
2.4 Development of oxy-fuel in large scale pulverised coal and fluidised beds 22
2.4.1 Pilot-scale oxy-fired pulverised coal plants 22
2.4.2 Progress of oxy-fired fluidised beds 23
2.5 Background of SO_3 chemistry 27
2.5.1 Homogeneous SO_3 reactions 27
2.5.2 Heterogeneous SO_3 reactions 30
2.6 SO_3 sampling methods 32
2.6.1 Controlled condensation method 32
2.6.2 Isopropanol absorption bottle method 34
2.6.3 Salt and glass bead methods 35
2.6.4 Indirect measurements of SO_3 36
2.6.5 Pentol SO_3 monitor 38
2.6.6 Acid dew point measurements 39
2.6.7 Summary of SO_3 sampling methods 40
2.7 Influence of oxy-fuel combustion on SO_3 formation 41
2.7.1 O_2/CO_2 environment 41
2.7.2 Effect of NO_x emissions 42
2.7.3 Effect of CO concentrations 44
2.7.4 Effect of steam 46

2.7.5 Temperature and residence time 47
2.7.6 Effect of fly ash 50
2.7.7 Pilot-scale so_3 measurements 53
2.7.8 Modelling studies of SO_3 formation 54
3 METHODOLOGY 61
3.1 Experiments in a fixed bed reactor 62
3.2 Experiments in a pilot-scale circulating fluidised bed reactor 63
3.3 Bench-scale SO_3 measurements in a bubbling fluidised bed 65
3.4 Materials 68
3.4.1 Materials for fixed bed tests 68
3.4.2 Materials for bubbling fluidised bed tests 68
3.5 Development of SO_3 sampling method 70
3.6 Experimental procedure for bubbling fluidised bed 74
3.7 Pressure drop measurements in BFB 76
4 RESULTS AND DISCUSSIONS 81
4.1 Uncatalysed SO_3 formation 81
4.1.1 Effect of bed temperature in fixed and bubbling fluidised bed 81
4.1.2 Effect of steam and oxygen 83
4.1.3 Effect of SO_2 concentrations 85
4.2 Catalysed SO_3 formation 87
4.2.1 Catalysed SO_3 tests in a fixed bed 87
4.2.2 Catalysed SO_3 tests in a bubbling fluidised bed 90
4.2.3 SO_3 tests in a 50 kW oxy-CFB unit 95
5 SUMMARY OF THE RESULTS 97
5.1 The applicability of the results 98
6 FINAL CONCLUSIONS AND FUTURE WORK 99
6.1 Conclusions 99
6.2 Future work 100
REFERENCES 103
APPENDICES 122
Appendix A Minimum fluidisation velocity 122
Appendix B Design of experiment 124
Appendix C Calibration of mass flow controllers 125
Appendix D Fly ash composition 127
Appendix E Illustration of glass condenser and sintered filter 129
Appendix F Sulfur balance 130
Appendix G Coals analysis 133
Appendix H Hydrodynamic experiments on a small-scale circulating fluidised bed reactor at elevated operating pressure, and under an O_2/CO_2 environment. 134

LIST OF FIGURES

Figure 1-1 Principal scheme of oxy-fuel combustion process 1

Figure 2-1 Simplified recycled flue gas scheme in oxy-fuel combustion (Hu and Yan, 2012) 14

Figure 2-2 Mineral transformation and particle formation pathway (Suriyawong *et al*., 2006) 20

Figure 2-3 Thermodynamic equilibrium SO_3/SO_2 conversion 28

Figure 2-4 Process contributing to formation of sulfur trioxide, sulfuric acid, and sulfates in residual oil-fired boilers (Modified from Walsh *et al*., (1972)) 31

Figure 2-5 Modified Controlled condensation method SO_3 sampling scheme (NCASI Southern Regional Center 1996) 32

Figure 2-6 Effect of pH on the relative concentrations of the SO_2 species in solution (Dellinger *et al*., 1980) 34

Figure 2-7 Isopropanol bottle method SO_3 measurements 34

Figure 2-8 Salt tube preparation 35

Figure 2-9 Arrangement SO_3 measurements by CaC_2O_4 (Ibanez *et al*., 2008) 37

Figure 3-1 Vertical fixed bed reactor system 62

Figure 3-2 Oxy-fuel CFB unit with flue gas recycle (Duan *et al*., 2014) 64

Figure 3-3 Sketch of bench scale bubbling fluidised bed 66

Figure 3-4 Photographs of bubbling fluidised bed rig 67

Figure 3-5 Particle size distribution of solid materials 70

Figure 3-6 Photographs of solid materials 70

Figure 3-7 SO_3 sampling train based on EPA method 8A 71

Figure 3-8 Accuracy of titration method 73

Figure 3-9 Pressure drop measurements at 400°C in BFB 77

Figure 3-10 Pressure drop measurements at 950°C in BFB 77

Figure 3-11 TGA test of FAs under air environment 78

Figure 3-12 (a,b,c) TGA tests for Fly ash-3, Fly ash-4 and Fly ash-1 FA 80

Figure 4-1 Effect of temperature on SO_3 formation in fixed bed rig 81

Figure 4-2 Uncatalysed SO_3/SO_2 conversion in BFB rig and comparison to the available data 82

Figure 4-3 Effect of H_2O on SO_3 formation under oxy-fuel condition in fixed bed rig (Inlet of SO_2-3000 ppm, O_2-6%, bal- CO_2, t-600°C)..... 84

Figure 4-4 Effect of O_2 concentration on SO_3 formation under oxy-fuel atmosphere in fixed bed rig (inlet SO_2-3000ppm; H_2O-10%; bal- CO_2 t-600^oC) 84

Figure 4-5 Effect of SO_2 concentration on SO_3 formation under oxy-fuel atmosphere in fixed bed rig (O_2-6%, H_2O-10%; bal-CO_2; t- 600^oC)..... 85

Figure 4-6 Effect of SO_2 concentrations in BFB rig (Flue gas composition: Air: O_2-4%, CO_2-17%, H_2O-6%, balance-N_2; Oxy: O_2 -5%, H_2O-11%, balance-CO_2)..... 86

Figure 4-7 Effect of fly ash on the SO_3 formation under oxy-fuel condition in fixed bed rig (O_2 concentration: 6%, H_2O concentration: 10%; CO_2 balance) 88

Figure 4-8 Effect of metal oxides on the SO_3 formation under oxy-fuel condition in fixed bed rig (O_2-6%, H_2O-10%; bal- CO_2)..... 89

Figure 4-9 Catalytic effect of FA on SO_3 formation at 400°C in BFB rig 91

Figure 4-10 Catalytic effect of FA on SO_3 formation at 950°C in BFB rig 91

Figure 4-11 Change of metal oxides in the fly ashes (before and after tests at 950°C) in BFB rig..... 95

Figure 4-12 SO_3 concentration during oxy-fuel CFB pilot test 96

Figure A-1 Minimum fluidisation velocity ……..124

Figure C-1 Calibration of nitrogen MFC (2 l/min)……..127

Figure C-2 Calibration of carbon dioxide MFC (1.5 l/min)……..127

Figure E-1 Clean glass condenser (a) and with condensed SO_3 (b).……..…..131

Figure E-2 Sintered filter with fly ash.……131

Figure F-1 SO_2 capture by fly ashes.……..133

LIST OF TABLES

Table 2-1 Performances of coal and gas-fired power plants (IEA 2012) 11

Table 2-2 Composition of CO_2 streams for storage (IEAGHG, 2011);(Talman, 2015) 12

Table 2-3 Effect of RFG on SO_2 concentration in the flue gas, based on 1000 ppm without RFG (Molburg *et al*., 2001)..... 15

Table 2-4 Pilot scale oxy-fired FB studies on emissions (modified from Wall *et al*., (2012)) 24

Table 2-5 SO_3 formation at excess and low O_2 concentrations (Reid, 1971).... 29

Table 2-6 Sulfuric acid dew-point (ADP) correlations: (Verhoff and Banchero, 1974);(ZareNezhad, 2009); 39

Table 2-7 Advantages and disadvantages of SO_3 methods 41

Table 2-8 List of homogeneous SO_3 studies conducted in quartz tube flow reactors..... 49

Table 2-9 A list of XRF analysis of fly ashes during the SO_3 studies..... 52

Table 2-10 A detailed lists of SO_3 measurement campaigns under oxy and air fuel combustion 56

Table 3-1 Test conditions in fixed bed rig (inlet gases per volume on a wet basis)..... 63

Table 3-2 Ultimate and proximate analysis of coal (air dried basis) (Duan *et al*., 2015) 64

Table 3-3 Chemical composition of fly ashes 69

Table 3-4 Test condition of SO_3 measurement in BFB rig 74

Table 3-5 Inlet mixture composition (per volume on a wet basis)..... 75

Table A-1 Experimental spreadsheet on U_{mf} 123

Table B-1 Number of tests……126

Table C-1 Assessment of SO_2 concentration by impingers…….……128

Table D-1 XRF analysis of bed materials after the tests at 950°C..……129

Table D-2 XRF analysis of fly ashes after the tests at 950°C……..……130

Table F-1 Sulfur balance from bench-scale BFB tests……..……133

Table F-2 Sulfur balance from the bench-scale BFB..……..……134

Table G-1 Ultimate, proximate analysis and HHV of coal...……...135

LIST OF EQUATIONS

Equation 2.1 13
Equation 2.2 13
Equation 2.3 27
Equation 2.4 39
Equation 2.5 39
Equation 2.6 39
Equation 3.7 72
Equation 3.8 72

LIST OF ABBREVIATIONS

ADP	Acid-dew point
ANL	Argonne National Laboratory
ASU	Air separation unit
BET	Brunauer-Emmett-Teller
BFBC	Bubbling fluidised bed combustor
CCM	Controlled condensation method
CCS	Carbon capture and storage
CER	Clean energy recuperator
CFB	Circulating fluidised bed
CFD	Computational fluid dynamics
DTF	Drop tube furnace
EPA	Environmental Protection Agency
EPRI	Electric power research institute
ESP	Electrostatic precipitator
FA	Fly ash
FC	Fireside corrosion
FGD	Flue gas desulfurisation
FTIR	Fourier transform infrared spectroscopy
GHG	Greenhouse gas emissions
IC	Ion chromatography
ID	Internal diameter
IEA	International Energy Agency
IFK	Institute of Combustion and Power Plant Technology
IGCC	Integrated gasification combined cycle
IR	Infrared spectrometry
MEA	Monoethanolamine
MFC	Mass flow controller
PBFB	Pressurised bubbling fluidised bed
PC	Pulverised coal
PD	Pressure drop

PM	Particulate matter
PPM	Parts per million
PSD	Particle size distribution
RFG	Recycled flue gas
SCR	Selective catalytic reduction
SEM	Scanning electron microscopy
SMD	Sauter mean diameter
SP	Suspension density
TGA	Thermogravimetric analysis
UV	Ultraviolet visible spectroscopy
VM	Volatile matter
WEO	World energy outlook
WGM	Wet gas meter
XRF	X-ray fluorescence

Chemicals

$Ba(ClO_4)_{2*}3H_2O$	barium perchlorate trihydrate
H_2O_2	hydrogen peroxide
$C_{16}H_{11}AsN_2O_{10}S_2$	thorin indicator
H_2SO_4	standard sulfuric acid solution

Notation

t	time, s
mf	value for $U=U_{mf}$
ΔP	pressure drop, kPa
U	superficial gas velocity, m/s
d_p	particle diameter, μm
Tdew	sulfuric acid dew-point temperature (°C)
$P_{species}$	partial pressure of gas species (kPa)
$C_{species}$	concentration of species (H_2SO_4, SO_2) (ppm)
V	volume of samples (L)

1 INTRODUCTION

According to the IEA, (2014);(2015), coal accounted for almost 30% of the world's total primary energy consumption in 2012 and 44% of global CO_2 emissions. The energy produced from renewable sources such as wind, biomass, geothermal or solar energy is unlikely to replace energy provided by fossil fuels in the near future. In this context carbon capture and storage (CCS) concept has been proposed as an alternative option to mitigate greenhouse gas emissions (GHG) from coal-fired power plants and industrial processes. It is reported by (IPCC, 2005) that CCS could potentially reduce CO_2 emissions by 80-90%. The CCS process involves the production of a highly enriched CO_2 stream from a fuel combustion followed by transportation and storage of CO_2 in storage facilities such as saline aquifers, depleted oil or gas reservoirs and mines. A number of studies are underway to evaluate the feasibility of CO_2 storage and the associated environmental issues.

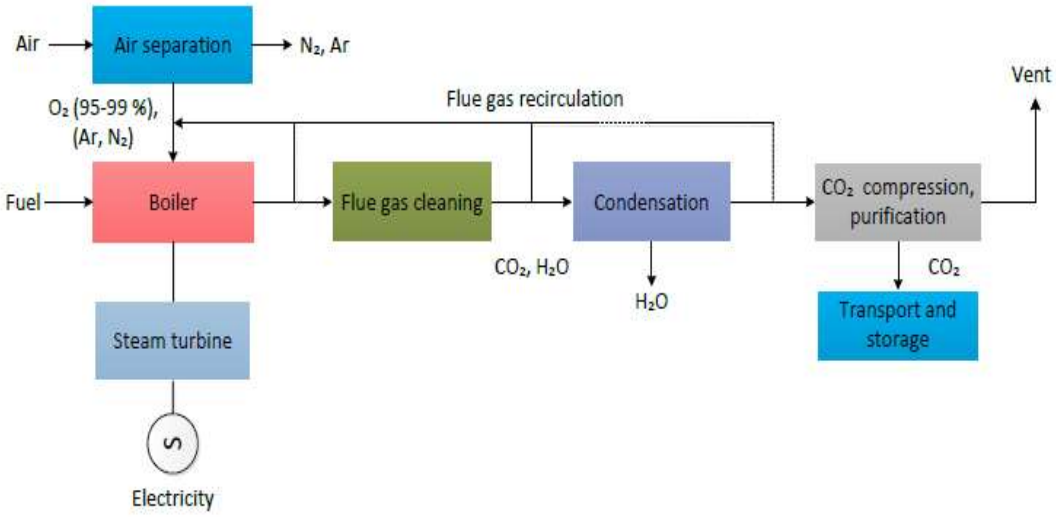

Figure 1-1 Principal scheme of oxy-fuel combustion process

The principal concept of oxy-fuel combustion is to burn fuel in a mixture of oxygen and recycled flue gas (RFG), see Figure 1-1. Thus, the combustion environment differs significantly from the typical air combustion. The nitrogen in the oxidiser stream is replaced by the RFG that typically contains mainly carbon

dioxide and steam (Toftegaard *et al*., 2010); (Wall *et al*., 2009). The amount of RFG in the main stream is controlled to moderate the combustion temperature in the boiler and keep it at levels similar to the air combustion (Buhre *et al*., 2005). As a result, a comparable heat transfer profile can be achieved along the vertical section of the boiler as in the typical air combustion (Buhre *et al*., 2005). However, the impurities contained in the flue gas increase sulfur dioxide, nitrogen oxides and steam concentrations considerably, due to the RFG (Liu and Shao, 2010). As a result, SO_2 concentrations in the oxy-fuel combustion can be several times higher than in the air combustion (Croiset and Thambimuthu, 2001);(Croiset *et al*., 1998). Thus, an increase of SO_2, O_2 and H_2O species could enhance SO_3 concentrations to a greater degree. This can lead to serious operational risks associated with the corrosion. The reaction of SO_3 and H_2O lead to the formation of sulfuric acid that condenses on the down-stream of the boilers (Moser, 2006);(Cao *et al*., 2010). In order to evaluate the formation of SO_3, several experimental tests are examined in this thesis during the combustion and post-combustion environments of air and oxy-fuel.

1.1 Influence of sulfur compounds in combustion systems

Sulfur-in-coal may vary from 0.2 to 11%, depending on the location and rank (Attar, 1978)(Raask *et al*., 1982). However, typical values fall generally between 0.3 and 4.3% (Glarborg, 2007). Typically, sulfur in coal is classified into two forms: organic and inorganic (Attar, 1978);(Cullis and Mulcahy, 1972). The amount of organic sulfur is approximately one-half to one-third of the total sulfur in coal (Cullis and Mulcahy, 1972);(Glassman and Yetter, 2008). Most organic and pyritic sulfur in coal is converted to sulfur dioxide during combustion and a part of the sulfur is retained in the ash. In this regard, studies on North Dakota coals has reported 83 to 93% conversion of sulfur in fuel to SO_2, depending on sulfur content in the coals (Zygarlicke *et al*., 2006). Similarly, 91% of S to SO_2 conversion for a US eastern bituminous coals was observed by Croiset and Thambimuthu, (2001). Swedish lignite was also investigated in a pilot-scale 100 kW oxy-PC unit and showed 67% of conversion (Fleig *et al*., 2011). Depending on the alkalinity content in the ash, part of sulfur reacts with alkaline or alkaline

earth metal compounds such as calcium, magnesium carbonates and sodium chloride (Cutler and Raask, 1984). As a result, roughly, 10 to 15% of SO_2 can be trapped by the alkaline compounds (Zygarlicke *et al*., 2006); (Cutler and Raask, 1984). The main challenge with burning sulfur contained coals in the boiler is associated with the corrosion aspects. The impact of sulfur in conventional PC boilers has been studied and reviewed extensively in the past (Attar, 1978);(Raask, 1982);(Cutler and Raask, 1984) and more recently in oxy-fuel combustion (Stanger and Wall, 2011). Most of the corrosion mechanisms due to the sulfur in conventional PC combustion are well known and apply to oxy-fuel combustion (Stanger and Wall, 2011).

Corrosion at high-temperatures is known as fireside corrosion (FC) that is caused by low melting points of alkali salt deposits. FC is one of the key reasons for tube failures in combustion systems that is caused by utilisation of coals with rich organically-bound sulfur, chlorine and sodium compounds (Bryers, 1996). This will lead to a damage of heat exchangers by loss of metal or formation of cracks which will be followed by mechanical damage (Harb and Smith, 1990). Corrosion at low temperatures occurs due to the formation of sulfuric acid. Sulfur during the combustion, also affects on the flame behaviour, significantly (Durie *et al*., 1970);(Zachariah and Smith, 1987). In fluidised beds, SO_2 inhibits carbon monoxide (CO) burn out rate and may decrease the rate of homogeneous CO oxidation (Miccio *et al*., 2001);(Schäfer and Bonn, 2000). Recent observations from a bench-scale natural-gas fired burner with a 26 kW, showed a clear decreasing trend of CO emissions when 100 ppm of SO_2 doped under sub-stoichiometric conditions (Glarborg, 2007).

1.2 Formation of SO_3 during the combustion

During the coal combustion a small fraction of SO_2 may be further oxidised to SO_3 (Srivastava *et al*., 2004);(Glarborg, 2007);(Cullis and Mulcahy, 1972);(Croiset and Thambimuthu, 2001). As reported by Nielsen *et al*., (2003), from 0.5 to 1.5 wt % of SO_2 present in the flue gas may further oxidise to SO_3. The SO_2 to SO_3 conversion is dependent on several parameters such as: combustion temperature, oxygen concentration and presence of catalytic

compounds in the fly ash (Fleig *et al*., 2009);(Fleig *et al*., 2012). Formation of SO_3 is undesirable in combustion process as it enhances corrosion problems and formation of aerosol emissions (Srivastava et al., 2004). By its nature, SO_3 is very reactive and converts easily to sulfuric acid in the presence of water vapour (Cullis and Mulcahy, 1972). SO_3 is thermodynamically favoured at lower temperatures. However, due to kinetic rate limitations and cooling rates in practical systems, the SO_3/SO_2 equilibrium is not observed in practical systems (Glarborg, 2007). Tan *et al*. (2006) has stated that the conversion of SO_2 to SO_3 in typical PC boilers may be up to 5%, depending on the sulfur content in the coal. SO_3 can also cause plume opacity in the stack by forming sulfuric acid droplets and particulate sulfate aerosols (Srivastava *et al*., 2004);(Cao *et al*., 2010). According to EPRI estimation, roughly 5 to 10 ppm of SO_3 in flue gas can result in a plume opacity of 20 and 50%, respectively (Peterson and Jones, 1994). Moser, (2006) has stated that the deposition of the H_2SO_4 on downstream surfaces can be avoided by increasing the outlet temperature of the flue gas. This means that the outlet temperature of the air preheater should be kept above the dew point. However, this will decrease the overall efficiency of the boiler significantly. An increase of 1.7ºC in the air heater outlet temperature results in a decrease of nearly 1% in the unit heat rate. The benefit derived from the removal of SO_3 and the consequential reduction of corrosion in the downstream could exceed $500,000 per year (Moser, 2006).

Application of selective catalytic reduction (SCR) technology in coal-fired power plants can cause further SO_2 oxidation (Srivastava *et al*., 2004); (Moser, 2006). This happens due the reduction of NO_x to molecular N_2 and H_2O by reaction of NO_x with injected NH_3. According Moser, (2006), this SO_2 oxidation in the SCR can vary from 0.3% to 2%. Slightly lower percentage have noted by Srivastava *et al*. (2004) of between 0.25 to 0.5% for bituminous and 0.75 to 1.25% for sub-bituminous coals. A more detailed study of SO_2 oxidation over honeycomb SCR catalysts was reported earlier by Svachula *et al*. (1993). According to these authors, the oxidation degree of SO_2 in SCR depends on vanadium content and wall thicknesses of the catalyst. It is also noteworthy that the reaction rate is of variable order in SO_2 and increasing with temperature. In addition, the reaction

rate is found to be independent of oxygen and water, and is strongly inhibited by ammonia and slightly enhanced by NOx (Svachula *et al*., 1993).

1.3 Aims and scope

The aim of the thesis is to extend the knowledge on the SO_3 formation during the low temperature combustion conditions typically found in air-fired and oxy-fired fluidised beds. The literature review made in this thesis has pointed out to the significant amount of work conducted at high temperature combustion conditions. Most of these combustion conditions characterises the SO_3 formation degree in pulverised coal combustors where combustion temperature found higher than 1000°C. Thus, the novelty of this thesis is to investigate the formation degree of SO_3 at the low-temperature conditions. In addition to that, oxy-fired fluidised beds combustion conditions are also investigated and compared to air combustion environment. As mentioned earlier, oxy-fuel combustion scheme has higher levels of O_2, H_2O and SO_2 concentrations compare to the air combustion environment. Thus, this could lead to a higher formation of SO_3 concentrations. The formation of SO_3 is an undesirable process during the combustion as it turns to convert to a sulfuric acid if the flue gas temperature goes below the dew point temperature. Thus, this could lead to serious operational risks due to the corrosion.

The objectives of current work were constructed based on the detailed literature survey on the SO_3 formation and series of experimental tests. The thesis also covers SO_3 measurements conducted in a pilot-scale 50 kW CFB unit during visit to Southeast University in China. For the bench-scale experiments, flue gas composition of oxy-fuel and air were simulated by synthetic gases to evaluate SO_2 to SO_3 conversion degree. Parameters such as O_2, SO_2 and H_2O concentrations were varied to investigate its effect on the SO_3. In addition to that, catalytic effects of fly ash compounds are investigated in this thesis by adding 4 different fly ashes in the bench-scale tests. Following objectives were derived for current thesis:

1. Literature review on the formation of SO_3 under air and oxy-fuel combustion environments:
    - Homogeneous and heterogeneous SO_3 formation;
    - SO_3 formation in the pulverised coal (PC) and fluidised beds (FB);
    - Methods of SO_3 measurements;
2. Development of SO_3 sampling train, based on EPA method 8A:
    - Controlled condensation method (CCM);
3. SO_3 measurements in a series of experimental rigs such as fixed bed, bubbling fluidised bed and pilot-scale oxy-CFB rig:
    - Low temperature SO_3 formation in a fixed bed rig;
    - SO_2 to SO_3 conversion in a bubbling fluidised bed under flue gas environments of air and oxy-fuel;
    - SO_3 measurements in a pilot-scale circulating fluidised bed;
    - Thermodynamic equilibrium prediction of SO_2 to SO_3 conversion;
4. Characterisation of fly ashes by thermogravimetric (TGA) and X-ray fluorescence (XRF) analysis;

1.4 Dissemination of PhD project

Provided list describes the main contribution of the research project prepared during the course of PhD program. The last two studies have been presented in the international conferences.

I. Sarbassov, Y., Zayoud, A., Mahanta, P., Gu, S., Ranganathan, P., Saha, U.K., 2015. 'Hydrodynamic experiments on a small-scale circulating fluidised bed reactor at elevated operating pressure, and an O_2/CO_2 environment' Thermal Science; Doi: 10.2298/TSCI150921068S;

II. Duan, L., Duan, Y., Sarbassov, Y., Li, Y., Anthony, E.J., 2015, 'SO_3 formation under oxy-CFB combustion conditions', International Journal of Greenhouse Gas Control, 43, 172–178;

III. Sarbassov, Y., Anthony, E.J., Duan, L., Manovic, V., 'Medium- and high-temperature SO_3 formation in a bubbling fluidized bed: effect of fly ashes under air and oxy-fuel combustion environments' (Submitted to Fuel Processing Technology);

IV. Sarbassov, Y., Anthony, E.J., Duan, L., Manovic, V., 'Review of sulfur trioxide emissions in oxy-fuel combustion: effect of flue gas recycling, catalytic effect of fly ash and modelling'. (Submitted to greenhouse gas science and technology*)*;

Conference papers:

I. Sarbassov, Y., Zayoud, A., Mahanta, P., Gu, S., Ranganathan, P., Saha, UK., Circulating fluidised bed hydrodynamics study at elevated pressure and atmospheric O_2/CO_2 environment, 22nd International Conference on the fluidised bed conversion, June 2015, Finland (Proceedings of the 22nd International Conference on the fluidised bed conversion);
II. Zayoud, A., Sarbassov, Y., Mahanta, P., Gu, S., Saha, UK., Influence of aeration on the hydrodynamic behaviour of pressurised circulating fluidised bed, 5th International and 41st National Conference on Fluid Mechanics and Fluid Power, Indian Institute of Technology Kanpur, December 2014, India (Proceedings of the 5th International and 41st National Conference on FMFP 2014, Fluid Mechanics and Fluid Power – Contemporary Research, Springer-2017, pp.105-114); Doi: 10.1007/978-81-322-2743-4_11;

The author of this thesis is the first author in three journal papers and in one conference paper. The first journal and two conference papers focused on the hydrodynamic aspects of solids circulation in the lab-scale circulating fluidised bed. Therefore, the author has not included these works into the main body of the thesis and placed journal paper in the Appendix G and H. The author of this thesis was the co-author in the second paper, which were conducted during the visit to Southeast University.

1.5 Content of the thesis

The current thesis consist 5 Chapters and Appendixes. XRF analysis of fly ashes are summarised in the Appendix. Chapter 1 provides an introduction into the thesis by describing the research aims and objectives and highlighting the key issues of sulfur during the combustion processes. The chapter also covers

a brief introduction to the SO_3 formation in the combustion. Chapter 2 provides the literature review for the oxy-fuel combustion technology, background on the SO_3 chemistry. Influence of oxy-fuel combustion environment on SO_3 concentration and SO_3 sampling methods are also provided in this section. Following chapter 3 describes the research methodology for each experimental test. Results and discussion are given in the Chapter 4. Finally the conclusion of the thesis is formulated in last Chapter 5.

2 LITERATURE REVIEW

The literature review in this thesis is divided into the following major sections:

- Oxy-fuel combustion concept including flue gas recirculation and emissions;
- Oxy-fuel combustion technology development in large-scale fluidised bed units;
- SO_3 formation in combustion and SO_3 sampling methods. This part is described by homogeneous and heterogeneous SO_3 chemistry along with the description of most available SO_3 sampling techniques.
- Effect of an oxy-fuel combustion environment on the formation of SO_3 is also discussed.

2.1 Oxy-fuel combustion technology

Oxy-fuel combustion is one of the CCS concept that was proposed by Abraham in 1982, to produce highly concentrated flue gas for enhanced oil recovery (Toftegaard *et al*., 2010); (Buhre *et al*., 2005). Later, Argonne National Laboratory carried out oxy-fuel investigations at a pilot-scale facility (Abele *et al*.,1987). In 1990, comprehensive work started on CCS technologies throughout Europe and USA (Edge et al., 2011). Babcock Wilcox and Air Liquid continued research on oxy-fuel in a collaboration with CANMET (Wall *et al*., 2009). A number of research publications can be found in the literature for oxy-fuel combustion in the pulverised coal combustors (Toftegaard *et al*., 2010). As noted in the previous section, the generated flue gas mainly consists of CO_2 and H_2O, plus small amount of contaminants such as NO_x and SO_x. The flue gas then goes through a cleaning process that occurs via a series of units such as electrostatic precipitator (ESP), flue gas desulfurisation (FGD) and selective catalytic reduction (SCR). Ash particles from the flue gases in downstream of boiler are removed by ESP unit before SCR. In practice, ESP system prevents degradation of catalyst in SCR unit. However, to avoid an accumulation of sulfur in the SCR system, a FGD unit must also be placed before SCR (Toftegaard *et al*., 2010). Due to the additional equipment for O_2 separation and flue gas

compression studies to date suggest that the net combustion efficiency points of oxy-fuel technology drops roughly from 7 to 11% (Davison, 2007); (Müller *et al*., 2012); (Wall *et al*., 2007). However, it should be mentioned that these studies are based on number of yet to be verified assumptions on plant performance and availability. The cost of technology can vary significantly depending on the plant location and type of coals (Davison, 2007).

Liu and Shao, (2010) have predicted the level of flue gas impurities in oxy-fuel combustion for CO_2 storage. The authors concluded that N_2/Ar levels in the flue gas varied from 1 to 6%, depending on O_2 purity from the ASU. O_2 concentration varied from 3 to 5%, depending on the combustion stoichiometry. Also, the water concentration in the flue gas fluctuated from 10 to 40%, depending on the fuel properties and partitioning of the RFG between dry and wet (Liu and Shao, 2010). Typical pollutant levels from modern coal and gas-fired power plants (SO_2, NOx and particulate matter-PM) are provided by IEA (2012), see Table 2-1. It can be seen that fluidised beds offers better solution with a comparatively low emission levels of SO_2 and NOx. However, to maintain the same level of emissions in pulverised coal (PC) technology, additional clean-up is required.

The produced CO_2 goes through purification and cleaning processes where the CO_2 is compressed and transported for storage at relatively high pressures (Anheden *et al*., 2008);(Anheden *et al*., 2004). The geological conditions for delivering the CO_2 stream have been reported by several authors (Dillon *et al*., 2005). The CO_2 requirement for transportation and storage was assessed by (Anheden *et al*., 2008). These authors noted that SO_2 content in CO_2-enriched gas must be < 200 mg/Nm^3 in aquifer storage and < 50 mg/Nm^3 for on-shore storage. Markewitz *et al*. (2012) has reported SO_x levels during the CO_2 transportation and noted that SO_x concentrations should be limited to 100 ppm. This level is associated with the emission limits in the event of gas leakage (Visser *et al*., 2008). SO_2 may also cause problems due to its sulfation behaviour in the presence of calcium containing ashes in the underground storage. If sulfates are formed in saline aquifer they will decrease the storage

Table 2-1 Performances of coal and gas-fired power plants (IEA 2012)

Plants (MW)	Cap fac[a] (%)	CO_2 emissions (g/kWh)	NO_x emission (mg/Nm^3)	SO_2 emission (mg/Nm^3)	PM[b] emission (mg/Nm^3)	CCS penalty (%)
PC-Ultra Super Critical (1050)[c]	80	740	<50 to 100 (by SCR)	<20 to 100 (by FGD)	<10	7 to 10 (post & oxy-fuel combustion)
CFBC (460)[d]	80	880 to 900	<200	<50 to 100 (in situ)	<50	
PC A-Ultra Super Critical [e] <(1000)	-	669[f]	<50 to 100 (by SCR)	<20 to 100 (by FGD)	<10	
IGCC (335)	70	669 to 740	<30	<20	<1	7
NGCC[g] (410)	80	400	<20	Almost none	0	8

porosity and consequently may affect the storage capacity parameters. Also, nearly complete dehydration of the flue gas is crucial, as it will reduce the mass flow rate and inhibit corrosion (Andersson and Johnsson, 2006);(Aspelund and Jordal, 2007). The change of mass flow is associated with the density of CO_2 stream which tends to decrease by increase of impurities (Burnol *et al*., 2015).

Presence of SO_2 results in higher heat capacities of CO_2 (Li *et al*., 2009). In addition, the isothermal compression work was found to be more sensitive for SO_2 than other species (Li *et al*., 2009). The presence of both SO_2 and water in

[a] Cap fac-capacity factor
[b] PM-particulate matter
[c] In operation (sliding pressure-type)
[d] In operation (Poland)
[e] Under development
[f] At temperature of 700 ºC
[g] NGCC-Natural gas fired combined cycle plant

the CO_2 stream may increase the risk of corrosion by formation of sulfuric acids (Anheden *et al*., 2008). For that reason, removal of impurities from the CO_2 stream by flue gas condensers and FGD units is necessary before the transportation (Anheden *et al*., 2008).

The impurities derived from three CCS technologies as compared by the IEA, (2012), was illustrated in Table 2-2. Three CO_2 purity scenarios were provided for an oxy-fuel combustion with 85.0%, 98.0 and 99.9% in the flue gas stream (IEAGHG, 2011);(Talman, 2015). It can be noted that the SO_2 and SO_3 compounds in CO_2 streams were higher in oxy-fuel combustion than in the pre-combustion and post-combustion CCS schemes. White *et al*., (2010) has

Table 2-2 Composition of CO_2 streams for storage (IEAGHG, 2011)**;**(Talman, 2015)

Compounds	Pre-combustion		Post-combustion			Oxy-fuel		
	Selexol	Rectisol	Low pur[h]	Med pur	High pur	Low pur	Med pur	High pur
CO_2 (vol%)	97.95	99.7	99.93	99.92	99.8	85.0	98.0	99.9
O_2 (vol%)			0.02	0.02	0.03	4.70	0.67	0.01
N_2 (vol%)	0.90	0.21	0.05[i]	0.05[1]	0.09[1]	5.80	0.71	0.01
Ar (vol%)	0.03	0.15				4.47	0.59	0.01
H_2O (ppm)	600	10	100	100	600	100	100	100
NO_x (ppm)			20	20	20	100	100	100
SO_2 (ppm)			10[2]	10[2]	20[j]	50	50	50
SO_3 (ppm)						20	20	20
CO (ppm)	400	400	10	10	20	50	50	50
H_2S+COS (ppm)	100	100						

[h] Pur - CO_2 purity
[i] Total concentrations of N_2+Ar
[j] Total concentrations of SO_2+SO_3

highlighted that the SO_2 and SO_3 compounds mainly removed in the form of H_2SO_4 in the CO_2 stream. Older data from the IEA on impurities were reported by IPCC, (2005). It is also noted that the flue gas should be dehydrated to a dew point of 5ºC below the temperature required for transportation in the presence of SO_2 and CO_2. It is believed that under these conditions SO_2 will not cause corrosion (Andersson and Johnsson, 2006).

2.2 Flue gas recirculation concept

The oxygen with >95% purity for combustion is mixed with the RFG before it enters the boiler. The amount of RFG is determined by flame temperature similar to typical air-fuel combustion. This consequently will give a comparable heat transfer profile through the boiler (Buhre *et al*., 2005). On the other hand, to reach similar adiabatic flame temperature in the furnace as in air combustion, O_2 concentrations in the oxidant stream should be kept higher than 30% (Wall, 2007);(Hu and Yan, 2012). Typically, this requires 2/3 of flue gas to be recycled. According to the previous studies of Toftegaard *et al*. (2010); Andersson and Johnsson, (2006); Handford *et al*. (2014) and Kather and Scheffknecht, (2009), an optimum RFG ratio lies between 0.6 to 0.8. The recycling rate is defined as the amount of RFG per mole of fuel (Hu and Yan, 2012):

$$\text{RFG rate} = v\left(\frac{\lambda_{\text{RFG}}}{[O_2]_{\text{Oxidant}}} - \frac{\lambda_{\text{RFG}}}{[O_2]_{\text{Asu}}}\right) \qquad \text{Equation 2.1}$$

where ν is the stoichiometric coefficient of O_2 for fuel used. $[O_2]_{asu}$ and $[O_2]_{oxidant}$ are O_2 concentration provided to the boiler and ASU, λ and ε are the stoichiometric ratio and excess oxygen in the oxidant and flue gas streams as seen in Figure 2-1.

Alternatively, this term can be presented as the recycled flue ratio.

$$\text{RFG ratio} = \frac{\text{Mol of recycled flue gas stream}}{\text{Total mol of flue gas stream of boiler outlet}} \times 100\% \qquad \text{Equation 2.2}$$

Various RFG schemes were proposed by Nakayama and Noguchi, (1992). In their studies, the difference between the dry and wet RFG is due to the presence or absence of a dehydration (condenser) unit in the system flow as

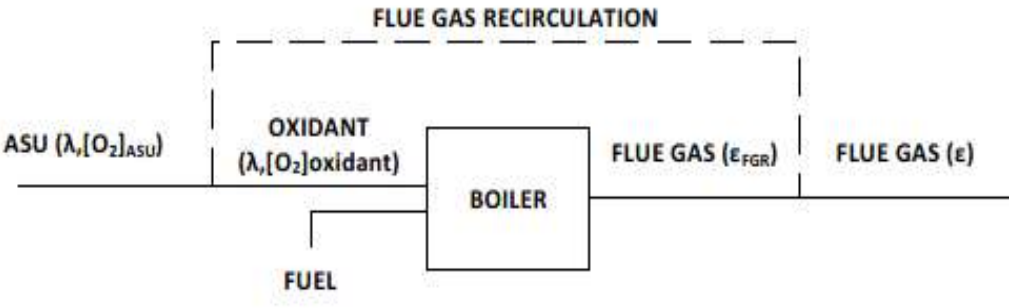

Figure 2-1 Simplified recycled flue gas scheme in oxy-fuel combustion
(Hu and Yan, 2012)

can be seen in Figure 1-1. The wet RFG is normally extracted before the flue gas condenser. Dry RFG is extracted after passing condenser. Dry RFG is required when restrictions on the moisture and SO_2 content in the flue gas exists (Normann *et al*., 2009). The model developed by Argonne National Laboratory (ANL), has presented a typical SO_2 concentration build up with an increase of RFG fraction, based on the 1000 ppm without recycled case, see Table 2-3 (Molburg *et al*., 2001).

In this regard, EPRI, (2007) reported that wet RFG can be employed after passing through the FGD unit if the SO_2 concentration in the flue gas exceeds 3000 ppm. RFG can be separated into primary and secondary streams for coal-fired power plants. This makes it advantageous to utilise low reactive bituminous coals. Primary recycle should be scrubbed, dried and cooled to a temperature of around 250ºC or more before entering the feeding mills (Toftegaard *et al*., 2010);(EPRI, 2007). This required for coal transportation and removing the moisture (Kather and Scheffknecht, 2009); (Zanganeh and Shafeen, 2007). Thus, the removal of water-soluble acid gases such as SO_3 and HCl could be ensured to reduce the risks of corrosion (Hu and Yan, 2012); (EPRI, 2007). Roughly, around 20% of the flue gas is taken as primary recycle, whereas the majority of the gas stream is extracted as the secondary recycling

Table 2-3 Effect of RFG on SO_2 concentration in the flue gas, based on 1000 ppm without RFG (Molburg *et al*., 2001)**.**

RFG fraction	Sulfur concentration (ppm)
0.7	3110
0.6	2370
0.5	1920
0.4	1650
0.3	1390
0.2	1230
0.1	1080
0	1000

stream (Toftegaard *et al*., 2010); (Dillon *et al*., 2005). In this regard, Kather and Scheffknecht, (2009) have suggested that the temperature of the RFG should be maintained between 200-300ºC. Similar temperature levels were also suggested elsewhere (Normann *et al*., 2009);(Günther *et al*., 2013). RFG temperature is determined mainly by technical parameters such as dimensions of the recirculation duct, recirculation fan and ESP (Kather and Scheffknecht, 2009). Higher flue gas temperature in the system can lead to a higher maintenance cost of hot recirculation fun (Kather and Scheffknecht, 2009).

2.3 Fundamental studies of the oxy-fuel combustion

2.3.1 SO_2 emissions

It is reported that in oxy-fuel combustion, SO_2 concentration (in ppm) is significantly higher compared to conventional air combustion (Croiset and Thambimuthu, 2001); (Stanger *et al*., 2011). Higher concentration of SO_2 in the oxy-fired flue gas occur due to the change of volumetric flow through the combustion furnace and RFG (Handford *et al*., 2014). However, in (mg/MJ) normalised basis SO_3 emissions found lower in oxy-fuel than in air combustion (Croiset and Thambimuthu, 2001); (Stanger *et al*., 2011); (Dhungel *et al*., 2011).

This is mainly attributed to higher retention of sulfur by the ash, removal of sulfur with condensate during the dry flue gas recycle (Croiset and Thambimuthu, 2001); (Dhungel *et al*., 2011). According to Liu and Shao, (2010), SO_2 concentrations of oxy-coal fired plant can be 6 times higher compared to an identical air combustion unit. The effect of RFG on combustion characteristics of US eastern bituminous coals was studied by Tan *et al*. (2006). The authors concluded that SO_2 concentrations in the furnace were 3-4 times higher than in air combustion (Tan *et al*., 2006). An almost identical level was noted by Fleig *et al*. (2011) in a lignite fired oxy-PC unit. However, comparatively lower concentrations of SO_2 were measured by Duan *et al*. (2014) in a 50-kW oxy-fired CFB unit. It should be noted that the SO_2 concentrations in this study were still higher than SO_2 seen in air combustion. Croiset and Thambimuthu, (2001) have observed almost double the SO_2 levels in the RFG tests compare to once-through tests in a 210 kW experimental unit. In addition, the authors indicated a decreasing trend of S to SO_2 conversion from 91% in air fired case. However, conversion in O_2/CO_2 atmosphere was 74% on average and 64% in the RFG tests. According to these authors, a possible reason for lower conversion could be due to the sulfur retention in the ash. This can be up to 3% of the initial sulfur contained in the coal and small fraction that oxidised to SO_3. Higher sulfur retention by ash was also noted in experimental tests in a 100 kW under oxy-fired unit (Fleig *et al*., 2011). Relatively, low conversions of S to SO_2 were noted by these authors reaching around 43% in oxy-fuel and 67% in the air tests. They also concluded that the low conversion occurs due to the sulfur retention in fly ash in the oxy case and suggesting that lignite has a higher self-retention performance under these conditions (Fleig *et al*., 2011).

At higher temperatures, sulfur species could decrease nitric oxides concentrations in the post-flame regions (Wendt *et al*.,1983);(Corley and Wendt, 1984);(Wendt and Ekmann, 1975). This occurs due to the catalyses of oxygen atom recombination reactions by SO_2 (Wendt and Ekmann, 1975). These mechanisms are described by Glarborg *et al*. (1996):

$$X + SO_2 + M \rightarrow XSO_2 + M \quad (1)$$

$$Y + XSO_2 \rightarrow XY + SO_2 \quad (2)$$

where X and Y may be H, O or OH, M – represents the third body. Typically, a third body is necessary to remove an excess energy from reaction to complete recombination and dissipate it as heat (Glassman and Yetter, 2008). It is reported that under fuel-lean combustion conditions, the inhibition is mainly governed by the recombination of O radicals involving SO_3 (Glarborg, 2007), while under fuel-rich or stoichiometric conditions the interaction of SO_2 with radicals is believed to be more complex (Lund *et al*., 2007);(Giménez-López *et al*., 2011). The most important radical removal step under stoichiometric and reducing conditions is caused by the recombination of SO_2 with hydrogen (H) to form an H/SO_2 adduct (Lund *et al*., 2007):

$$SO_2 + H + M \leftrightarrow H/SO_2 + M \quad (3)$$

This followed by recycling of this adduct to SO_2 by reaction with H or OH. H/SO_2 is expected to be HOSO (hydroxidooxidosulfur) radical than HSO_2 due to its thermal stability (Lund *et al*., 2007).

The presence of SO_2 also has an inhibition effect on moist CO oxidation in N_2 diluted environments. The inhibition was more pronounced at high O atom levels; however the presence of NO in the system significantly reduced the SO_2 effect (Glarborg *et al*., 1996). This work has been extended recently by Giménez-López *et al*. (2011) who explored this phenomenon experimentally under CO_2 diluted atmosphere to simulate oxy-fuel conditions. The authors concluded that an important inhibition effect was evident in a CO_2 atmosphere as compared to N_2 rich environment. This was due to the competition between CO_2 and O_2 for H radicals that reduces the formation of chain carriers via the O_2+H chain branching reaction. Lower inhibition was seen when the stoichiometry becomes oxidising.

2.3.2 NO_x emissions

Major review of nitrogen oxides in oxy-fuel combustion were reported previously by Normann *et al*. (2009) and Toftegaard *et al*. (2010). Therefore, this thesis reports only on latest investigations of NO_x emissions in oxy-fuel combustion. For more detailed review and the fundamentals of NO_x formation, the reader is referred to above mentioned review papers. It should be highlighted that most of the investigation in this aspect have concluded that there are reduced NO concentrations in the O_2/CO_2 atmospheres than in the air. This occurs due to the replacement of N_2 by CO_2, which does not favour the prompt and thermal reaction for NO_x formation (Normann *et al*., 2009); (Toftegaard *et al*., 2010). In addition to that higher concentrations of CO_2 and CO derived from oxy-fuel combustion contributes to the reduced of NO_x emissions in contrast to the air combustion environment (Toftegaard *et al*., 2010). Results from 50 kW oxy-CFB unit has also confirmed lower NO_x in 21% O_2/79% CO_2 compare to conventional air case which occurred due to the lower temperature and presence of CO (Duan *et al*., 2011a). Stadler *et al*. (2011), indicated 50% of NO_x reduction for swirl flame oxy-coal combustion and 40% with flameless combustion mode. The oxygen concentration of 18 to 27% in swirl flames resulted to a slight NO_x reduction under dry RFG condition. However, in wet RFG condition NO_x were much lower. Lately, a few studies on this aspect have been carried out such as the one by Brix *et al*., (2013) who studied NO_x formation at a fundamental level to see the effect particle temperature from single and group of char particles. It was shown that the formation of NO from lignite char was not influenced from the switching of gas between N_2 to CO_2. NO yield was lower for bituminous coal in O_2/CO_2 environment. The conversion to NO for both lignite and bituminous chars decreased with an increase of O_2 and particle sizes (Brix *et al*., 2013). Effect of impurities as NO and N_2O concentrations of fuel derived NO_x concentrations were tested by Yoshiie *et al*. (2015). The authors concluded that N_2O concentrations were slightly higher in oxy-fuel atmosphere due to the recirculated N_2O. This conclusion was supported by Roy *et al*. (2014) and Wang *et al*. (2015). However, no significant effect of impurities was noted in their work at 21% of O_2 concentration. In this regard, the early work reported by Shaddix

and Molina, (2011) has illustrated the net NO_x production when 550 ppm of NO injected. The NO reburn were between 20% and 40%, depending on the type of coal and this difference noted only when O_2 concentrations increased to 36%. Moreover, along with an independent effect of temperature on N_2O reduction, the catalytic effect of Fe_2O_3 provided an obvious contribution on N_2O reduction in the presence of CO (Wang *et al*., 2015). It should be highlighted that the presence of steam was excluded in some of these studies and the results are limited by the size of the setup. It is highlighted that the addition of steam resulted in a 30% decrease in NO_x production in oxy-fuel condition, while 44% reduction were noted in air combustion CFB unit with nitrogen content of 1.7% in coal (Stewart *et al*., 2012). However, these values were less than those results noted by Roy *et al*. (2014). The effect of steam on reduction was 5.5% for NO_x and 10% for N_2O by utilising Victorian brown coal with nitrogen content of 0.72% (Roy *et al*., 2014). The lower nitrogen content of fuels could be the main reason for different conversion ratio. More recently Spanish high rank coals such as anthracite, bituminous, lignite and three types of Ca-based sorbents were investigated in a bench size bubbling fluidised bed (Obras-loscertales *et al*., 2015). As noted previously, a reduction of total fuel-N conversion to NO and N_2O was achieved in oxy-fuel condition. In the case of sorbents, it is concluded that lowest NO emissions were seen in the sorbent with lowest sulfur retention. In addition bigger particle size and longer residence time of sorbents corresponded to the reduction of NO emissions. Moisture in the fuel slightly enhanced the reduction of NO emissions further, whereas no significant change in N_2O was detected. An increasing O_2 content to the combustor generally increases the NO_x emission and was associated with an increase of fuel input. Tests in pulverised coal (PC) unit also confirmed an increase of NO_x emissions with O_2 concentration (Ndibe *et al*., 2013);(Shaddix and Molina, 2011).

2.3.3 Ash and deposit formation

Transformation of the mineral matter in flame depends on the temperature and gas environment (Bryers, 1996);(Sheng *et al*., 2007). Thus, replacing N_2 by CO_2

in oxy-fuel combustion could result in a different ash composition. The metal transformation mechanisms during air-coal combustion was revised by Linak and Wendt, (1994). These authors developed a controlling mechanism for particle formation which later modified by Suriyawong *et al*. (2006). Based on these studies, the mineral transformation and particle formation pathways in typical coal combustion are illustrated in Figure 2-2. Suriyawong *et al*., (2006) tested subbituminous coal in a drop tube furnace (DTF) under N_2/CO_2 and O_2/CO_2 environments. Their conclusion was that the mean size of submicron ash particles (<0.5 μm) under O_2/CO_2 was smaller compared to the N_2/CO_2 firing mode. However, an increase of O_2 content in the mixture resulted to increase of mean size submicron particles. This occurred due to the faster vaporisation rate, which resulted from higher coal particle temperature.

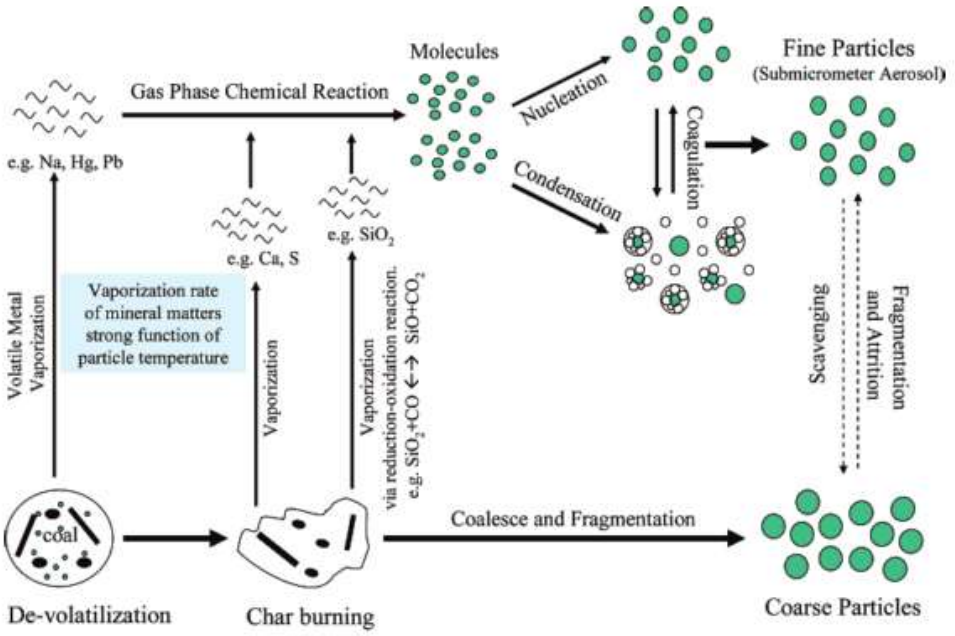

Figure 2-2 Mineral transformation and particle formation pathway

(Suriyawong *et al*., 2006)

Sheng *et al.*, (2007) has concluded that the size distribution of the residue ash particles was not affected by O_2/CO_2 environment. However, a significant change was noted in submicron particles, including both their composition and

size distribution. This is consistent with the results of Suriyawong *et al*., (2006), where an enrichment of CaO and Fe_2O_3 was noted in the fragmentation mode. However, their later work with X-ray diffraction (XRD) suggested no significant impact of two environments on ash mineral formation (Sheng and Li, 2008). The following conclusions were withdrawn from spectroscopic analysis of O_2/CO_2 environment: 1) more iron melted into the glass silicates; 2) less iron oxide formed due to the low char combustion temperature and 3) a high CO concentration within the particles slowed the transformations of pyrite and siderite to the oxides. Thus, this situation favoured transformation to form iron oxides (Sheng and Li, 2008). A similar particle size distribution (PSD) of bulk ash particles was noted by Li *et al*. (2013), in a 25 kW down-fired PC combustor. A higher formation of PM was seen in O_2/CO_2 than in air combustion at identical temperatures. This could be due to the higher vaporisation and nucleation under enriched O_2 concentration and longer residence time. However, the lower ash deposition rate was noticed in oxy-fuel than in air. These authors believe that the ash deposition should be attributed to the aerodynamics between combustion mode rather than chemical or physical differences (Li *et al*., 2013). These conclusions agreed with Yu *et al*. (2011), who has tested three US coals for ash and deposition formation. An enhanced deposition rate was seen in oxy-fuel combustion that was indicated by larger thickness of the ash layer. Fly and bottom ash characterisation from 100 kW oxy-fired CFB unit showed a higher degree of unburnt carbon (UC) in the fly ash than that found in bottom ash. According to these authors, this is due to the short residence time of CFB unit (Wu *et al*., 2011). It was also concluded that $CaCO_3$ content in fly ash was higher than in the ash from conventional combustion mode. This was confirmed by TGA analysis where char reacted with $CaSO_4$ at the temperatures higher than 880ºC. The Brunauer-Emmett-Teller (BET) surface area and pore volume of fly ash were much higher than in bed ash (Wu *et al*., 2011). More recently, the vaporisation of organically bound metals and ash agglomeration of Victorian lignite, brown and Chinese bituminous coals were tested in a DTF rig (Zhang *et al*., 2011). Experimental condition included the influence of impurities such as HCl, SO_2 and steam at

1000ºC (Jiao *et al*., 2011). These authors highlighted the fact that organically bound metals are the main source for ash agglomeration as well as the effect of impurities. Vaporisation of metals via chlorination was favoured mainly due to the presence of HCl. The vaporisation of Al and Ti oxides was also notable. The presence of SO_2 promoted sulfation of Na to condensed into liquid droplet which increased the fine ash yield, while steam in the presence of HCl and SO_2 favoured the transformation of chlorides into molten alumina-silicates (Jiao *et al*., 2011). These authors explored a similar approach using Victorian brown coal at different temperatures and as expected, a different transformation of metallic vapours was noted. At 800°C, the transformation of inorganic vapours was governed by pyrolysis (Zhang *et al*., 2011). It was also noted that higher concentration of SO_2 could lead to the formation of secondary products, including sulfur retention in the fly ash (MacDowell *et al*., 2010).

2.4 Development of oxy-fuel in large scale pulverised coal and fluidised beds

2.4.1 Pilot-scale oxy-fired pulverised coal plants

At the industrial scale, the world's first full scale oxy-fuel PC Schwartz Pumpe 30 MWth plant has been demonstrated in 2008 by Vattenfall (Faber *et al*., 2011). According to Strömberg *et al*. (2009), CO_2 is transported by refrigerated trucks to industrial and storage sides. Later in 2009, natural gas-fired 30 MW_{th} Lacq project was commissioned by Total. This project for the first time connected to the sequestration pipeline. The Lacq project does not include any inert-removal, and injects CO_2 with 92% purity down to the depth of 4500 m into a depleted gas field (Aimard *et al*., 2008). The Callide oxy-fuel project with 30 MW output has also been operating for some time in Australia. This project is the first demonstration of retrofit to an existing coal-fired power plant (Spero *et al*., 2008). On-going projects at commercial demonstration-scale include the Jaenschwalde 250 MW by Vattenfall. A list of on-going CCS projects can be

found in the updated database of Massachusetts Institute of Technology Energy Initiatives[k].

2.4.2 Progress of oxy-fired fluidised beds

By 2009, around 900 air-fired CFB boilers were in operation or under construction worldwide with a capacity range of 50 to 400 MWe (Suraniti *et al*., 2009). This represents a remarkable progress of technology in a short period of time. On a larger scale, a 100 MWe oxy-CFB demonstration plant has been announced by Alstom. However, at present no further information is available in the open literature on this project. Foster Wheeler (FW) has conducted 8 months of trial runs at CanmetENERGY in a 0.8 MWth pilot-scale CFB unit and demonstrated excellent combustion performance (Kuivalainen *et al*., 2010). CanmetENERGY conducted a number of oxy-fired tests since 2003 onwards in FB reactors with the capacity range of 0.1 to 0.8 MW (Jia *et al*., 2011). FW introduced a first supercritical CFB plant (Lagisza power plant) in Poland and also successfully commissioned 30 MW oxy-fired CFB plant in Spain (Anthony, 2013);(Wall *et al*., 2012). Preliminary results of 30 MW oxy-CFB unit have been published by Lupion *et al*. (2013) and more recently from Gómez *et al*. (2014). According to Gómez *et al*. (2014), over 90% of sulfur capture was achieved by limestone addition. Foster Wheeler has also announced a plan to develop 300 MW supercritical Flexi-burn CFB demonstration plant in cooperation with ENDESA (Kuivalainen *et al*., 2010). At pilot-scale level, oxy-fuel tests on CFB units were also being carried out by Technical research centre in Finland (VTT) and Lappeenranta University of Technology. Oxy-fuel combustion is also being investigated by a number of research groups using bubbling and circulating fluidised bed units and these are summarised in Table 2-4.

[k] Carbon Capture and Sequestration Technologies, MIT Energy Initiatives

Table 2-4 Pilot scale oxy-fired FB studies on emissions (modified from Wall *et al*., (2012))

Organisation	Cap	Aim of research	Type of fuel	RFG mode	Other information	References
Alstom, Windsor, CT, USA	3 MW (FB)	Feasibility study of oxy-fuel in fluidised bed		Not considered	Not available in open literature	Wall *et al*., (2012)
CanmetENERGY, Canada	0.1 and 0.8 MW (CFB)	CO_2, NO_x, SO_2 and Combustion characteristics, NOx, SO_2 emissions, ash characterisation	Anthracite, petroleum coke	Dry/Wet	Support of national Canadian program on oxy-fuel CFB	Jia *et al*., (2012)
Foster Wheeler, VTT and Lappeenranta University	0.1 MW (CFB)	Provided design and operational data for oxy-fuel operation		Wet	FW used VTT and CanmetENERGY units to test numerous fuels and limestones as a prelude to their demonstration plant at CUIDEN.	Eriksson *et al*., (2007)
Metso power	4 MWth	Developing	N/A[lm]	Wet	Cooperation between	Seddighi *et al*.,

[l] CAP-Capacity

Organisation	Cap	Aim of research	Type of fuel	RFG mode	Other information	References
(present name Valmet Corporation), Finland	(CFB)	commercial technology			Metso and Fortum, with fundamental studies performed by Chalmers University, Sweden.	(2013); (2015)
CIRCE, University of Zaragoza, Spain	90 kW (BFB)	Fundamental studies, NOx, SO_2 emissions	Bituminous high-sulfur lignite			Lupiáñez *et al*.,(2011); (2013)
ICB-CSIC, Spain	3 kWth (BFB)	Fundamental studies, NOx, SO_2 emissions	Anthracite, Bituminous, Lignite			Obras-Loscertales *et al*., (2015) Diego *et al*., (2013)
Czestochowa University of Technology, Poland	0.1 MW (CFB)	General data, including (CO, NOx and SO_2)	Bituminous coal	N/A	Unit has also been used to support Foster Wheeler' program	Czakiert *et al*., (2006);(2010)
Southeast University, China	50 kW (CFB)	Combustion characteristics, NOx, SO_2 emissions,	US and Chinese bituminous coals,	Dry/Wet		Duan *et al*., (2011)

[m] N/A –Not available

Organisation	Cap	Aim of research	Type of fuel	RFG mode	Other information	References
			petroleum coke			
Institute of Engineering Thermophysics, Beijing	0.1 MWth -1 MWth (CFB)	Generation of fundamental data	Datong bituminous coal	Dry	Operation of unit was conducted at enriched O_2 concentration in the furnace (50%)	Li *et al*., (2015)
University of Stuttgart, Germany	0.15 MWth (CFB)	Solid burn out, CO, NOx emissions	El Cerrejon bituminous coal	N/A		Hofbauer *et al*., (2014)
CUIDEN, Foster Wheeler	30 MW CFB	First industrial scale flexi-burn CFB unit	Anthracite	N/A	Higher sulfur capture efficiency at 880-890 ºC; Small improvements in sulfur capture observed for Ca/S molar ratio higher than 2.6	Lupion *et al*., (2013); Gómez *et al*., (2014)

2.5 Background of SO_3 chemistry

2.5.1 Homogeneous SO_3 reactions

Past studies by Cullis and Mulcahy, (1972) and Jorgensen *et al*. (2007) noted that photochemical tests on the direct oxidation have been tried in the past to measure SO_3. This direct homogeneous oxidation of SO_2 can be represented by the global reaction:

$$SO_2 + O_2 \rightleftharpoons SO_3 + O \qquad + 161.9\,\mathrm{kJ/mol} \tag{4}$$

However, SO_3 formation via reaction (4) becomes significantly less important at temperature below than 900°C (Cullis and Mulcahy, 1972). While direct oxidation of SO_2 to SO_3 is rather limited, it can be produced in much larger amounts catalytically. In addition to that, two dominant reaction pathways are recognised for homogeneous SO_2 oxidation to SO_3. Here primary oxidation is the direct reaction of SO_2 with oxygen radicals that occurs at post-flame zones area of combustor where the temperature is higher than 900°C (Duan *et al*., 2015):

$$SO_2 + O\ (+M) \rightleftharpoons SO_3\ (+M) \tag{5}$$

Burdett *et al*. (1984) investigated the rate of direct oxidation reaction in the temperature range of 630 to 1080°C. These authors tested SO_3 formation in $O_2/N_2/SO_2$ flow and proposed following kinetic equation to predict homogeneous SO_3 (Burdett *et al*., 1984):

$$\frac{d[SO_3]}{dt} = \frac{k_1}{RT}[SO_2][O_2] = \frac{A[SO_2][O_2]}{RT} e^{(-B/T)} \qquad \text{Equation 2.3}$$

Where $k_1 = A\ exp(-B/T)$, $A = 2.6\ (\pm\ 1.3) * 10^{12}\ mol^{-1}\ cm^3\ s^{-1}$, $B = 23000 \pm 1200\ K$. $[SO_2]$,$[O_2]$ and $[SO_3]$ are partial pressures (kPa). More detailed data on kinetics of reactions 4 and 5 can be found elsewhere (Mulcahy *et al*., 1969);(Mulcahy *et al.,1966)*;(Yilmaz *et al*., 2006);(Merryman and Levy, 1979);(Naidoo *et al*., 2005). The second pathway occurs under moist condition, where oxidation of SO_2 is

enhanced in the presence of water vapour that increases via O/H radical concentration:

$$SO_2 + OH\,(+M) \rightleftharpoons HOSO_2(+M) \quad (6)$$

$$HOSO_2 + O_2 \rightleftharpoons SO_3 + HO_2 \quad (7)$$

It is reported that the first route is the main source of SO_3 at temperature higher than 900°C (Glarborg, 2007), while second route is believed to contribute to the SO_3 formation during the cooling of flue gases (Glarborg, 2007);(Jorgensen *et al*., 2007). Formation of SO_3 based on reactions (5) and (6) is thermodynamically favoured when exhaust gases undergoes the cooling process. While reaction (7) is found to be insignificant at temperature of 730°C and above in terms of producing SO_3 (Blitz *et al*., 2003).

The thermodynamic equilibrium curves of homogeneous SO_3/SO_2 conversion were plotted with an online calculator developed by Colorado State University,

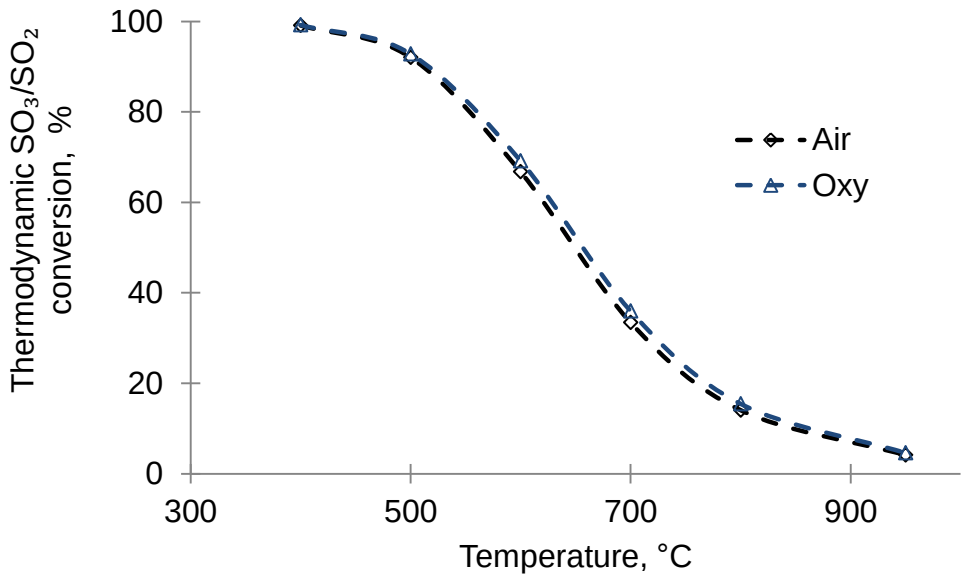

Figure 2-3 Thermodynamic equilibrium SO_3/SO_2 conversion

Air: SO_2-1000 ppm, O_2-4%, CO_2-15%, H_2O-6%, N_2-balance;

Oxy: SO_2-1000 ppm, O_2-5%, H_2O-11%, CO_2-balance;

(2016). Typical air and oxy-fired flue gas compositions were selected with SO_2 level of 1000 ppm both air and oxy flue gases, see Figure 2-3. O_2 and H_2O concentrations were changed from air to oxy, while diluted N_2 was replaced by CO_2 environment to evaluate SO_3/SO_2 conversion at the temperature ranges of 400 and 950°C. As noted in the literature, the formation of SO_3 is favoured at low temperatures and is significantly reduced at high temperatures. It can be seen from Figure 2-3 that the SO_3/SO_2 conversion was 100% at 400°C and 4.6% at 950°C. This equilibrium curves roughly agrees to the results presented by Belo *et al.* (2014). It is also interesting to point out that the change from air to oxy flue gas composition showed similar results at temperatures close to 400 and 950°C. It can be seen that homogeneous SO_3/SO_3 conversion of post-combustion environment for air and oxy provides a small difference with the temperature range of 500 to 800°C.

Early data from power plants have showed the effect of excess O_2 concentrations on the formation of SO_3, see Table 2-5. However, operation with a lower O_2 level lead to a significant reduction of SO_3.

Table 2-5 SO_3 formation at excess and low O_2 concentrations (Reid, 1971)

Power plants	O_2 level, %	SO_3 (ppm)	Dew point, (°C)
Marchwood	3.0	20	130-160
	0.5	2-7	116-124
Poole	4.0	45	160
	<0.6	5	82
Denes	1.7	N/a[n]	>130
	>1.7	N/a	130
Ince	4.5	18	N/a
	1.0	7	N/a

[n] N/a – Not available

2.5.2 Heterogeneous SO_3 reactions

There have been a number of investigations on the catalytic oxidation of SO_2 (Urbanek and Trela, 1980). Most of these experimental results indicated higher conversion of SO_2 to SO_3 were achieved via heterogeneous reactions (Marrier and Dibbst, 1974);(Zhang *et al*., 2006);(Tronconi *et al*., 1999);(Dunn *et al*., 1998) Catalytic conversion of SO_2 to SO_3 by fly ash was investigated in a bench scale reactor by Marier and Dibbs, (1974). They concluded that the conversion of SO_2 to SO_3 was strongly enhanced due to the iron oxide in the fly ash whereas the reverse effect was noted in the presence of unburnt carbon in the fly ash (Marrier and Dibbst, 1974). Similar and supporting results were produced by Zhang *et al*. (2006). The highest conversion of SO_2 to SO_3 was noticed at 700°C with residence time of 1.8 s and free carbon ash test in the work of (Zhang *et al*., 2006). Extended experiments on sulfation of SO_2 by CaO and MgO mixed with iron oxide indicated direct relation to the catalytic conversion SO_2 to SO_3 (Marrier and Dibbst, 1974). Efficient SO_2 capture from flue gases by CaO and MgO was due to the catalytic conversion of SO_2 to SO_3 in an oxidising condition. Similar work on the kinetics of SO_3 adsorption by calcium and magnesium oxides were provided by Thibault *et al*. (1982). These authors concluded that uptake rates are controlled by intergranular diffusion and independent of gross particle size. Also, the uptake rate was faster for MgO than CaO. However, a subsequent study suggested that this may be due to the difference of grain size and porosity (Thibault *et al*., 1982). A modelling approach called density functional theory was applied by Benjamin *et al*. (2015), to explore binding mechanisms of SO_3 to other metal compounds. CaO, MgO, Na_2O and K_2O minerals that are typically found in fly ashes included in the model. The authors observed that SO_3 binds strongly with alkali and alkaline metals, with the effect being more pronounced with alkali metals (i.e. Mg<Ca<Na<K) through the formation of a sulfate (SO_4^{2-}) (Benjamin *et al*., 2015). Cao *et al*., (2010) has outlined two main interaction of fly ash with SO_3 based on the temperature. First, fly ash could serve as SO_3 adsorbent under low temperature typical for the bottom section of the boilers. At temperatures lower than the dew point of SO_3, SO_3 is converted to H_2SO_4 mist droplets in the

presence of the water. Subsequently, these droplets condense on fly ash surfaces. The pore structure of the fly ash, which is associated with the carbon residue is responsible for condensation or adsorption of SO_3. The second interaction occurs at the temperature higher than 150°C, where SO_3 may react with multiple fly ash compounds such as metal oxides (CaO, MgO), alkali metal oxides (Na_2O, K_2O) and ammonia (NH_3). Chang *et al*., (1978) investigated an infrared adsorption of SO_2 on γ-Alumina (Al_2O_3 aluminium oxide) outlining two main factors: the number of hydroxyl groups and temperature of the catalyst. Infrared spectroscopy showed that SO_2 adsorbed on Al_2O_3 in the form of sulfite species SO_3. SO_2 also could be oxidised on Al_2O_3 to form aluminium sulfate. Vanadium catalyst contains a mixture of metal compounds of vanadium and alkali metal dispersed on a silica-based support. SO_2 to SO_3 oxidation by vanadia catalysts have been studied widely for SCR technology (Dunn *et al*., 1998). The formation of sulfur trioxide, sulfuric acid and sulfates were investigated by Walsh *et al*. (1972) for oil-fired boilers. As a result of this work, following illustration was developed for SO_3 formation, see Figure 2-4.

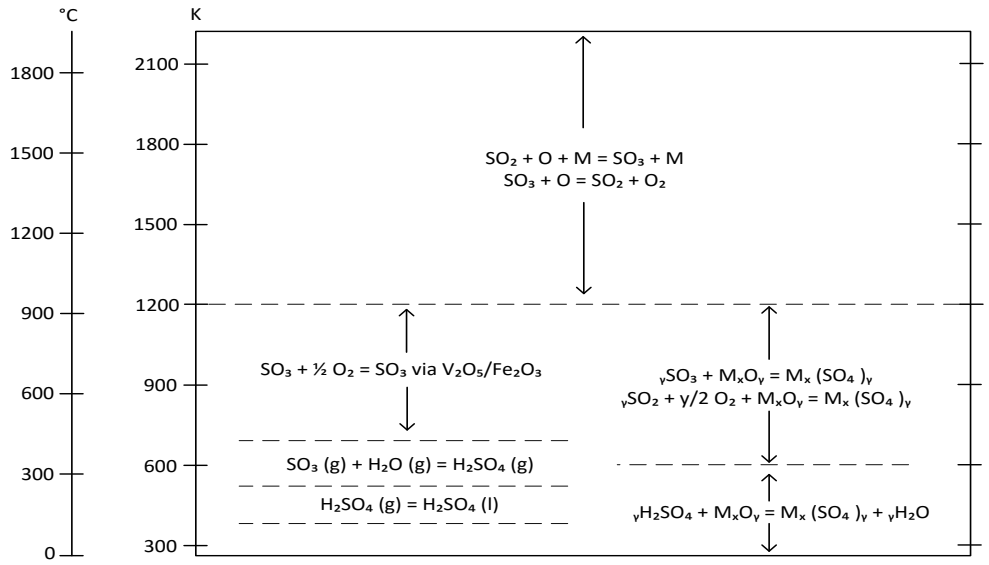

Figure 2-4 Process contributing to formation of sulfur trioxide, sulfuric acid, and sulfates in residual oil-fired boilers (Modified from Walsh *et al*., (1972))

2.6 SO_3 sampling methods

2.6.1 Controlled condensation method

The controlled-condensation method (CCM) is the most widely used method for SO_3 measurements (Jaworowski and Mack, 1979). The CCM method is often classified as British Standard BS 1756-4:1977 and American Standards D-3226-73T. The principle of the CCM method is based on the cooling down of extracting flue gas to the temperature which lies between the acid dew point and water dew point. SO_3 is condensed in the quartz filter as well as in glass walls of the sampling train as shown in Figure 2-5. As recommended by EPA standard, 30 minutes of sampling time are required with a flow rate of 10 L/min. After gas sampling, a known quantity of distilled deionised water is used to flush out the filter and condenser to collect the H_2SO_4. The accumulated H_2SO_4 concentrations are then determined by the titration method. Barium perchlorate (0.005M) solution is used as titrant to produce a quantitative colorimetric indication of the sulfur present in the sampling gas stream. As shown in Figure 2-5, the quartz filter is used to capture particulates before entering the

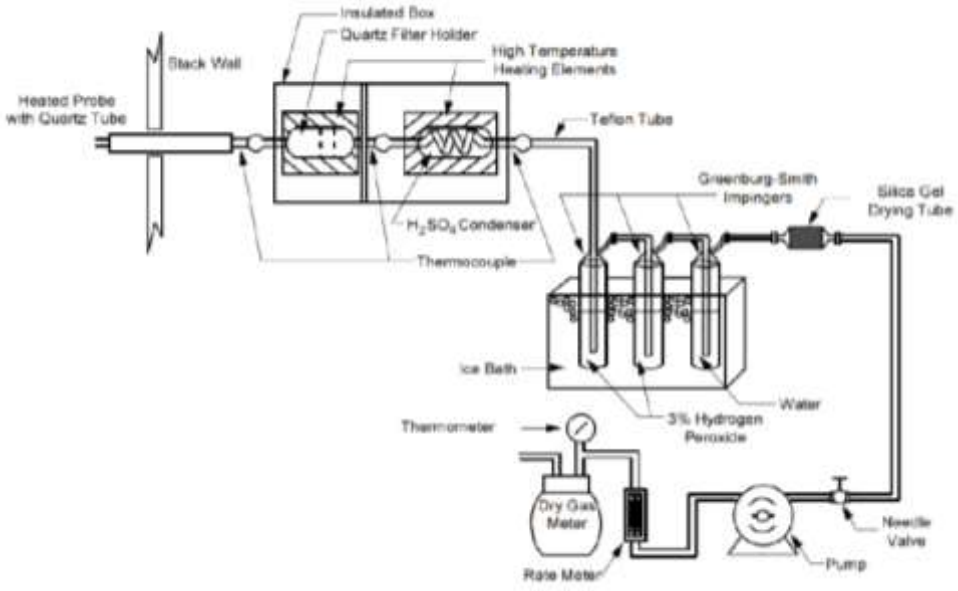

Figure 2-5 Modified Controlled condensation method SO_3 sampling scheme (NCASI Southern Regional Center 1996)

condenser impingers. The probe and quartz filter should be maintained at 260°C to avoid the formation of aerosol particles and sulfuric acid condensation (NCASI, 1996);(Maddalone *et al*., 1979).

The filtration of ash particles from the sampling gas is a crucial step for SO_3 measurements as the interaction of ash and SO_3 in the sampling train could lead to both positive and negative errors (Maddalone *et al*., 1979). The glass condenser should be maintained at the temperature of 80 to 90°C (Maddalone *et al*., 1979). It is concluded that the series run of CCM at laboratory scale was able to collect 95% of H_2SO_4 with the variation of ±6.7% (Maddalone *et al*., 1979). These authors extended experiments in the field and concluded that the accuracy of CCM method was less than indicated by results achieved at laboratory scale. The mechanism of CCM is well described by Dellinger *et al*. (1980). Sulfur dioxide is introduced into the water, where it can react with water and dissociation into bisulfate and sulphite ions (Dellinger *et al*., 1980):

$$SO_2 + H_2O \rightarrow SO_2 * H_2O \quad (8)$$

However, the oxidation of sulfur dioxide depends on the concentration of sulfite ion in the solution, which makes the reaction pH dependent, see Figure 2-6:

$$SO_2 + H_2O \rightarrow H^+ + HSO_3^- \quad (9)$$

$$HSO_3^- \rightarrow H^+ + SO_3^{2-} \quad (10)$$

$$SO_3^{2-} + ½\, O_2 \rightarrow SO_4^{2-} \quad (11)$$

Figure 2-6 illustrates the calculated mole fraction of sulfur species as a function of pH at 25°C in aqueous solution. It can be seen that sulfites dominate in alkaline solution while bisulfite predominates in the pH range of 3-7 (Dellinger *et al*., 1980). It is commonly accepted that at normal sampling condition, the impinger solution must be slightly acidic, thus preventing sulfite formation and subsequent oxidation (Dellinger *et al*., 1980). Therefore, purging of impingers with the air is recommended by EPA standard to remove SO_2.

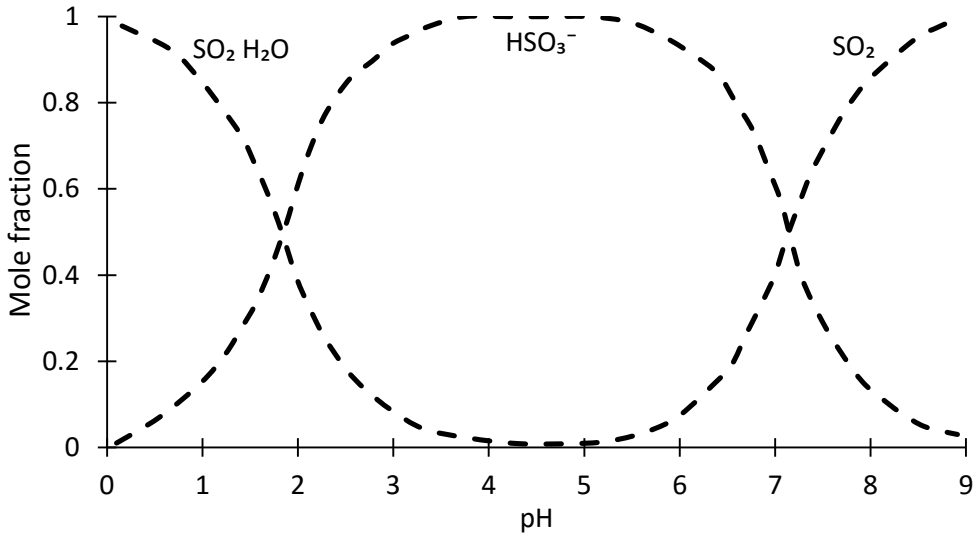

Figure 2-6 Effect of pH on the relative concentrations of the SO_2 species in solution (Dellinger *et al*., 1980)

2.6.2 Isopropanol absorption bottle method

This method is based on EPA Method 8A with some modifications. The schematic illustration of the isopropanol absorption method is shown in Figure 2-7. The iso-kinetically extracted flue gas is first cooled down as in the CCM by a glass condenser and passed through four bottles. As shown in Figure 2-7, all bottles are kept in the ice bath vessel. The first bottle is filled with 10 ml of 80% isopropanol solution diluted in the water. Following two bottles are filled with 3% hydrogen peroxide solution. The fourth bottle is used to capture moisture content of the flue gas with silica gel. According to Cooper, (1995), most common error occuring during the sampling of SO_3 in this method

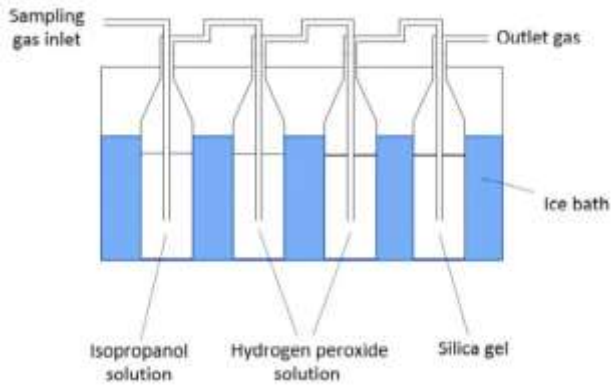

Figure 2-7 Isopropanol bottle method SO_3 measurements

was the absorption and oxidation of SO_2. Similar limitations were mentioned by Fleig *et al*. (2012), where large amount of SO_2 were absorbed in the isoproponol solution and resulted in positive bias.

2.6.3 Salt and glass bead methods

The first description of salt method was provided by Kelman *et al.* (1952) in the early 1950s and this was later applied to industrial plant for SO_3 measurements by Cooper *et al*. (1995). The advantages of this method as highlighted by the authors were: 1) no interferences from SO_2, which is occasionally encountered in the isopropanol bottle method; 2) simplicity to conduct sampling. Flue gas containing SO_2 and SO_3 passes through the dry layer of sodium chloride (NaCl). As a result, sulfur trioxide reacts with sodium chloride (Kelman *et al*., 1952). This method was applied to detect SO_3 concentration in 100 kW rig at Chalmers University (Vainio *et al*., 2013). Schematic view of the salt method is shown in Figure 2-8, where salt is fixed in the tube with glass wool (Cooper *et al*., 1994);(Cooper, 1995). With decrease of the flue gas temperature to approximately 500ºC, SO_3 starts to react with water vapour to form gaseous sulfuric acid (H_2SO_4) (Fleig *et al*., 2012);(Vainio *et al*., 2013).

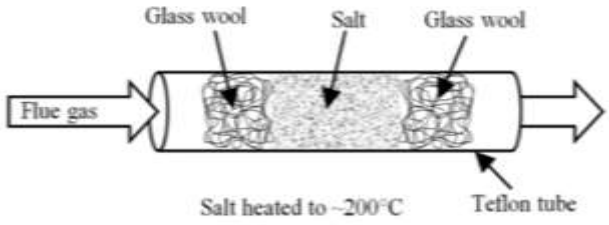

Figure 2-8 Salt tube preparation

(Vainio *et al*. 2013)

$$SO_3(g) + H_2O(g) \rightarrow H_2SO_4(g) \quad (12)$$

Further H_2SO_4 reacts with sodium chloride (NaCl) to form sodium sulfate (Na_2SO_4) and sodium bisulfate ($NaHSO_4$) (Vainio *et al*., 2013). Reactions occurring during the salt method are given as:

$$NaCl(s) + H_2SO_4(g) \rightarrow NaHSO_4(s) + HCl\,(g) \quad (13)$$

$$2NaCl\,(s) + H_2SO_4(g) \rightarrow Na_2SO_4\,(s) + 2HCl\,(g) \quad (14)$$

$$NaHSO_4(s) + NaCl\,(s) \rightarrow Na_2SO_4(s) + HCl\,(g) \quad (15)$$

$$4NaCl\,(s) + 2SO_2(g) + 2H_2O\,(g) + O_2(g) \rightarrow 2Na_2SO_4(s) + 4HCl\,(g) \quad (16)$$

The last reaction is undesirable as it leads to a positive measurement bias (Fleig *et al*., 2012). Sulfation of NaCl is a slow reaction and mainly depends on temperature and SO_2 concentration. Cooper, (1995) concluded that this method could be improved further. Later, this method were extended by Vainio *et al*. (2013), by testing other types of salts (KCl, K_2CO_3, and $CaCl_2$) along with (NaCl). However, the authors concluded that tests with NaCl and KCl showed comparable results to the CCM.

2.6.4 Indirect measurements of SO_3

An indirect measurement is another available method to speed up the analysis part of SO_3 (Ibanez *et al*., 2008). Here, a different method for assaying SO_3 concentrations in the flue gas has been described by Ibanez *et al*. (2008) who proposed using a calcium oxalate:

$$SO_3 + CaC_2O_4 \rightarrow CaSO_4 + CO_2 + CO \quad (17)$$

This method is also dependent on precise temperature control and the reaction vessel should be maintained at 325°C. A mixture of gas is passed through a plug of prepared CaC_2O_4 then through two optical cells in series, see Figure 2-9. The SO_2 (g) content in sampling gas is monitored by means of a UV spectrometry, while the SO_3 concentration in the gas is quantified indirectly with CO_2 in second cell IR spectrometry. These authors note that the preparation of reagent and calibration should be done very carefully to produce reliable results. A similar approach has been developed by Fateev and Clausen, (2011). However, only preliminary results have been provided by them Fateev and Clausen, (2011).

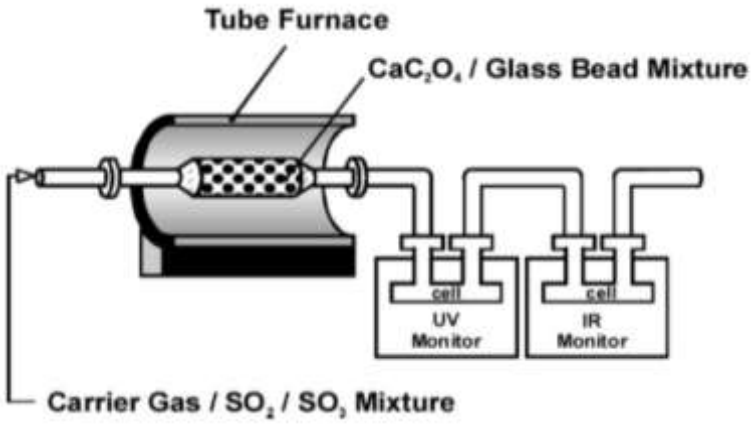

Figure 2-9 Arrangement SO_3 measurements by CaC_2O_4 (Ibanez *et al*., 2008)

The option of continuous SO_3 measurements by Fourier transform infrared (FTIR) and differential optical absorption spectroscopy (DOAS) instruments were described by EPRI, (2004). Subsequently a modified cross duct probe design has been developed to improve SO_3 measurements by FTIR. The results of 3 days of continuous measurements with FTIR was compared with CCM method and the total H_2SO_4 and SO_3 were measured were in good agreement, however variation of SO_3 across probes were 10% (Himes, 2006). An indirect test of SO_3 with FTIR has also been attempted by measuring hydrogen chloride (HCl) from reaction of NaCl and H_2SO_4. It is highlighted that for the consistent measurement of SO_3, the exit gas temperature should be kept between 200-400°C. However, at the temperature of 200°C, only about one-half of SO_3 was converted to HCl (Vainio et al., 2013). Chamberlain et al. (2013) has also attempted to measure SO_3 concentrations with FTIR under pulverised air and oxy-coal combustion tests. However the uncertainty of measurement was ±20 ppm in absolute values. Given this range of uncertainty, the authors could not determine any difference of SO_3 concentrations between air and oxy-fuel combustion. It should be noted here that an indirect measurement concept will have difficulties in achieving high accuracy and repeatability. Therefore, both of these methods still need to be improved before they can be used in practice. Furthermore, in the case of CaC_2O_4 technique, it is unclear how to SO_3 could be

quantified in CO_2 rich environment. Roy *et al*. (2014) has carried out such tests a lab scale oxy-fuel experiments. However, these authors did not comment on the consistency of this method and how other combustion parameters could affect on the final results. For that reason, supplementary research is required.

2.6.5 Pentol SO_3 monitor

Previously this device was called the Severn Science reactive gas analyser (Jackson *et al*., 1981). The initial description of this continuous measurement method was given by Jackson et al. (1981). The principle of this instrument is that SO_3 and H_2SO_4 in the gas sample are absorbed as (SO_4^{2-}) in an aqueous solution of isopropanol solution diluted in water. During the sampling, the solution is continuously passed through a bed of barium chloranilate where the following reaction occurs:

$$SO_4^{2-} + BaC_6O_4Cl_2 + H^+ \rightarrow BaSO_4 + HC_6O_4Cl_2^- \quad (18)$$

The released acid chloranilate ions absorb at 535 nm[o], producing a purple-coloured solution, and the concentration of this chemical is continuously measured by flow photometer. More sulfate in the solution means a higher the absorption level. The amount of sulfate in the solution is proportional to the SO_3 concentration entering the analyser (SO_3 Monitor brochure). According to the Dennis and Hayhurst, (1988), this instrument was slow to achieve steady state performance and required moisture in fluidisation gases to ensure reliable readings. Cooper, (1995) has applied Severn Science gas analyser at an Orimulsion power plant, where the average results were 25% higher than the CCM approach. The authors have discussed a possible reasons such as absorption of SO_2 in the isopropanol and partial oxidation of SO_3^{2-} to SO_4^{2-}. These were confirmed by noting peaks for SO_3^{2-} and SO_4^{2-} by ion chromatograph analysis (Cooper, 1995). However, the latest study made by Fleig *et al*. (2012) concluded its reliability for longer continuous measurements. However, the average readings were still less than 20% compared to CCM (Fleig *et al*.,

[o] Nm – nanometres

(2012). It is clear from the discussion above that there are still many limitations related to accuracy of SO_3 measurements which need to be resolved.

2.6.6 Acid dew point measurements

The sulfuric acid dew point (ADP) temperature is one of the conventional ways to estimate the amount of SO_3 and H_2O present in the flue gases. Taylor (Taylor, 1951) has concluded that the condensation of sulfuric acid is a function of surface temperature of sampling tube and water vapour content in the flue gases. Previous measurements of acid dew points were conducted by using a cooled electrical conductivity probe to determine the temperature where condensation occurs (Stuart, 2010). The probe has two electrodes and thermocouple attached in the probe. By measuring the temperature of the probe, the dew point is determined by a sudden increase in the conductivity between electrodes on the surfaces due to the condensed liquid sulfuric solution. Currently, a series of advanced portable devices are available in market (Lancom 200) to measure ADP temperature of the flue gases (Stuart, 2010). The ADP temperature changes with the moisture content of the flue gases, which is particularly important for oxy-fuel combustion environment.

Table 2-6 Sulfuric acid dew-point (ADP) correlations: (Verhoff and Banchero, 1974);(ZareNezhad, 2009);

Authors	Correlations	
Verhoff and Banchero	$\frac{1}{T_{Dew}+273.15} = 0.002276 - 0.00002943\ln p_{H_2O} - 0.0000858\ln p_{H_2SO_4} + 0.00000620(\ln p_{H_2SO_4})(\ln p_{H_2O})$	Equation 2.3
Okkes	$T_{Dew} = 203.25 + 27.6\log p_{H_2O} + 10.86\log p_{SO_3} + 1.06(\log p_{SO_3} + 8)^{2.19}$	Equation 2.4
ZareNezhad	$T_{Dew} = 150 + 11.664\ln(p_{SO_3}) + 8.1328\ln(p_{H_2O}) - 0.383226\ln(p_{SO_3})\ln(p_{H_2O})$	Equation 2.5

Available correlations to estimate the ADP temperature are illustrated in **Error! Reference source not found.**. According to Verhoff and Banchero, (1974), two methods have been developed to define the vapour and liquid equilibrium for aqueous sulfuric acid solutions. First method was determined by measuring the vapour-liquid compositions and temperature at the equilibrium. However, the second method takes into account liquid and pure components to estimate the equilibrium vapour and liquid compositions via thermodynamics. Based on these two methods, Verhoff and Banchero, (1974) have proposed a correlation to predict the dew point temperature of sulfuric acid. More recently, ZareNezhad has proposed a new correlation to predict the flue gas sulfuric acid (ZareNezhad, 2009). Based on these correlations, Stanger et al. (2011) has compared both correlations for flue gas composition derived from oxy-fuel combustion. The authors have concluded that Verhoff and Banchero method over-predicts experimental dew points at low SO_3 concentrations and high moisture content. However, the Okkes' correlation has been found to be better suited for flue gases with moisture content higher than 25% (Stanger *et al*., 2011).

2.6.7 Summary of SO_3 sampling methods

Following subsection provides a comparative information for all described SO_3 sampling methods by highlighting its advantages and disadvantages, see Table 2-7. It can be noted that the controlled condensation method is found to be the most reliable method to measure SO_3 concentration of flue gases. In addition to that, CCM method typically used as a reference case to the rest available methods noted in this section. Salt method is also suitable for SO_3 measurements, however still requires an alternative data for validation. Pentol SO_3 monitor provides a reasonable data along with CCM method and suitable for longer period. In addition, it should be highlighted that all described methods require a specific skills for the operator to measure SO_3.

Table 2-7 Advantages and disadvantages of SO_3 methods

SO_3 techniques	Advantages	Disadvantages
Controlled condensation method	High accuracy within a reasonable range; used mainly as reference method;	Temperature control of flue gas, time for post processing if manual titration is selected;
Isopropanol absorption bottle method	Not available	SO_2 is absorbed and oxidises by isopropanol by leading to a positive bias;
Salt and glass bead methods	Easy to handle; less expensive to manufacture; suitable for measurements	Needs to be cross-checked with CCM;
Indirect measurements of SO_3	Expenses can be avoided to manufacture SO_3 sampling train;	Not reliable; requires to keep flue gas temperature between 300 and 400°C;
Pentol SO_3 monitor	Complete and portable gas analyser; suitable for long continuous measurements;	Requires very careful precaution. Has a difference in contrast to CCM.
Acid dew point measurements	Provides better results close to dew-point temperature of the flue gas only;	Provides only a rough estimation of SO_3 or H_2SO_4; found sensitive to the change of the acid dew-point temperature

2.7 Influence of oxy-fuel combustion on SO_3 formation

2.7.1 O_2/CO_2 environment

SO_3 concentrations under O_2/CO_2 environment are several times higher than in a typical air combustion environment due to FGR and higher concentrations of O_2 in combustion process (Croiset and Thambimuthu, 2001);(Ahn *et al*., 2011). Higher SO_3 and SO_2 concentrations along with wet RFG will produce a higher ADP temperature. As a result, this could lead to serious corrosion risks in the

boilers as noted in section 1.3. At the bench scale level, the formation of SO_3 in O_2/CO_2 environment was investigated by several researchers (Fleig *et al*. 2013);(Fleig *et al*. 2011);(Spörl *et al*. 2014);(Belo *et al*. 2014). According to these authors, an enriched O_2 concentration in oxy-fuel combustion contributes to the higher SO_3 formation. (Belo et al. 2014) has observed that higher O_2 concentrations between 3%, 5% and 10% resulted in SO_2 oxidation of the level of 3-10%. These results agree well with the equilibrium calculation of Zheng and Furimsky, (2003). At higher temperatures, Fleig *et al*. (2011);(2013) concluded that the replacing N_2 by CO_2 had a strong effect. This might be due to higher effectiveness of third-body collisions. At lower temperatures, CO_2 found thermally more stable and the third-body efficiency of CO_2 expected to be low. Fleig *et al*. (2013) has noted that an increase of SO_3 formation in the CO_2 environment was more pronounced, reaching values 30% higher value than in the N_2. A sensitivity analysis at 1027°C indicated that SO_3 was enhanced due to the increase of radical production in the CO_2 atmosphere than in N_2 as indicated below:

$$HO_2\ (+M)\ \rightleftharpoons\ H + O_2\ (+M) \tag{19}$$

$$H + O_2 \rightleftharpoons\ O + OH \tag{20}$$

The formation of H radicals is increased via reaction (19) which reacts with O_2 to form OH radicals, reaction (20). The hydroperoxyl radicals (HO_2) are formed via its decompositions in reaction (7). In addition, the RFG which increases the level of impurities such as NOx, SO_2 and CO are also believed to enhance the SO_3 formation to some extent. The effect of impurities on SO_3 formation during the oxy-fuel described below.

2.7.2 Effect of NO_x emissions

NO_x emissions from combustion may have catalytic effect on SO_2/SO_3 conversion ratio even at low temperatures (Cullis and Mulcahy, 1972);(Armitage and Cullis, 1971);(Wendt and Sternling, 1973). The effect of nitrogen oxides can occur either through direct or through indirect route by interaction with the

radical pool composition (Glarborg, 2007). At low temperatures, the oxidation of SO_2 may react directly with NO_2 to promote SO_3 as (Armitage and Cullis, 1971):

$$NO + NO + O_2 \rightleftharpoons NO_2 + NO_2 \quad (21)$$

$$NO_2 + SO_2 \rightleftharpoons NO + SO_3 \quad (22)$$

According to Wendt and Sternling, (1973) at high concentrations of NO, the SO_2 oxidation was second order in NO and had low activation energy. However, at low concentrations of NO, the SO_2 oxidation found as first-order in NO with high activation energy. At low concentrations of NO, the reaction (21) is slow, and the SO_2 oxidation could follow the following reactions routes (Wendt and Sternling, 1973):

$$NO + O_2 \rightleftharpoons NO_3 \quad (23)$$

$$NO_3 + SO_2 \rightleftharpoons SO_3 + NO_2 \quad (24)$$

In addition to the direct SO_2 oxidation, during the cooling NO may increase SO_3 indirectly by converting HO_2 in reactions (6) and (7) back to OH radicals as (Glarborg, 2007):

$$NO + HO_2 \rightleftharpoons NO_2 + OH \quad (25)$$

This has been noted by Fleig *et al*. (2011) when small amount of NO (100 ppm) favoured the formation of SO_3. These authors also noted an increase of SO_3 when more OH radicals were available through reaction (25) at the temperature higher than 1027°C. As a result, higher SO_3 concentrations were formed through reactions (6) and (7) (Fleig *et al*., 2011). These authors also highlighted notable increase of SO_3 in the presence of around 50 ppm NO concentrations in oxy-fuel environment compare to air. According to the authors, this might be due to the difference of reaction rate (26):

$$H + O_2(+M) \rightleftharpoons HO_2(+M) \quad (26)$$

According to the previous study of Glarborg, (2007), the rate of reaction (26) is higher for the CO_2 diluted environment than in N_2 which favours the HO_2 formation and could reduce SO_3 to SO_2 by the reaction (-7)[p] and followed by (-6). An excess formation of OH via reaction (25), promotes secondary formation of SO_3 via reactions (6) and (7). This effect was more pronounced in CO_2 environment (Fleig *et al*., 2011). Only limited information is mentioned about the third-body effect. In the extended numerical work of Fleig *et al*, (2011), a higher value of third-body coefficient of 2.5 for CO_2 (instead of 1.0) resulted in negligible reduction of SO_3 by 2% only. This still was higher than in air case. Thus, as noted by Wendt and Sternling, (1973), the impact of SO_2 oxidation by nitrogen oxide during the cooling is likely to be small and that the effect of NO could be assumed negligible in oxy-fuel combustion.

2.7.3 Effect of CO concentrations

Previous studies have shown that the CO concentration under oxy-fuel conditions is higher than in the air combustion environment (Zheng and Furimsky, 2003);(Kühnemuth et al., 2014). The higher O_2 concentration in the primary gas corresponds to the higher flame temperature. As a result, this enhances the formation of CO significantly (Seddighi *et al*., 2013). It has also been noticed that most CO formation occurs in near or close to the burner region (Seddighi *et al*., 2013);(Glarborg and Bentzen, 2007). Under CO_2 rich environment the thermal dissociation of CO_2 could also contribute to a higher CO concentration due to the dissociation reaction (Glarborg and Bentzen, 2007):

$$\mathrm{CO_2\ (+M)} \rightleftharpoons \mathrm{CO + O\ (+M)} \qquad (27)$$

However, this reaction only likely to occur only at temperatures significantly higher than 930°C (Glarborg and Bentzen, 2007). The presence of CO_2 can compete with O_2 for the atomic hydrogen, and will lead to the formation of CO as (Kühnemuth *et al*., 2014);(Glarborg and Bentzen, 2007):

[p] (-) reverse reaction

$$CO_2 + H \rightleftharpoons CO + OH \quad (28)$$

Simultaneously, during the formation of high CO concentrations in the flame zone, the recombination of CO with OH can take place Merryman and Levy, (1979) and this will increase the formation of H radicals (28):

$$CO + OH \rightleftharpoons CO_2 + H \quad (29)$$

Consequently, this will compete with reaction (6) for OH radicals and reduce the formation of SO_3 as noticed in the experiments of Wang *et al*. (2015) and Fleig *et al*. (2013). It is worth mentioning that an early experiment from the staged combustion of CH_4/H_2S/air mixture environment showed clear enhanced SO_3 formation in the presence of 1100 ppm of CO (Merryman and Levy, 1979). The maximum SO_2 oxidation took place at flame temperatures between 1300 and 1650°C for single and staged combustion. Slightly narrow temperature range of 1100 to 1300°C was observed for the test with secondary air supply. These authors postulated that the maximum SO_3 formation was only a transient phenomenon. It is highlighted that the SO_3 concentration changes as the reactions continue in the downstream gas. In addition, there was no enhancement of SO_3 at the residence time beyond about 0.09 s. These authors believe that enhanced SO_3 behaviour was dependent on air/fuel ratio of the each combustion stage and the delay interval between first and second stages (Merryman and Levy, 1979). An similar conclusion was drawn by Bayless *et al*. (2000). Based on the experimental work of Fleig *et al*. (2013), an addition of 1000 ppm CO into the system increased the SO_3 formation significantly compared to the test without a CO addition. The measured SO_3 concentrations were three times higher at a temperature of 927°C with 3% of O_2, while the this difference was smaller at 1200°C. However, further increase of CO to 3000 ppm showed only a small difference compare to the 1000 ppm added CO. In summary, it appears that the maximum SO_3 formation in the presence of CO, takes place at temperatures between 827 and 1027°C. Whereas, less formation of SO_3 at temperatures higher than 1127°C was noted by Fleig *et al*. (2013). This indicates that formation of SO_3 is affected significantly by the temperature

where burn out of the fuel takes place. In general, these results agree well with the earlier study of Merryman and Levy, (1979).

2.7.4 Effect of steam

The RFG in oxy-fuel combustion can increase the water vapour level up to 25-35% in the combustion furnace (Hecht *et al*., 2012). This increase of H_2O content in the combustion may promote an increase of the secondary SO_3 formation route via $HOSO_2$, see reactions (6) and (7). In the homogeneous test made by Fleig *et al*. (2013), a more pronounced effect of water on SO_3 was noticed at the temperatures between 1130 and 1200°C. In the presence of steam, OH radical can be formed by the reaction of H_2O with O radical (Yilmaz *et al*., 2006):

$$H_2O + O \rightleftharpoons OH + OH \quad (30)$$

and simultaneously by the decomposition steam as noted by Wine *et al*., (1984):

$$H_2O \rightleftharpoons OH + H \quad (31)$$

As seen, the decomposition of HO_2 and higher OH release through reaction (19) and (20) concentrations shifts reaction (31) to the right side to enhance SO_3 formation. This in principle could favour to an increase of SO_3 formation via reactions (5) and (6). In addition to that the third-body efficiency of H_2O is found to be higher than the CO_2 and N_2 (Fleig *et al*., 2013). Fleig *et al*., (2013) has also pointed out that increase of H_2O from 0.1% to 1.1% and 8.7% produces higher SO_3 concentrations at temperatures between 927 and 1127°C. At 1174°C and 8.7% of H_2O, highest SO_3 concentration was reached of around 23 ppm. However, in the tests with presence of combustibles, the inhibiting effect of steam in SO_3 formation was observed (Fleig *et al*., 2013). This observation agrees well with the previous conclusion of Glarborg *et al*. (1996). In contrast to that, a less pronounced effect of H_2O on SO_3 was noted by Belo *et al*. (2014).
The effect of steam on SO_3 was also investigated recently by Wang *et al*. (2015). In their work, higher concentrations of steam from 15 to 35% were

provided to simulate wet RFG. The authors reported that SO_3 concentration was decreased with increase of steam content in homogeneous tests. Wang *et al*., (2015) have claimed that lower formation of SO_3 was due to the inhibiting effect of steam. In oxy-fuel combustion tests, further increase of H_2O to 35% produced a stronger inhibiting effect on SO_3 formation. This is consistent with the result of by Fleig *et al*. (2013) obtained in the presence of fuel combustion. The various inconsistencies between Wang *et al*. (2015) and other studies may be explained by the fact that there is a complex set of reactions occurring in the homogeneous and heterogeneous environments due to the high water content. The inhibiting effect of H_2O in homogeneous cases can affect SO_3 consumption reactions as a result of reactions (4), (20) and (31), followed by:

$$SO_3 + H \rightleftharpoons SO_2 + OH \quad (32)$$

$$SO_3 + O \rightleftharpoons SO_2 + O_2 \quad (33)$$

$$SO_3 + OH \rightleftharpoons SO_2 + H_2O \quad (34)$$

According to Hindiyarti *et al*. (2007) and Glarborg *et al*. (1996), major consumption of SO_3 in combustion could be due to reaction (32) and (33). They claimed that the rate constant for reaction (32) is several magnitudes higher than that of reaction (5) at a similar temperature. In addition, H_2O concentrations were higher than SO_2 concentrations in their experiments. Under this condition, steam was more likely to compete for O radical. As a result, O-radical form OH radicals resulting in lower SO_3 formation through reaction (5).

2.7.5 Temperature and residence time

Flint and Lindsay, (1951) and Burdett *et al.* (1984), carried out pioneering investigations on the oxidation of SO_2 in quartz tube reactors. In both tests an there was increasing homogeneous SO_3 formation with increasing temperature and residence time, see Table 2-8. Later, a similar approach was carried out using an air environment by Belo *et al.* (2014). As shown in Table 2-8, the homogeneous conversion ratio increased from 0.04% to 0.77% by increasing

temperature from 400ºC to 1000ºC. In their test, a significant increase of conversion of SO_2 to SO_3 was noted when the reaction temperature exceeded 700ºC. Nevertheless, temperatures higher than 900ºC were required to see significant conversion for the residence time in their study of 1 s (Belo *et al*. 2014). At this residence time, the maximum conversion was 0.36%. This agrees well with the previous results of Flint and Lindsay, (1951) and Burdett *et al*. (1984).

It is well known that at a lower temperature range, SO_3 is formed by oxidation of molecular oxidation via the reaction (6) and (7) and that SO_3 formation is thermodynamically favoured with decreasing temperature. However, the reaction rate is very slow and such systems cannot reach equilibrium at a short residence time. Fleig *et al*., (2013) have carried out experimental work on homogeneous SO_3 formation over a much wider temperature range, see Table 2-8. These authors concluded that SO_3 formation was less than 1 ppm under the temperature <727°C. Lower level of SO_3 seen in their work was due to the short residence time, as noted by Flint and Lindsay, (1951) and the low level of H_2O (1.11%) in their work.

Table 2-8 List of homogeneous SO_3 studies conducted in quartz tube flow reactors

Authors	Sizes, mm (d x l)	Temp (ºC)	Inlet gas condition	Flow rate, (L/min)	Residence time, (s)	Max temp, (ºC)	$SO_3/(SO_2+SO_3)$) (%)
Barret *et al.,* (1966)	25.4 x 610	1030-1530	Air + 0.7% SO_2	3.4	5.5-5.7	1530	0.2
Flint and Lindsay, (1951)	14 x 1829	500-900	Air (+ H_2O-8%), SO_2(1400 ppm)	1.7-8.5	0.9-9.6	900	0.36 - 4.8
Burdett *et al*., (1984)	10 x 450	850-1066	SO_2(0-5500 ppm); O_2 (0-21%); bal-N_2/	0.5-5	Up to 6	960	0.36
Belo *et al*., (2014)	12 x 250	400-1000	Gas mixture (SO_2-1000 ppm, H_2O-3%, O_2-5%, bal-N_2)	0.5-1.5	0.3-0.9	1000	0.14 – 0.77
Fleig *et al*., (2013)	50 x 900	527-1400	SO_2-1000 ppm, O_2-3%, H_2O-1.1%, bal-N_2/CO_2,	1.0	Up to 5	1400	0.1-1.7
Wang *et al*., (2015)	50 x 1500	350-1050	O_2-5%, SO_2 –500, 1500, 2500 ppm, H_2O-0.03%, bal-CO_2,	2.0	N/S[q]	950	500[r]-0.11 1500-0.16 2500-0.21

[q] Not specified (N/S). Based on size of tube and flow rate, calculation shows long residence time for this work
[r] 500, 1000 and 2500 means tests with SO_2 concentration

2.7.6 Effect of fly ash

As noted in section 3.2, the fly ash components are potentially important for SO_3 formation. It has been reported that metal oxides as Fe_2O_3, Al_2O_3 and CuO could serve as a catalyst for SO_2 oxidation, while some alkali and earth metal oxides as MgO, CaO can adsorb SO_3 (Marrier and Dibbst, 1974). The catalytic effect of fly ash on SO_3 formation in oxy condition was investigated by Belo *et al*. (2014), who reported the following conclusions: 1) the total conversion of SO_2 to SO_3 under heterogeneous test 1.8% 2) the effect of Fe_2O_3 on SO_2 to SO_3 conversion was more pronounced compare to other ash components at constant 1000 ppm of SO_2 concentration; 3) fly ashes derived from air and oxy-fuel modes showed no significant difference in conversion ratio under constant SO_2 concentration, N_2 and CO_2 atmospheres demonstrated no significant effect on the heterogeneous conversion of SO_2 to SO_3. SO_3 concentrations increased to 17.84 ppm at 700°C in the presence of ash test, while 0.98 ppm of SO3 was observed in the homogeneous test (Belo *et al*., 2014). Although, the general trend of SO_2 to SO_3 conversion is consistent with past studies of Marier and Dibbst, (1974), a stronger catalytic effect at temperatures of 400 and 500°C was noted by Duan *et al*. (2015) compare to the tests of Belo *et al.* (2014). However at 700°C, the catalytic effect in the tests of Belo *et al.* (2014) was more pronounced. Higher concentration of CaO tends to react with SO_2. A similar result was noted in the pilot-scale tests of Ahn *et al.* (2011), when PRB coal was utilised, which has a CaO content in the ash of 22.2%. SO_3 formation from burning PRB coal was lowest comparatively to Utah and Illinois coals. By contrast, an enhanced of SO_3 formation observed for the Illinois coal, which has significantly less CaO content (1.9%) in the ash and a high content of sulfur, as shown in Table 2-9 and Table 2-10.

Based on the available information, it may be concluded that a pronounced catalytic effect were observed in bench scale tests rather than the pilot-scale tests. However, large scale units could perform differently due to the differences in heat transfer rates in a large boiler, inconsistency in fuel composition and loading requirements. Interestingly, the effect of Fe was not observed in the

presence of combustibles at pilot-scale test of IFK (Spörl *et al*., 2014). For this reason, detailed experiments with a wide range of coals are still required under oxy-fuel combustion condition to evaluate the degree of catalytic oxidation and absorption by fly ash in laboratory experiments.

Table 2-9 A list of XRF analysis of fly ashes during the SO_3 studies

	Solid Fuel	SiO_2	Al_2O_3	Fe_2O_3	CaO	MgO	Na_2O	K_2O	TiO_2	P_2O_5	SO_3
Belo *et al*., (2014)	A	52.9	34	7.13	1.41	0.98	0.16	0.52	2.16	0.28	0.24
	B	69	24.2	2.16	0.87	0.74	0.28	0.60	1.65	0.18	0.28
	C	53	26.5	8.34	4.66	1.67	0.98	1.06	1.13	1.51	0.97
Sporl *et al*., (2014)	A	58.9	26.2	6.8	1.2	0.7	0.1	0.4	2.4	0.2	0.3
	B	64.4	21.5	1.2	0.4	0.7	02	0.4	3.9	0.0	7.2
	C	33.2	23.0	11.4	7.0	1.8	1.3	0.9	1.2	1.8	22.7
Couling *et al*., (2011)	Williamson coal	50	20.5	15.9	5.18	1.14	0.68	2.41	1.05	0.1	4.78
Ahn *et al.,* (2011)	PRB coal	30.46	14.78	5.20	22.19	5.17	1.94	0.35	1.30	1.07	8.83
	Utah coal	60.89	14.52	5.09	6.11	1.39	1.41	0.57	0.88	0.59	2.33
	Illinois coal	49.28	17.66	14.57	1.87	0.98	1.51	2.26	0.85	0.11	2.22
Kenney *et al*., (2011)	Sub-Bit coal	34.56	16.05	6.16	19.79	4.23	1.24	0.50	1.29	0.81	11.67
	Low-S Bit coal	56.30	30.78	5.58	0.84	0.82	0.23	2.67	1.78	0.15	0.71
	High-S Bit coal	50.85	20.53	15.56	3.52	0.96	1.02	2.11	0.94	0.52	2.81
	Lignite	41.99	13.96	6.47	14.84	4.50	1.56	1.93	0.54	0.18	11.99
Duan *et al*., (2015)	Bituminous coal	45.12	34.14	4.16	8.66	1.36	0.46	0.99	1.53	0.09	3.06
	Bituminous coal	37.84	18.52	10.37	19.99	4.51	2.55	0.37	1.09	1.09	3.07
Wang *et al*., (2015)	Lignite	64.39	18.04	3.42	4.68	1.27	0.90	0.93	0.48	0.95	4.69
	Bituminous coal	48.82	29.81	3.99	4.57	1.12	1.12	1.17	0.64	0.26	8.23
Jurado *et al*., (2014)	Cerrejon coal	60.69	22.01	7.43	2.27	2.90	1.06	2.32	0.92	0.21	
	CCP-biomass	44.36	2.49	2.47	7.78	3.96	0.36	24.72	0.12	12.04	

2.7.7 Pilot-scale so_3 measurements

At the pilot-scale, Ahn *et al.* (2011) studied sulfur trioxide formation extensively in a 1.5 MW oxy-PC and a 330 kW oxy-CFB combustor units. Three types of US coal were tested (PRB, Utah and Illinous) in their SO_3 test campaign. The sulfur content of these coals is provided in Table 2-10. During the Illinious coal test with S content-3.98%, the SO_3 concentrations increased from 4 to 6 times on average at 530°C. However, sampling at higher temperatures close to 930°C, similar SO_3 concentrations were observed for oxy-fuel and air combustion in PC tests. The overall SO_3 concentrations measured at higher temperatures were less than the concentrations found at 527°C. This suggests that the secondary formation of SO_3 and the catalytic effect of metal oxide dominates in pilot-scale tests. In oxy-CFB tests, only Utah coal was investigated. The trend of SO_3 emissions was consistent with oxy-PC combustion, however on normalised base (mass per unit energy input), no difference was found between oxy and air-firing modes. Later, SO_3 measurements conducted at IFK in a 500 kW oxy-PC combustor (Spörl *et al*., 2014). This system had an ESP was along with a SCR (Spörl *et al*., 2014) and the SO_3 sampling was made from inlet and outlet of ESP and SCR, respectively. Roughly 62% of the SO_3 capture was noted under oxy-fuel combustion in the SCR unit. Higher SO_3 was noted in oxy-fuel runs and there was less influence of the SCR on the ADP temperature in these experiments (Spörl *et al*., 2011);(Monckert *et al*., 2008). Babcock-Hitachi tested SO_3 emissions in 1.5 MWth oxy-fuel combustion facility which included SCR, Clean Energy Recuperator (CER), Flue Gas Recirculation Dry Precipitator (DESP) and Wet Electrostatic Precipitator (WESP)(Mitsui *et al*., 2011). Two different coals were used in this experiment with low sulfur, but high ash contents. SO_3 concentrations at the DESP outlet was reduced to less than 1 ppm by decreasing the flue gas temperature to 90°C at the DESP inlet. Similar results were obtained for air and oxy-fuel combustion. It is worth noting that most SO_3 was trapped in the CER unit (Mitsui *et al*., 2011).

There is a lack of experiments in the literature for SO_3 formation from oxy biomass or co-firing combustion. In this regard, several SO_3 measurements were produced by Jurado *et al*. (2014), in a 100 kW oxy-PC unit during co-firing combustion test. Cerrejon coal/Cereal co-products were blended in the proportion of 50/50% and 75/25%. Wet RFG was employed in this test with varied steam content. Adjusting their results to a comparable SO_3 data received during air and oxy-fuel combustion environment, SO_3 concentrations indicated a slightly higher trend with an increase of biomass percentage in the mixture. These authors pointed out that this higher conversion seen in their co-firing experiments could be due to the higher content of alkali (K_2O) in biomass fly ash. Other SO_3 measurements taken for pilot-scale and industrial-level combustors are summarised Table 2-10. Currently it appears for pilot-scale tests on SO_3, CCM method was mostly applied.

2.7.8 Modelling studies of SO_3 formation

Only a few numerical studies on SO_3 formation are available for the O_2/CO_2 environment as compared to air combustion. Burdett *et al*. (1983) has predicted the effect of operating bed pressure on SO_2 to SO_3 conversion in the (Burdett *et al*., 1983). The predicted plot of bed pressure (600 kPa) and temperature of 900°C with 10% of O_2 in the flue gas clearly indicated an increasing trend of SO_3 formation. And this work suggests that under such condition, the potential increase of sulfur-in-fuel to SO_3 could be as high as 20%. However, these conclusions still need to be verified experimentally. Later, Burdett *et al*. (1984) has proposed a kinetic model to predict homogeneous reaction rates. Fleig *et al*., (2011) modelled homogeneous gas-phase SO_3 formation for oxy-fuel combustion condition with a model which is described by Gimenez-Lopez *et al*. (2011) and which was initially developed by Glarborg *et al*. (1998). CHEMKIN-PRO was used to model homogeneous reaction by making assumptions such as: plug flow reactor, and assuming a pre-defined reaction temperature and residence time. The resulting homogeneous model predicts less SO_3 at the temperature higher than 1400°C. More recently, Belo *et al*. (2014), implemented the kinetic model of Burdett *et al*. (1984) for residence times of 0.3 to 0.9 s as

shown in Table 2-8. Thermodynamic equilibrium calculations showed maximum conversion SO_2 to SO_3 at low temperatures and further increase of temperature to 900 and 1000°C decreased the SO_3 by about 6.8 and 3.2%, respectively (Belo *et al*., 2014). Gas phase SO_3 formation was also modelled by Schneider and Bogdan, (2003) for an oil-fired boiler.

Table 2-10 A detailed lists of SO_3 measurement campaigns under oxy and air fuel combustion

Authors	Type of fuel and sulfur content	Type of reactor	Measuring tools	Methodology to detect SO_3	SO_3 (ppm)
Abele *et al*., (1987)	Sub-bituminous (S-0.57%);			CCM	Air-0.03; Oxy-0.76;
Tan *et al*., (2006)	East-bituminous (S-.95%); Sub-bituminous (S-0.22%); Lignite (S-0.6%);	0.3 MW_{th} Vertical combustor	Data acquisition Honeywell Series S9000e controller; GA[s];	Not specified	Air-27 ng/J[t]; Oxy-75 ng/J; Oxy-0.14 ng/J;
Ahn *et al*., (2011)	PRB (S wt.%-0.23), Utah (S wt.%-0.53), Illinois (Swt.%-3.98)	1.5 MW PC combustor;	SO_2 Gas analyser (CAI Model 601 NDIR) and FTIR (Nicolet Magna-IR 550)	CCM	PRB Air: below 5[t] Utah Air: 5[u] Utah Oxy: 5[t] Illinois Air: 31[t] Illinois Oxy: 117[t]
Eddings *et al*., (2010)	Illinois coal pellets (Swt.%-4.0)	BFB reactor	FTIR	CCM	Air: 12[t] Oxy: 10[t]

[s] GA- gas analyser;
[t] ng/J-nanograms per joule
[u] Average value is taking into account

Authors	Type of fuel and sulfur content	Type of reactor	Measuring tools	Methodology to detect SO_3	SO_3 (ppm)
Kiga *et al*., (1997) Stanger and Wall, (2011)	Australian low sulfur coals with: A (S-0.45%); B (S-0.96%); C (S-0.38%);	1.2 MW IHI Aioi facility	Non-dispersive infra-red gas analyser (HORIBA ENDA-1610), GC (Shimadzu 14APFP);		Coal A: Air-2; Coal A: Oxy-7; Coal B: Air-9; Coal B: Oxy-9; Coal C: Air-3 Coal C: Oxy-11
Fleig *et al*., (2012)	Propane and SO_3 injected to unit;	100 kW Oxy fired test unit combustor	Nondispersive infrared (NDIR) analysers (NGA 2000 Fisher Rosemount); IC (ICS -90 DIONEX)	CCM used as reference case to other methods: 1. Isopropanol absorption bottle method, 2. Salt method; 3. Pentol SO_3 monitor;	CCM results: Air case: 34; Oxy-case 25[v]:9; Oxy-case 30: 56; Oxy-case 35: 25
Vainio *et al*., (2013)	Mixture of gases: (SO_2, H_2O, O_2, N_2 and H_2SO_4)	Bench scale horizontal tube reactor	ICS-90 Ion chromatography (DIONEX)	Salt method: four types of salts has tested (NaCl, KCl, K_2CO_3, $CaCl_2$)	Salt method results: NaCl: Air – 30[t]; NaCl: Oxy – 46[t];

[v] Oxy-30: 30 means O_2 concentration percentage in the oxidiser stream at the inlet;

Authors	Type of fuel and sulfur content	Type of reactor	Measuring tools	Methodology to detect SO_3	SO_3 (ppm)
Spörl *et al*., (2014)	Australian coals with sulfur: (A-0.3%; B-0.7%; C-0.7%)	20 kW combustion rig; L x D (2.5 x 0.2 m); Flow rate: 11.5 m^3/hour;	IC (DIN EN ISO 10304)	CCM	Coal A: Air – 2; Oxy: 6 – 35[w]; Coal B: Air – 8; Oxy: 18 – 50; Coal C: Air – 1; Oxy: 2– 30;
Monckert *et al*., (2008)	Klein Kopje, Lausitz, Rhenish, Ensdorf (S-1%)	0.5 MW down-fired Oxy -PC	SEM-BSE, SEM-MAP	CCM	Air: 8; Oxy: 85;
Roy *et al*., (2014)	Victorian coals Loy Yang, Morvell and Yallourn (S- 0.5%)	10 kW oxy-fired BFB	Gas analyser (MX6 iBrid) GC (Agilent GC 7890A);	Calcium oxalate with glass beads;	Dry Oxy: 11 mg/MJ; Air: 15 mg/MJ; Dry Oxy-fuel 14 mg/MJ;
Wang *et al.*, (2015)	Lignite coal (S-0.6%); Bituminous coal (S-3.69%)	Oxy PC unit	ICS -90 DIONEX	CCM	Oxy Bituminous coal: 500 to 3000[x]; 13 to 105[y]; Oxy Lignite: 500 to 3000; 0.5 to 80
Hemis, (2006)	Illinois bituminous coal	Hoosier Energy' Merom Station	FTIR; IC (Desert Analytics);	FTIR and CCM	Air tests: Day-1 FTIR-37.33 versus CCM-30.4; Day-2 FTIR-

[w] Range of SO_3 values are provided for this particular test as initial parameters were different;
[x] 500 to 3000 means SO_2 concentration in the test conditions;
[y] 13 to 105, Corresponding SO_3 concentration in regard to SO_2 concentrations;

Authors	Type of fuel and sulfur content	Type of reactor	Measuring tools	Methodology to detect SO_3	SO_3 (ppm)
					37.66 versus CCM-29.1;
Cao *et al*., (2010)	Bituminous & subbituminous coals (S-3.5%); Three FAs	Fixed bed rig, Full-scale utility boilers	IC (DX-120);	Modified CCM	Air. Site1: Bituminous coal SCR inl-22; SCR out–24; APH[z] out–7; ESP in-6; FGD inl–7; FGD out–4; Site 2: SCR inl-23; SCR out-24; APH out-21; ESP out-17; FGD in-17.5; FGD out-15; Site 3: Sub-bituminous: below 2 at all locations
Kenney *et al*., (2011)	LSB[aa] (S-0.9%), HSB[bb] (S-3.2%); Sub-bituminous (S-0.3 %), Dried lignite (S-0.7%);	Oxy fired pilot plant; 15 MW_{th}, Alstom;	N/A	SO_3 executed from Economiser outlet locations of boiler; CCM.	Sub-bit Air: 0.5[t]; Oxy with SO_x control: 1.6[t]; LSB air: 28.8; oxy: 39.4; HSB air-41; Oxy-186.3; Lignite air-30; oxy-45.9;

[z] AHP – air preheater;
[aa] LSB-low sulfur bituminous
[bb] HSB-high sulfur bituminous

Authors	Type of fuel and sulfur content	Type of reactor	Measuring tools	Methodology to detect SO_3	SO_3 (ppm)
Jurado et al., (2014)	EI Cerrejon coal (EC) (S-0.58%); Cereal co-product (CC) (S-0.16%)	0.1 MW pulverised oxy-fuel combustor	FTIR, ESEM/EDX, XRD	CCM	Air: EC-3.7; EC/CC (50/50%)-20.2; CC-25.4; Oxy: EC-20.6; EC/CC (50/50%)-35.9; EC/CC (75/25%)-16.8;
Davis, (2011)	USA Williamson coal (S-1.7%);	E.ON 1 MW Combustion Test Facility	XRF, SEM	SO_3 Monitor (Severn Science analyser); CCM	Not specified;
Dhungel *et al*., (2011)	Medium sulfur bituminous Coal	ERTF[cc] 0.16 MW Oxy fired system;	Dry sorbent injection; Gas analyser	CCM	Not specified;

[cc] ERTF-Emission Reduction Test Facility

3 METHODOLOGY

In this section, the first two experimental tests were conducted during the visit to Southeast University and are described first. This work is followed by the latest SO_3 measurements which were conducted in a bench-scale bubbling fluidised bed rig at Cranfield University.

The data obtained from pilot-scale oxy-CFB tests provide a realistic data on sulfur to SO_3 conversion during the air and oxy combustion environments. However, it should be noted that operation of a pilot-scale CFB unit is difficult for a long period of time, as it requires longer time for preparation and analysis of the test. The amount of SO_3 concentration achieved in the air and oxy environments was defined by average value of repeated tests. In contrast, bench-scale experiments allowed to gather the SO_3 at a wider range of parameters which is difficult to obtain in the pilot-scale CFB unit. A second study in the bench-scale bubbling fluidised bed represents a typical operation parameters of the BFB reactor in air and oxy conditions. The results from both bench-scale tests provide a presentable data that simulates and predicts the SO_3 formation in pilot-scale and demonstration units. Tests were conducted three and in some tests two times. Therefore, the final data for the similar test condition was presented by average value. In some tests, particularly in bubbling fluidised bed rig, few tests were done two times. The methodology section also describes the experimental procedure and design of experiment

3.1 Experiments in a fixed bed (FB) reactor

A vertical tube reactor was used for the tests involving homogeneous and heterogeneous reactions, as shown in Figure 3-1. The system consists of a 15.5 mm inner diameter (ID) quartz tube flow reactor placed in an electrically heated furnace. The total length of the quartz tube was 1115 mm. A porous quartz plate was placed at the centre of the quartz tube to support the solids in the reactor. The furnace below the plate is used to preheat the gas into the reaction zone. The isothermal length above the plate is calibrated as 420mm. Another porous quartz plate was placed at the exit of the quartz tube to prevent the escape of solids from the reactor. High purity (>99.99%) reactant gases (O_2, SO_2, and N_2/CO_2) were supplied by gas bottles and were metered by the flow meters before entering the gas mixer.

Deionised water was metered and pumped into a steam generator by a metering pump (BT 100-2 J, Longer Pump, China). The steam generator was controlled to operate at 200°C. The steam and other gases were mixed in the gas mixer which is also heated and then sent to the reactor. The entire gas line was electrically heated to avoid condensation. The total gas flow rate into the reactor was 3.17 L/min (100 kPa, 0°C) to maintain the residence time of gas at 1.5 s under the actual condition. Test conditions and variables are presented in Table 3-1. The amount of SO_3 and SO_2 present in the condensed acid in the hydrogen peroxide solutions were quantified through a titration method using barium

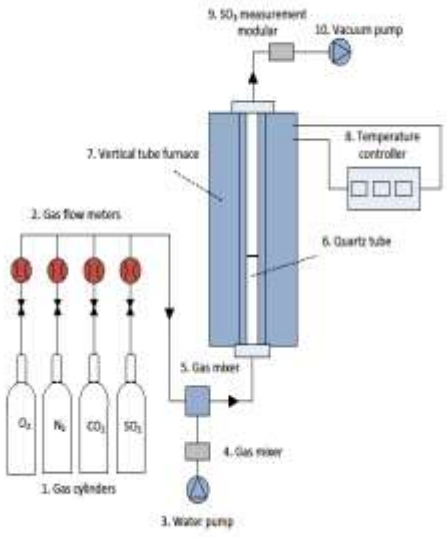

Figure 3-1 Vertical fixed bed reactor system (Modified from Duan *et al*., 2015)

perchlorate with a thorin indicator, according to the EPA method 8A. All samples were titrated at twice to get accurate results. More details of the SO_3 sampling and measurements are described in section 3.4.

Table 3-1 Test conditions in fixed bed rig (inlet gases per volume on a wet basis)

Variables	Operational values
Temperature, (°C)	400, 500, 600, 700
SO_2 concentrations (ppm)	2000, 3000, 4000, 5000
O_2 concentrations (%)	3, 6, 11, 16
Steam concentrations, (%)	5, 10, 15

3.2 Experiments in a pilot-scale circulating fluidised bed (CFB) reactor

Several SO_3 measurements were conducted in a 50 kW_{th} oxy-fired CFB unit with wet RFG to evaluate the formation of SO_3 under real combustion environment. The sketch of oxy-CFB unit is illustrated in Figure 3-2. The pilot scale oxy-CFB unit consist: riser, fuel feeding system, gas feeding system, cooler, bag filter and supply of pre-heated RFG. A bituminous coal was burned in air and oxy combustion tests. The ultimate and proximate analysis of the bituminous coal used in the test is shown in Table 3-2. The mass flow rate of coal was around 7.2 kg per hour. Oxygen concentration in the oxy-fuel combustion conditions was 23.4%. This corresponded to the reactor temperature of 881°C for air and 891°C under oxy-fuel combustion. More details concerning the rig can be found elsewhere (Duan *et al*., 2014). The following gases were monitored during the experiments: 1) oxygen concentrations in the inlet and outlet of the reactor were measured by ZrO_2 oxygen sensors; 2) SO_2 concentrations were read during the tests by a gas analyser (NGA2000,

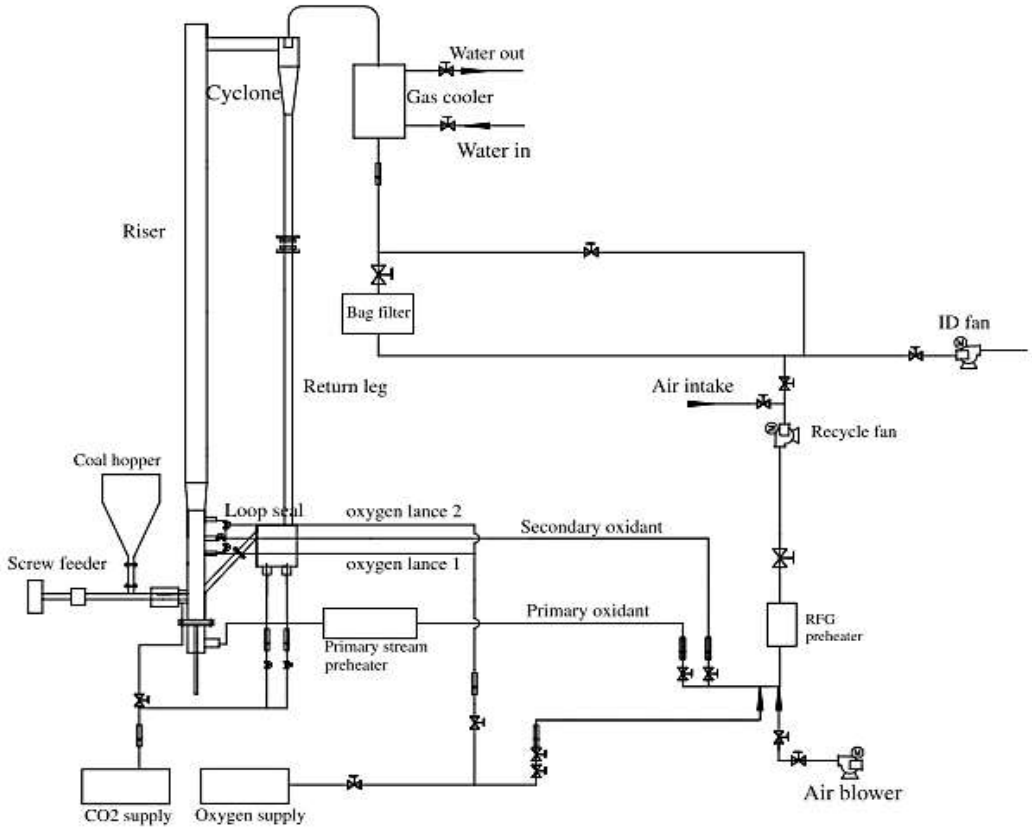

Figure 3-2 Oxy-fuel CFB unit with flue gas recycle (Duan *et al*., 2014)

Table 3-2 Ultimate and proximate analysis of coal (air dried basis) (Duan *et al*., 2015)

Ultimate analysis (wt.%)		Proximate analysis (wt.%)	
Carbon (C)	65.00	Fixed carbon (FC)	51.68
Hydrogen (H)	3.85	Volatile (V)	28.38
Oxygen (O)	9.95	Ash (A)	16.18
Nitrogen (N)	0.76	Moisture (M)	3.76
Sulfur (S)	0.50	Heating value (MJ/kg)	25.05

Emerson, USA); 3) H_2O concentration in the flue gas was measured by a moisture analyser (MAC125, MAC INSTRUMENTS, USA);

3.3 SO_3 measurements in a bubbling fluidised bed (BFB) rig

Fundamental data collection of SO_3 formation is continued in a bench scale bubbling fluidised bed reactor. A schematic diagram of a bench-scale bubbling fluidised bed rig is illustrated in Figure 3-3. The reactor consists of the following: inner and outer stainless steel tubes that serves as the reactor, together with gas lines for (O_2, CO_2, SO_2, N_2) and a water pump, an electrically-heated furnace to achieve the desired temperatures and a solids feeding port. At the hot exit line, a sintered filter and gas analyser is installed for solids removal and gas monitor. The dimension of inner tube (ID) was 25 mm with a height of 550 mm. The outer tube has an ID of 38 mm and a height of 1180 mm. The distributor plate is made of 4 layers of stainless steel (316) mesh clamped with an open cap to the bottom part of inner reactor. The reactor temperature and the pressure drop across the bed were measured by K-type thermocouple and pressure transducers, respectively. The total length of a tube made for an exit gas (ID-4.2 mm) was 700 mm. The purpose of using smaller diameter pipe was to reduce the residence time of the gas exiting the reactor to prevent SO_3 condensation. The residence time of the exit gas in exhaust section was less than 1 s. According to the studies of Lindsay and Flint, (1951), SO_3 capture by tube wall could be avoided if a short residence time is ensured in the sample lines to the SO_3 analyser. A similar approach for the sampling line for such measurements has been used by Dennis and Hayhurst, (1988). Moreover, the whole length of the gas sampling line was heated with a string heating element and maintained at temperature 290-300°C. As a result, the exit gas temperature was controlled from 185 to 190°C. Another reason for maintaining heater at such temperatures is to avoid the formation of aerosols in the quartz filter fitted in the SO_3 sampling train (Maddalone *et al*., 1979).

All readings were recorded by the data acquisition system (Picolog). The mixture of gases and steam were fed to the bottom part of the outer tube to pass through the pre-heating section. The flow rate of gases to the reactor was controlled by calibrated mass flow controllers (MFC-Bronkhorst). N_2 and CO_2 mass flow controllers are calibrated by connecting MFC straight to the

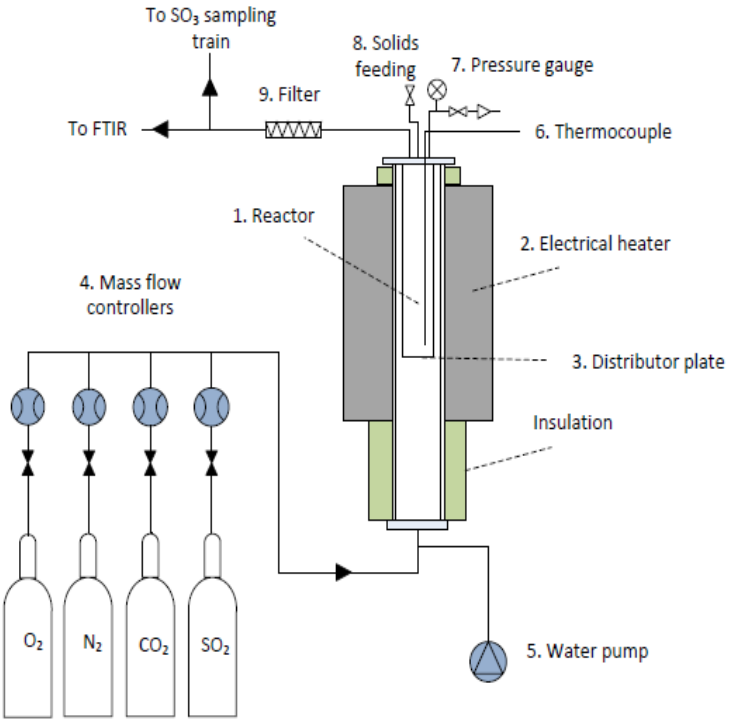

Figure 3-3 Sketch of bench scale bubbling fluidised bed

calibrated wet gas meter under constant flow rate. The calibration of N_2 and CO_2 MFCs are given Appendix C. As a result of calibration procedure, the difference between the WGM and MFC was taking into account during the tests. Deionised water is provided by a high pressure pump and supplied in a straight line to the pre-heated section of the outer tube to avoid a steam condensation in the bottom section of the outer tube.

The water pump is also checked before the tests by running water into to the 50 ml of glass beaker (Pyrex). The time of flow is fixed and collected volume of water was measured visually. After passing the main heated section of the reactor, concentrations of an exit gas were measured by a Fourier transform infra-red (FTIR, Protea, model FTPA-002). A schematic of the rig and auxiliaries is presented in Figure 3-4 (a, b, c).

(a)

(b)

(c)

(d)

Figure 3-4 Photographs of bubbling fluidised bed rig

(a) Front view that includes: reactor, electrical furnace, oven for glass condenser and vacuum pump; (b) side view illustrates control system for gases, data acquisition system via PC and FTIR gas analyser; (c) upper part of the rig includes pressure gauge, solid feeding port with two valves, exit gas line and thermocouple port; (d) riser (reactor) with distributor plate;

3.4 Materials

3.4.1 Materials for fixed bed tests

Uncatalysed tests in the quartz tube reactor were conducted in the absence of solids. During the catalysed tests, three different metal oxides (0-10μm) including α-Fe_2O_3, V_2O_5 and CuO with purity higher than 99% and two different kinds of fly ash-1 and fly ash-2 (0-45μm) were used as the catalysts. 1.6 g Fe_2O_3, 0.795 g CuO and 1.82 g V_2O_5 were used respectively in the heterogeneous tests to make them at the same molar amount. 1.0 g FA was used in the FA tests. The chemical composition of the used fly ashes is given in Table 3-3.

3.4.2 Materials for bubbling fluidised bed tests

Experiments in BFB rig used silica sand with a mean particle size of 260 μm. In addition, three different fly ashes (FA) were used to investigate the catalytic effect of minerals on the formation of SO_3. Fly ashes were supplied from: CanmetENERGY (Canada), British power station (UK) and Southeast University (China). Further these materials are entitled as Fly ash-3 (Canadian), Fly ash-4 (British FA) and Fly ash-1 (Southeast). The last fly ash was produced from a 50 kW oxy-fired CFB unit described in the section 3.2. Further details about the coal from which the FA was produced and the combustion units themselves can be found elsewhere (Duan *et al*. 2014). The chemical composition of the Fly ash-3 and Fly ash-4 is given in Table 3-3 along with the fly ashes from fixed bed tests. Due to the low bulk density of FA, smaller particles were sieved for the catalysed tests. The particle size (PSD) of fly ashes used in this work was between 90 and 212 μm, with a mean diameter (d_p) of 150 μm. However, a higher particle size was sieved for the Fly ash-1, as shown in Figure 3-5.

Table 3-3 Chemical composition of fly ashes

Composition	Fly ash 1 (FB, BFB)	Fly ash 2 (FB)	Fly ash-3(BFB)	Fly ash-4 (BFB)
Na_2O	0.46	2.55	0.2	1.25
MgO	1.36	4.51	9.02	2.5
Al_2O_3	34.14	18.52	9.12	29.5
SiO_2	45.12	37.84	25.44	48.0
K_2O	0.99	0.37	0.78	3.0
CaO	8.66	19.99	29.95	3.0
Fe_2O_3	4.16	10.37	8.59	9.0
TiO_2	1.53	1.09	0.21	0.95
SO_3	3.06	3.07	n/a	n/a
P_2O_5	0.09	1.09	0.11	n/a

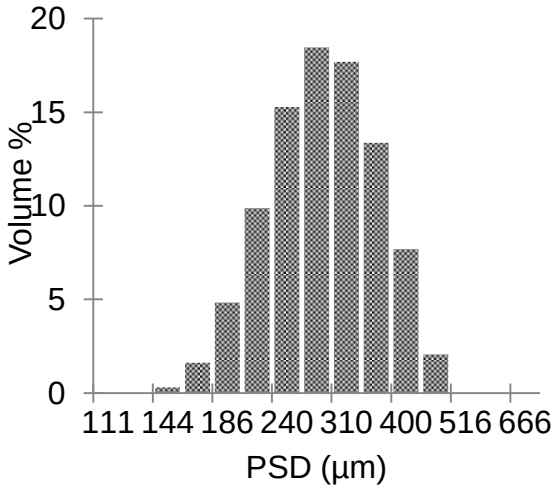

(a) Silica sand

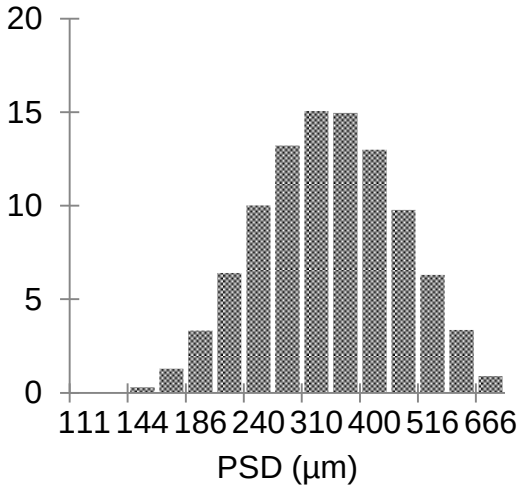

(b) Fly ash-1

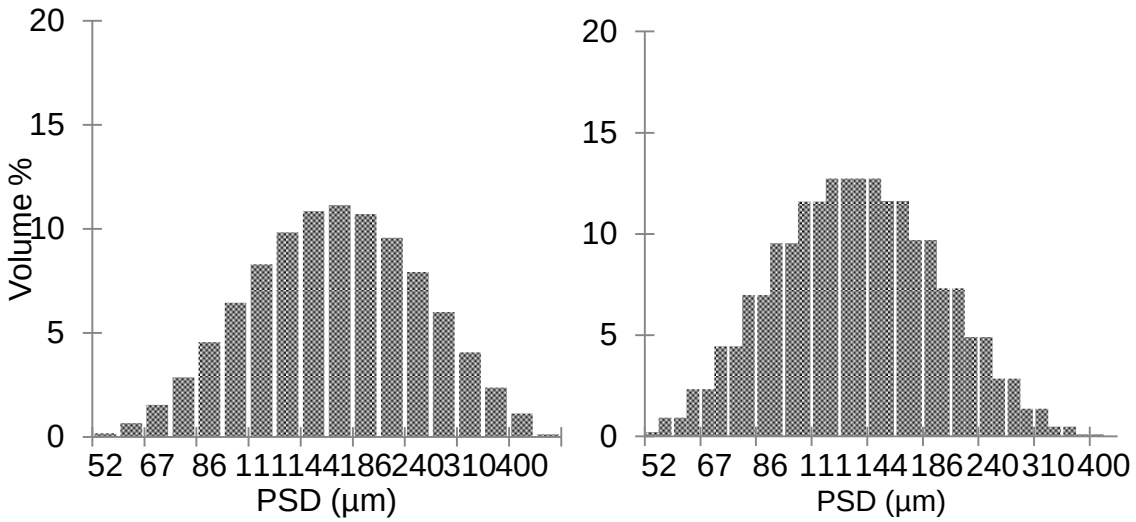

(c) Fly ash-3 FA **(d) Fly ash-4 FA**

Figure 3-5 Particle size distribution of solid materials

Four layers of fine metal mesh with the porosity grade of 75 and 120 µm were fixed to sustain solids in the reactor. The PSD of solids is shown in Figure 3-5. At the exit of the reactor, a thumb type sintered filter with a porosity grade of 60 µm was placed to prevent solids escape from the reactor. All tubes in exhaust section were made of stainless steel. Initial illustration of solids is presented in Figure 3-6.

Figure 3-6 Photographs of solid materials

3.5 Development of SO_3 sampling method

For the next experimental campaign conducted at Cranfield University, a new SO_3 sampling train was designed based on the EPA method 8A. According to

previous investigators, the CCM appears to be the most common method for measuring SO_3 (Jaworowski and Mack, 1979);(Maddalone *et al*., 1979);(Fleig *et al*., 2012). Due to the size limitations of the rig, the total sampling flow of exit gas was several times lower than the sampling flow rate recommended by EPA method 8A. Therefore, the sampling time was extended to match a minimum gas volume of 300 L. At 950°C, the duration of sampling was around 4 h, while only 2 h were required at 400°C. The SO_3 sampling train is shown in Figure 3-7. The sampling probe of an exit gas is connected to the quartz tube and sealed with a high temperature ceramic paste. The exit gas is filtered a second time in the glass sampling train by the quartz filter and paper. The quartz filter had a porosity size of 100 µm. Secondary paper filter is required to remove fine particles from the gas stream as it can result in positive errors.

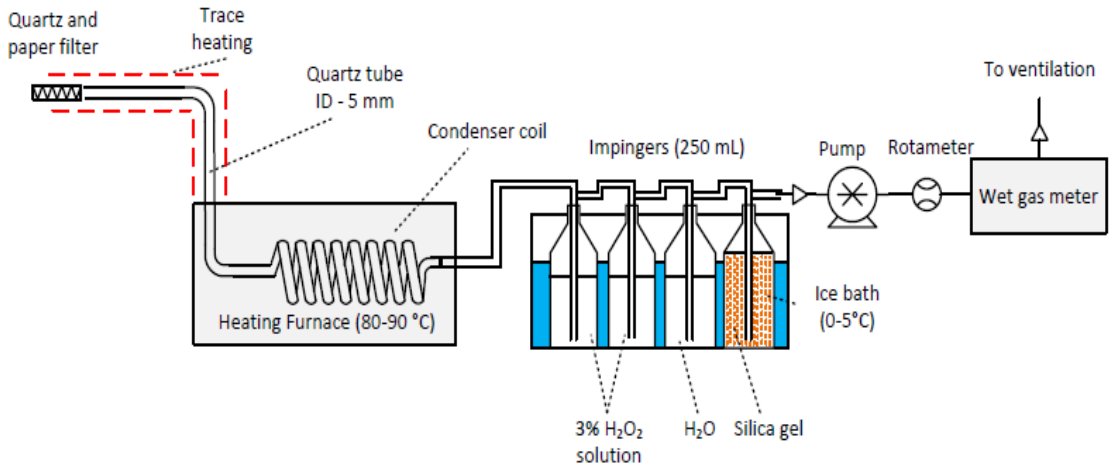

Figure 3-7 SO_3 sampling train based on EPA method 8A

The probe and filter are maintained at the temperature of 290-300°C to avoid the formation of aerosols. After passing the filter, the sampling gas undergoes a temperature drop in the glass condenser which maintained at the temperature of 80 to 90°C. At this temperature, an existing SO_3 in the exit gas condenses at the wall of the glass condenser. The image of glass condenser fixed in the oven is provided in Appendix E. The remaining gas passes through a 3% of hydrogen peroxide (H_2O_2) solution; here any SO_2 is converted to sulfuric acid even at low temperature. The gas moisture is removed by silica gel and the gas then goes to a wet gas meter (WGM). A calibrated WGM was used in this test to avoid

flow measurement errors, see Figure C-1 and C-2 in Appendix C. The WGM was fixed in a horizontal plate and positioned by a spirit level. The top of water level was monitored in the WGM.

For the SO_3 analysis, a solution containing 1.95 g of barium perchlorate trihydrate (99.9%-Ba, CAS: 10294-39-0; Stream Chemicals, Newburyport, MA 01950, USA) was dissolved in a 200 ml of de-ionised water at room temperature. Then, 800 ml pure iso-propanol is added to make 1000 ml of barium standard solution. The solution is stored in a 1000 ml glass bottle and kept closed at room temperature. The solution is stable for the period of two weeks. For the SO_2 measurements, the first two bottles were filled with 100 ml of solution containing 3% hydrogen peroxide, followed by 100 ml of de-ionised water and silica gel in the last bottle. All 4 impingers were maintained at the temperature bellow 5°C during the test. The temperature in the water bath was monitored by K-type thermocouple during the test and kept at the temperature below 5°C, by adding a fresh ice during the sampling period. The glass condenser, probe and first two impingers were titrated separately by barium perchlorate trihydrate solution. 2-4 drops of thorin indicator was used to titrate the solution until a pink colour was achieved.

Finally, the quality of barium perchlorate trihydrate solution was also determined by diluting the standard sulfuric acid into 5, 10, 25 and 50 mmoles as shown in Figure 3-8. As a result, a high titration accuracy was achieved.

The SO_3 concentration and SO_2 concentrations (C) were defined by the following equations 3.7 and 3.8, respectively:

$$C_{H_2SO_4} = K_1 \frac{(V_t - V_{tb})\, N \left(\frac{V_{soln}}{V_a}\right)}{V_{m(std)}} \qquad \text{Equation 3.7}$$

$$C_{SO_2} = K_2 \frac{(V_t - V_{tb})\, N \left(\frac{V_{soln}}{V_a}\right)}{V_{m(std)}} \qquad \text{Equation 3.8}$$

Where:

- K_1 = 0.04904 g/milliequivalent (g/meq) for metric units;
- K_2 = 0.03203 g/milliequivalent (g/meq) for metric units;
- V_t = Volume of barium standard solution titrant used for the sample, ml;
- V_{tb} = Volume of barium standard solution titrant used for the blank, ml;
- V_{soln} = Total volume of solution in which the H_2SO_4 or SO_2 sample is contained, 250 ml or 1000 ml, respectively;
- V_a = Volume of sample aliquot titrated;
- V_m = Volume of gas sample as measured by wet gas meter;
- N = Normality of barium perchlorate titrant, g-equivalents/liter;

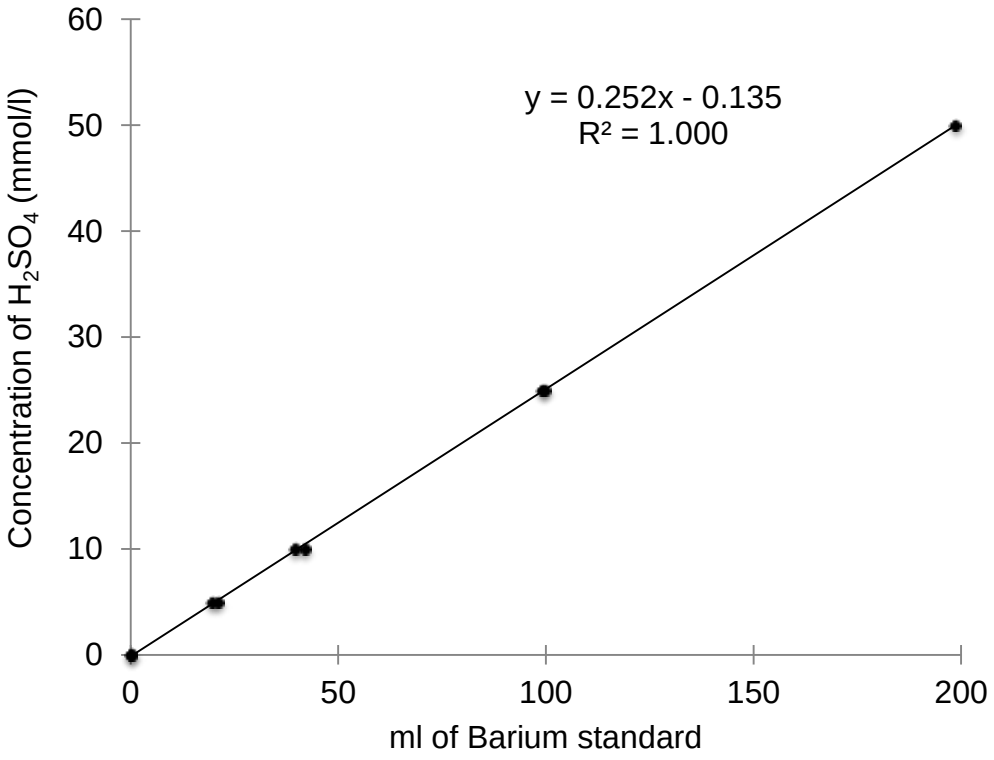

Figure 3-8 Accuracy of titration method

3.6 Experimental procedure for bubbling fluidised bed

For these experiments, a factorial approach was chosen for the experimental design with lower and higher values for SO_2 concentrations and bed temperatures (T_{bed}) as shown in Table 3-4 and Appendix B. Two levels of SO_2 concentrations of 1000 and 4000 ppm were used to simulate average and high sulfur coal combustion flue gases in BFBs. The 4000 ppm SO_2 content represents high-sulfur coal combustion in an oxy-fuel combustion environment

Table 3-4 Test condition of SO_3 measurement in BFB rig

Test parameters:	Lower range	Higher range
Operating temperature, °C	400	950
SO_2 inlet, (wet basis) ppm	1000	4000
Flow rate, L/min	2.6	1.4
Sampling volume (EPA[dd]), m³	0.3	0.3
Sampling time, hours	1.9	3.9

with wet RFG. As discussed above, the wet RFG in oxy-fuel combustion increases steam content in the combustion furnace (Liu and Shao, 2010). Therefore, this environment was represented by increasing the steam content in the reactor from 6% to 11% by volume, as seen in Table 3-5. Here, low temperature (400°C) tests represent the formation of SO_3 at the back end of combustion furnace while, higher temperature case (950°C), represents post-flame combustion environment in the fluidised bed. Reactant gases were supplied by bottles and metered by mass flow controllers. The flue gas compositions of these tests are illustrated in Table 3-5. These tests can be designated as:

- *Uncatalysed tests:* Uncatalysed formation of SO_3 under BFB condition. These tests were performed in the presence of 20 g of washed and

[dd] EPA protocol on measuring sulfur trioxide and sulfur dioxide emissions

sieved silica sand and conducted according to the conditions shown in Table 3-4. It is assumed that silica sand had no significant effect on the formation of SO_3.

- *Catalysed tests:* Catalysed formation of SO_3 tests were conducted in the presence of 20 g of silica sand and 10 g of fly ash. Each fly ash was sieved and then weighted precisely. However, in this tests fly ash was dropped into the hot reactor;
- *Ash characterisation:* This part of the study employed a thermogravimetric analyser (TGA) to determine the amount unburnt carbon in the ashes and XRF analysis of bed ashes after the tests. TGA (model TGA Q500) tests were conducted for each ash under air and inert gas to investigate the mass change with temperature up to 900°C.

Uncatalysed tests in the absence of fly ashes conducted according to the Table 3-5 and were repeated two times. The catalysed tests were also conducted according to the Table 3-5, in the presence of 10 g of ashes. For catalysed tests with fly ashes, tests with Fly ash-3 were repeated two times while second and third fly ashes performed once. Also, the Fly ash-1 was tested only at 950°C under SO_2 concentrations of 1000 ppm. Single tests were done for this case as the results were in an acceptable range.

Table 3-5 Inlet mixture composition (per volume on a wet basis)

Test runs	Mode	Temp °C	SO_2 (ppm)	O_2 (%)	H_2O (%)	N_2 (%)	CO_2 (%)
1	Air	400	1000	4	6	Bal	15
2	Air	400	4000	4	6	Bal	15
3	Air	950	1000	4	6	Bal	15
4	Air	950	4000	4	6	Bal	15
5	Oxy	400	1000	5	12	0	Bal
6	Oxy	400	4000	5	12	0	Bal
7	Oxy	950	1000	5	12	0	Bal
8	Oxy	950	4000	5	12	0	Bal

Prior to starting each test, all exit gas tubes and metal connections were checked for leakages. Afterwards, the reactor heated up at a rate of 20°C/min to reach the desired temperature. 20 g of silica sand was dropped to the reactor when the set temperature is reached. Once, the steady-state condition was achieved as determined by FTIR readings, the exit line are switched to the SO_3 sampling line. The reason for this approach was due to the limitation of volumetric flow through the reactor. At typical fluidising conditions (20°C and 100 kPa), the volumetric flow rate was 2.6 L/min at 400°C and 1.4 L/min at 950°C, to maintain a similar superficial gas velocity in the reactor. The residence time in the reactor was ~3 s under actual conditions which is equivalent to a fluidisation velocity (U/U_{mf}) of around 3.8 which corresponds to a vigorously bubbling fluidised bed. The minimum fluidisation velocity (U_{mf}) is calculated by Wen and Yu correlation (Kunii and Levenspiel, 1991). The minimum fluidisation (U_{mf}) velocity value was obtained from Wen and Yu correlation and compared with the experimental (U_{mf}) in the BFB rig, see Appendix A. Good agreement were achieved between Wen and Yu correlation and an experimental data. The apparent density of bed materials was calculated by the water displacement method. The apparent density of silica sand was 2500 kg/m^3, while for Fly ash-3 ash was 950 kg/m^3 and roughly 750 kg/m^3 for Fly ash-4 and Fly ash-1 ashes.

3.7 Pressure drop measurements in BFB

Pressure drop profiles at 400°C and 950°C are illustrated in Figure 3-9 and Figure 3-10. It can be seen from Figure 3-9 that feeding 20 g of silica sand increased ΔP across the bed to 0.36 to 0.40 kPa. An addition of 10 g of ash particles increased ΔP further to 0.55 to 0.59 kPa. The ΔP during heating stage was between 0.01 and 0.05 kPa in the empty reactor. This ΔP was due to the resistance of the distributor plate. A fluctuation in ΔP profiles was also noted with ash tests. This could be due to the adjustable vacuum pump for SO_3 sampling. A gradual decrease of ΔP profiles was noted in the tests with Fly ash-4. This could be explained by the lower density of FA particles that escaped the reactor and remained in the sintered filter. Similar profiles for ΔP were observed

for the test carried out at 950°C. The repeated fluctuation of ΔP in the test with Fly ash-4 at 950°C appears to be as a result of split feed of ash.

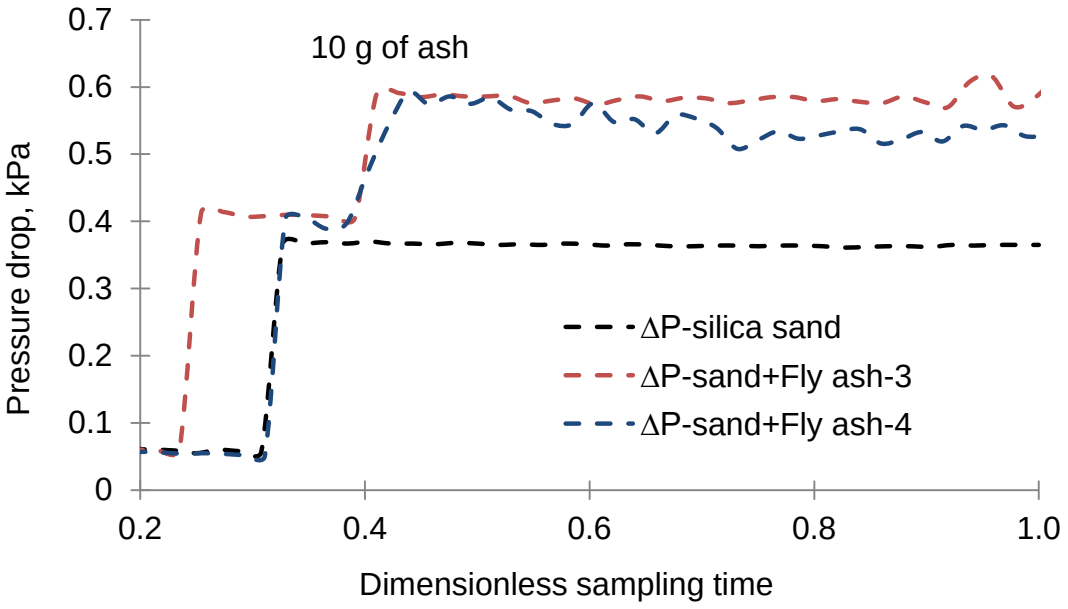

Figure 3-9 Pressure drop measurements at 400°C in BFB

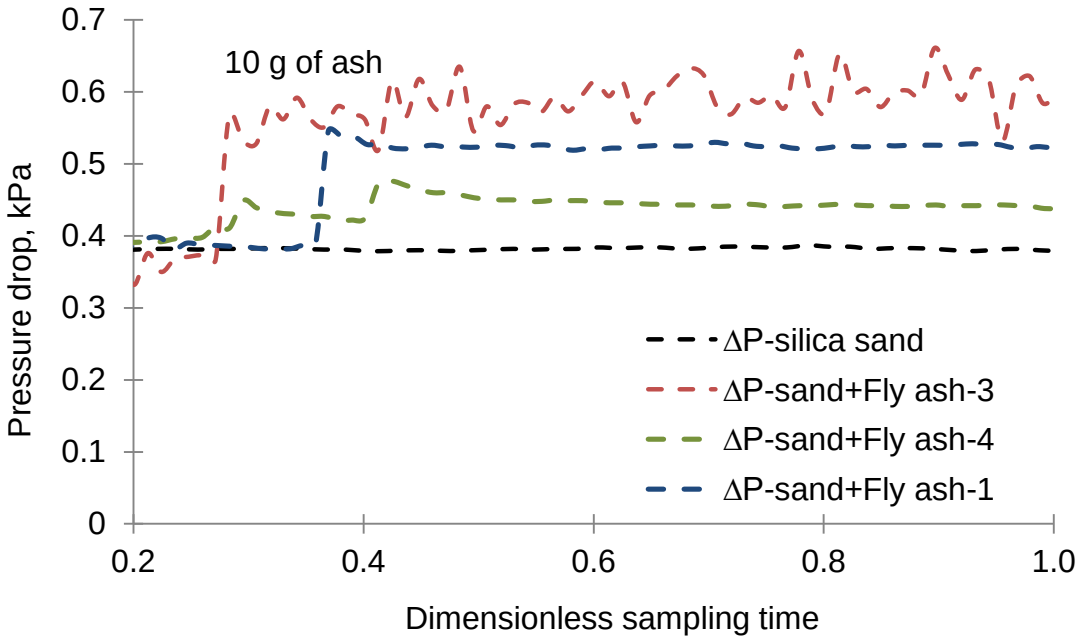

Figure 3-10 Pressure drop measurements at 950°C in BFB

However, ΔP for the Fly ash-4 and Fly ash-1 decreased notably after feeding at 950°C. This change of ΔP could be explained by amount of unburnt carbon

content in the ash. In order to confirm this, fly ash particles were tested by thermogravimetric analyses (model TGA Q500), as illustrated in Figure 3-11 and Figure 3-12 (a, b and c).

In a typical experiment, 0.02 g of sample was placed in a platinum based pan supported by a balance within the TGA instrument. Filtered air and N_2 with the purity of 99.987% were supplied from the air compressor and from gas cylinder, respectively. The volumetric flow rate of gas was fixed at a rate of 100 mL/min (measured at STP). The heating rate of the TGA chamber was set to 20°C/min, while the maximum temperature for each test was 900°C. The maximum temperature of the TGA chamber was limited by the instruction of the model. The off-gas from the TGA was sent to the ventilation system. As illustrated by Fan and Brown (2001), the unburnt carbon in the ash is typically determined by TGA weight loss. The ash sample is heated till 500°C in an inert environment where the weight loss can be 2.5% due to the release of moisture and volatile

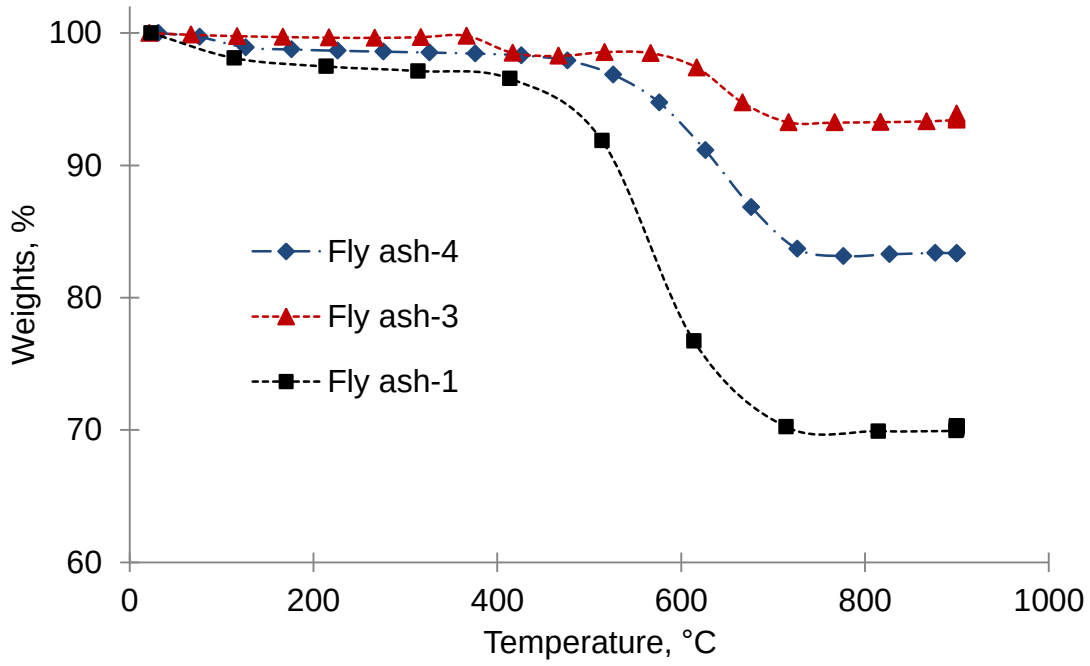

Figure 3-11 TGA test of FAs under air environment

matter. Then, oxidation of solids starts when oxygen is introduced into the chamber. The total loss is defined as total change during the TGA test, while unburnt carbon in the ash is determined as weight loss after the oxygen is

introduced. It can be seen from Figure 3-11 that Fly ash-1 had the highest unburnt carbon content, as the total weight loss of the sample dropped almost to 30%. The weight loss of Fly ash-1 at 500°C under N_2 and air was around 4%, see Figure 3-12 (c). As a result, the unburnt carbon of this ash is accounted roughly to 26%. Unburnt carbon values for Fly ash-4 and Fly ash-3 were 14% and 5%, respectively, see Figure 3-11. The weight losses of Fly ash-4 and Fly ash-3 at 500°C were 2%, which found in a good agreement of Fan and Brown (2001) studies. Unburnt carbon for the Fly ash-1 could be due to the short residence time through the pilot-scale oxy-CFB unit. More details concerning this work can be found in the work of Duan *et al*. (2015). Here, ΔP with Fly ash-3 showed a more stable profile compared to the Fly ash-4 and Fly ash-1.

This means that ΔP in the BFB is affected by the oxidation of unburnt carbon in the fly ashes. The mass change curves in TGA, provided a reasonable explanation of the observed ΔP in the BFB tests.

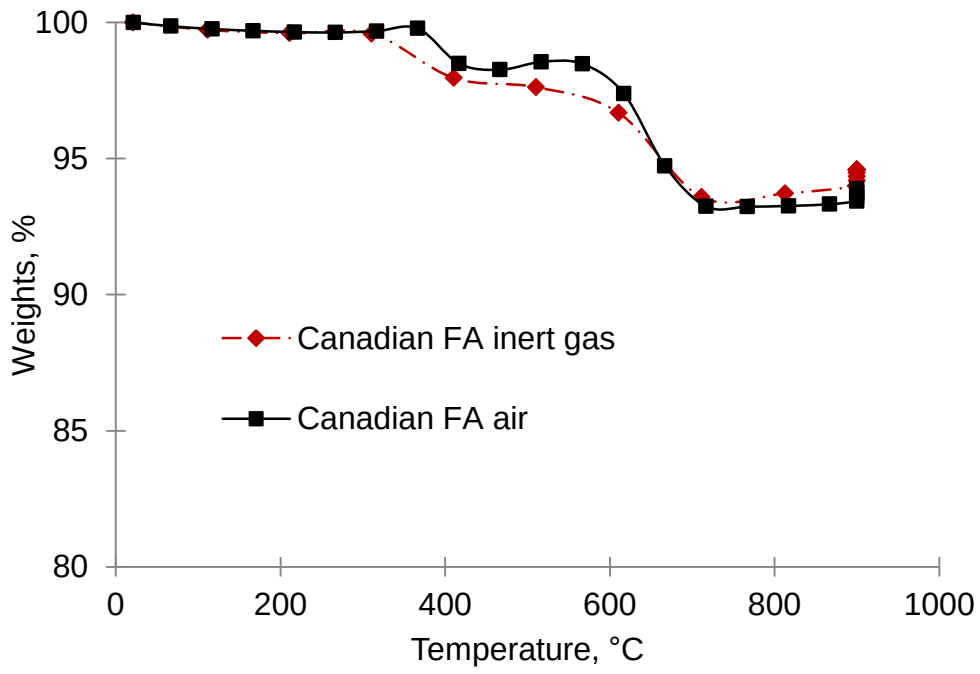

(a) Fly ash-3

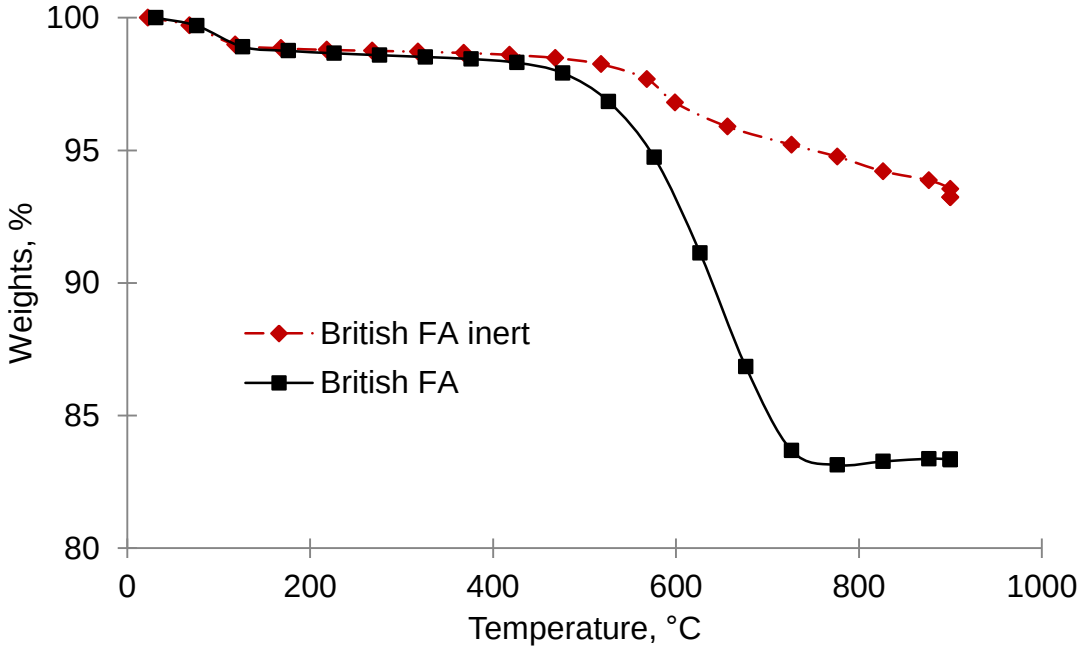

(b) Fly ash-4

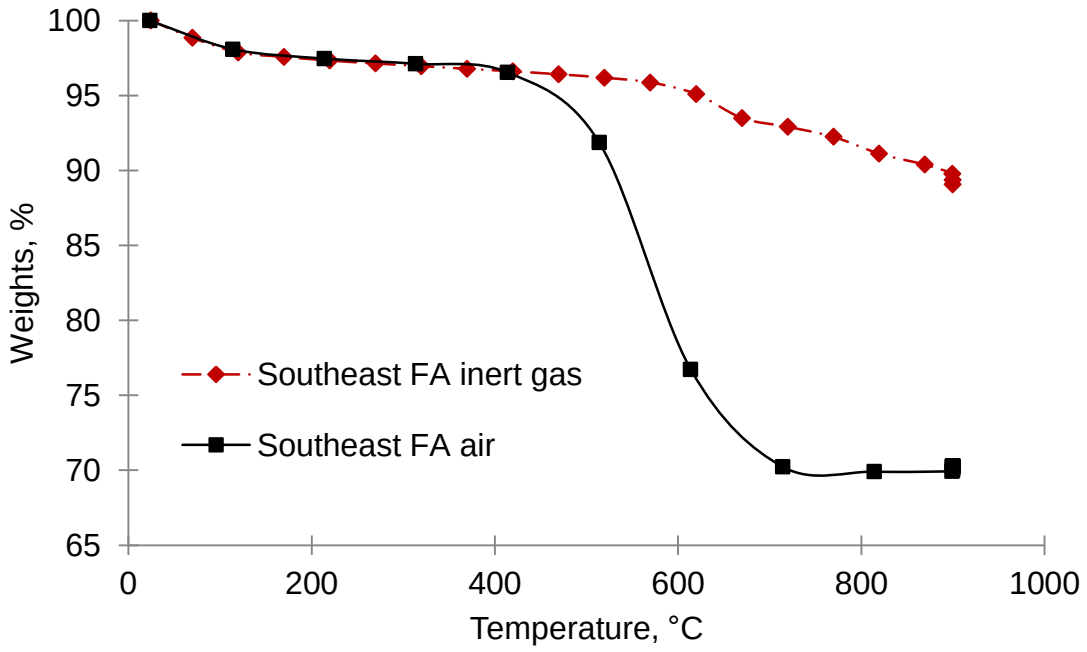

(c) Fly ash-1

Figure 3-12 (a,b,c) TGA tests for Fly ash-3, Fly ash-4 and Fly ash-1 FA

4 RESULTS AND DISCUSSIONS

4.1 Uncatalysed SO_3 formation

4.1.1 Effect of bed temperature in fixed and bubbling fluidised bed

The SO_3 concentration from 400 to 700°C and under different gas compositions environments is shown in Figure 4-1. As temperature increases from 400 to 700°C, SO_3 concentration increases for all different atmospheres tested in the fixed bed reactor. This trend observed under a constant inlet concentration of SO_2 at 3000 ppm. As described in the section 2.5, SO_3 is formed by the oxidation of the molecular oxygen via reaction (6) and (7) for the temperature range in this study. The formation of SO_3 is thermodynamically favoured as the

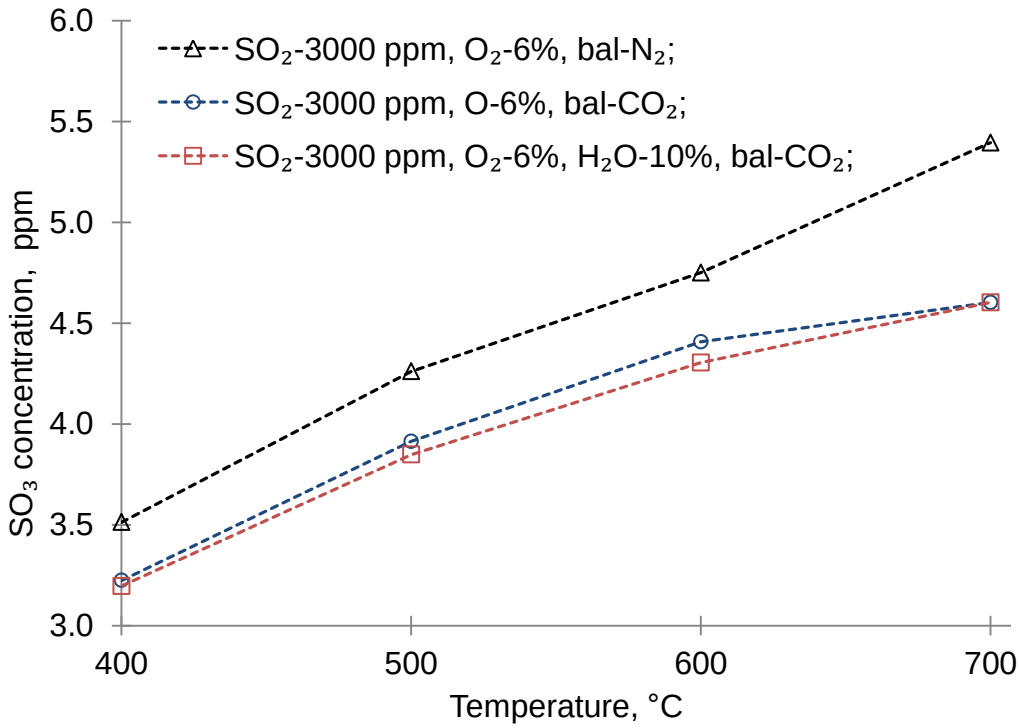

Figure 4-1 Effect of temperature on SO_3 formation in fixed bed rig

temperature falls, but the reaction rate is very slow and it cannot reach equilibrium during the short residence time typically used in most studies. The results are consistent with previous studies of Belo *et al.* (2014) and Fleig *et al.*

(2013). Replacing N_2 by CO_2 has showed very slight effect on the SO_3 formation at the tested temperatures, which indicates CO_2 serve essentially as an inert in the SO_3 formation. This behaviour is different from the results of Fleig *et al*. (2013), where CO_2 favours SO_3 formation at higher temperature range. At lower temperature, CO_2 is thermally stable and the third body efficiency of CO_2 in reaction (6) under this condition is also expected to be low.

The effect of temperature on SO_3/SO_2 conversion from the bubbling fluidised bed tests is illustrated in Figure 4-2. The SO_3 concentrations were measured during the simulated flue gas composition of air. The actual concentrations were plotted as SO_2/SO_3 conversion rate and compared with available studies. It can

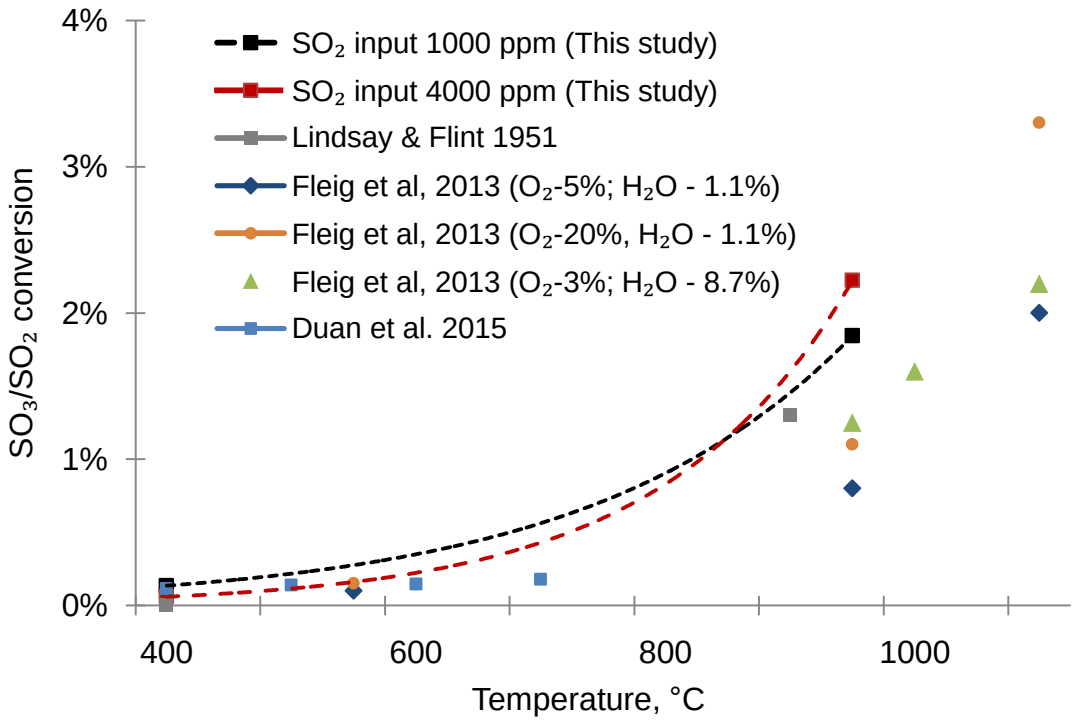

Figure 4-2 Uncatalysed SO_3/SO_2 conversion in BFB rig and comparison to the available data

This study: SO_2-1000/4000ppm, O_2-4%, CO_2-17%, H_2O-6%, bal-N_2, res.t[ee]-3s;
Lindsay and Flint, 1951; SO_2-1400 ppm, O_2-21%, H_2O-8%, bal-N_2, res t-4.3 s;
Fleig et al. 2013, SO_2-1000ppm, O_2-5/20%, H_2O-1.1/8.7%, bal-N_2, res.t-5s;
Duan et al. 2015, SO_2-3000ppm, O_2-5%, H_2O-6%, bal-N_2, res.t-1.5s;

[ee] Res.t-residence time (SI unit-seconds)

be seen that the SO_3/SO_2 conversion at 400°C is negligible and found in the range 0.1% in both levels of SO_2 concentrations. An increase of SO_3/SO_2 conversion with temperature was noted. The SO_3/SO_2 conversion at 950°C was 1.84% and 2.22%, with SO_2 of 1000 and 4000 ppm, respectively. In order to ensure the quality of the obtained data, the results are plotted against the previous studies from the literature, see Figure 4-2. In the fixed bed SO_3 measurements under oxy-fuel conditions, this trend was 0.12% at 400°C and increased gradually to 0.18% at 700°C that corresponds to 3.5 and 5.4 ppm of SO_3 as shown in Figure 4-1. At the temperature range of 400 and 1000°C, Belo *et al*. (2014) has indicated an exponential curve of SO_3/SO_2 conversion by using the kinetic model proposed by Burdett *et al*., (1984). According to these studies, it can be concluded that the formation of SO_3 favours at relatively higher temperatures close to 700°C. It is also observed earlier by Lindsay and Flint, (1951) that the formation of SO_3 at below 500°C is insignificant. Similar observation was also noted by Fleig *et al*. (2013), at the temperatures below 500°C. The authors have tested SO_3 formation in the heated vertical tube reactor at different flue gas composition conditions, where O_2 and H_2O concentrations were varied as seen Figure 4-2.

4.1.2 Effect of steam and oxygen

Effect of steam concentration over the temperature can be noted in Figure 4-1. More pronounced effect was observed at 700°C. This matches with the trend of Fleig *et al*. (2013), who has investigated SO_3 at temperature range between 573 and 1173°C. They suggested that the increase in H_2O concentration promotes SO_3 formation by increasing secondary SO_3 formation via $HOSO_2$ and to some extent by increasing direct SO_2 oxidation. However, Belo *et al*. (2014) found H_2O concentration from 3 to 9% at 900°C did not have much effect on the conversion of SO_2 to SO_3. Results of this study confirm that the presence of steam contributes significantly to SO_2 oxidation, presumably by means of OH radical formation. Further results on the steam effect are shown in Figure 4-3. As the H_2O concentration increases from 5% to 15%, SO_3 concentration

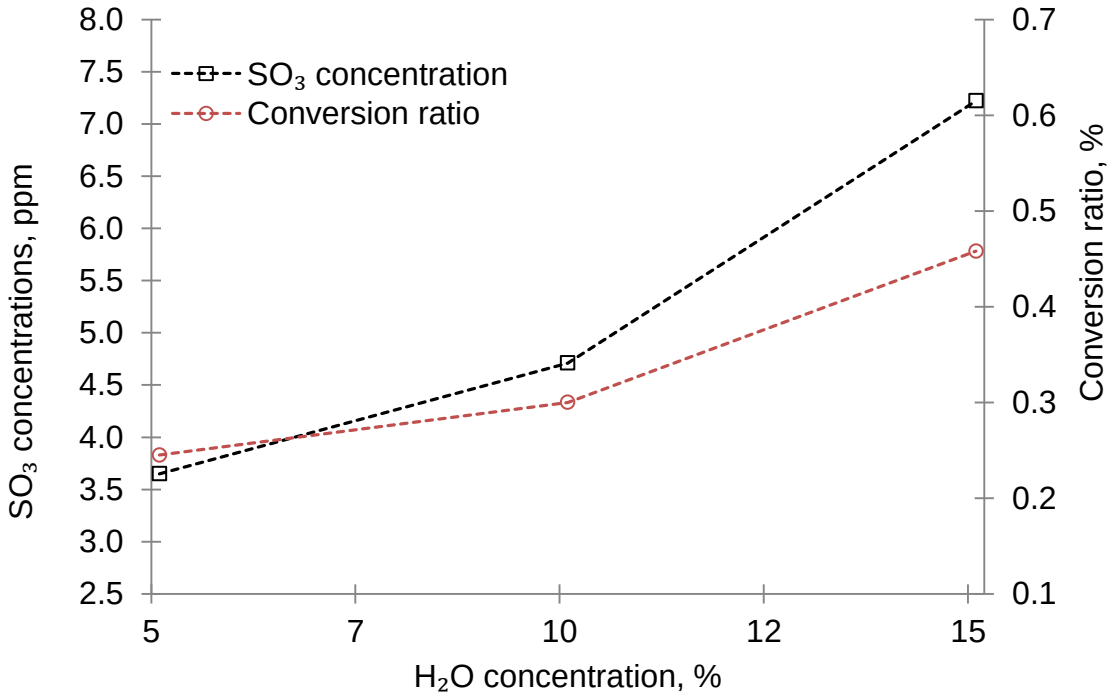

Figure 4-3 Effect of H_2O on SO_3 formation under oxy-fuel condition in fixed bed rig (Inlet of SO_2-3000 ppm, O_2-6%, bal- CO_2, t-600°C)

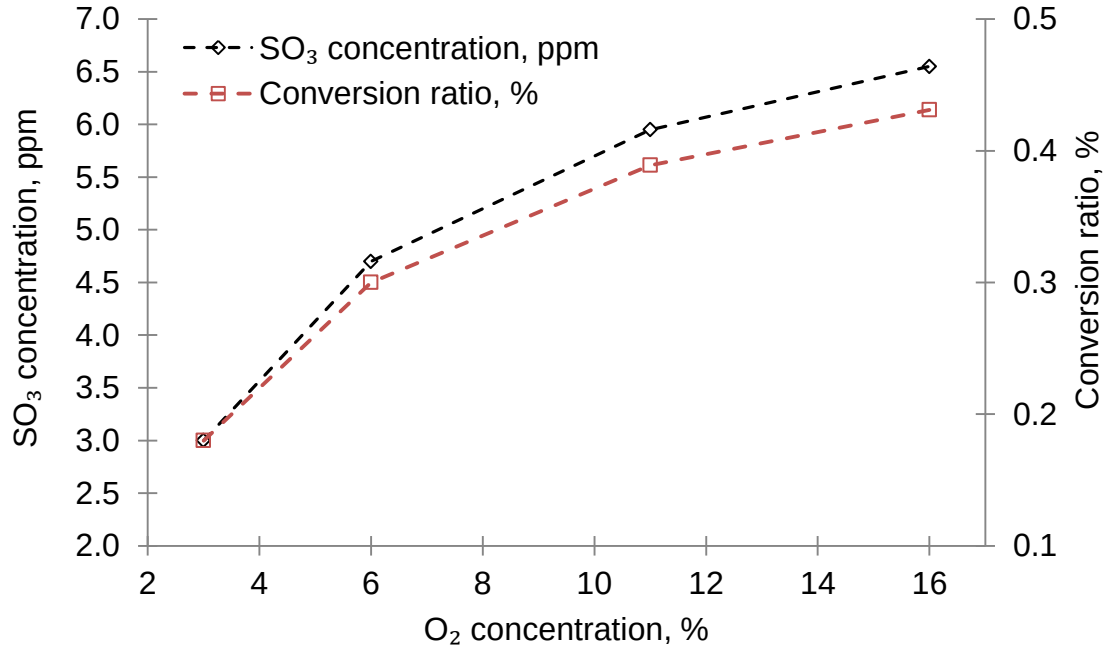

Figure 4-4 Effect of O_2 concentration on SO_3 formation under oxy-fuel atmosphere in fixed bed rig (inlet SO_2-3000ppm; H_2O-10%; bal- CO_2 t-600^{o}C)

increases from 3.7 ppm to 7.1 ppm, while the SO_2 conversion ratio increases from 0.24% to 0.46%. Figure 4-4 shows the effect of O_2 concentration on SO_3 formation. As anticipated, the oxygen enrichment elevates the SO_3 formation because there is more molecular oxygen available. At the low temperature used in this study, the excess oxygen serves as molecular oxygen which shifts the reaction (7) to the right side. As O_2 concentration increases from 3% to 6%, SO_3 concentration increases from 3.0 ppm to 4.7 ppm. Further increasing O_2 does not lead to significant increase of SO_3 formation and an increase in the associated SO_2 conversion ratio.

4.1.3 Effect of SO_2 concentrations

Effect of SO_2 concentrations on SO_3 formation during the fixed bed tests is shown in Figure 4-5. SO_2 concentration varied from 2000 ppm to 5000 ppm in this study and was chosen to represent the oxy-fuel combustion condition with RFG. A good linear fit can be achieved for the SO_3 concentration over the SO_2 concentration. As the O_2 concentration (6% in this study) is higher than the SO_2

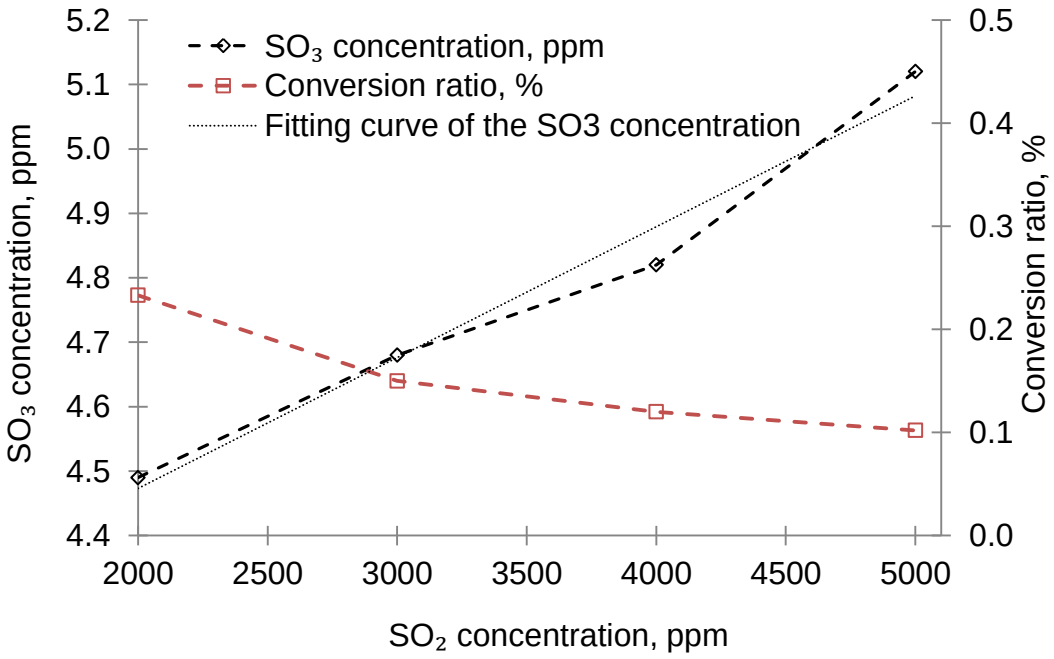

Figure 4-5 Effect of SO_2 concentration on SO_3 formation under oxy-fuel atmosphere in fixed bed rig (O_2-6%, H_2O-10%; bal-CO_2; t- 600^oC)

concentration, a pseudo-first-order reaction can describe the SO_3 formation very well. It can be also seen that the conversion ratio decreases as the SO_2 concentration increases, which corresponds to the conclusion in previous studies Belo *et al*. (2014) and Fleig *et al*. (2013).

The increasing trend of increasing SO_3 formation with increasing SO_2 concentration was also noted in bubbling fluidised bed tests, see Figure 4-6. The increase of SO_3 concentrations with SO_2 were noted at both temperatures. At 400°C, the effect of SO_2 on SO_3 concentrations was higher under air flue gas composition. The SO_3 concentrations under of an air environment increased from 1.6 to 2.2 ppm, while under an oxy-fuel environment the formation was less 1 ppm. However, it is expected that oxy-fuel combustion generates higher SO_3 concentrations in comparison to air. However, the trend of SO_3 formation at 400°C shows gradual increase that agrees with the results seen in the literature. It should be noted that the formation of SO_3 at low temperatures is significantly low. Therefore, some experimental error present in these tests. At 950°C, slightly different trend of SO_3 was observed under constant concentrations of

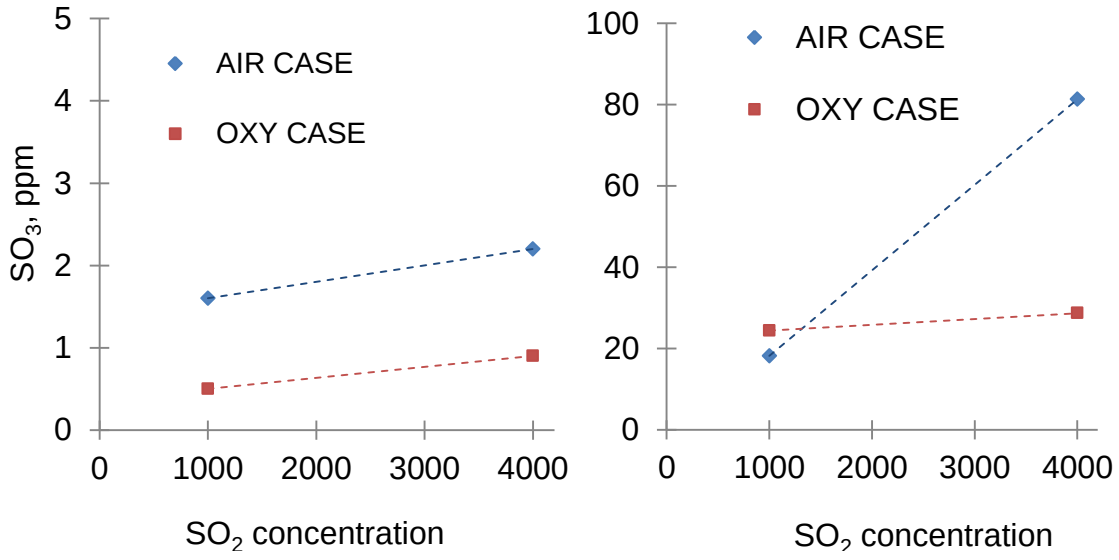

Figure 4-6 Effect of SO_2 concentrations in BFB rig (Flue gas composition: Air: O_2-4%, CO_2-17%, H_2O-6%, balance-N_2; Oxy: O_2 -5%, H_2O-11%, balance-CO_2)

SO_2-1000 ppm. The test with oxy environment was higher than the test condition of the air. In the case with high SO_2 content, 81 ppm of SO_3 was measured while only 29 ppm of SO_3 was seen in the oxy-fuel environment. Higher concentrations of SO_3 in Figure 4-6(b) could be described by condensation of SO_2 in the sampling train. This is associated with temperature control of the exit line. It could be concluded that SO_3 formation increases with increase of SO_2 concentrations at both 400 and 950°C temperatures.

4.2 Catalysed SO_3 formation

4.2.1 Catalysed SO_3 tests in a fixed bed

Fe_2O_3, V_2O_5 and CuO all play clear catalytic effect on SO_3 formation under oxy-fuel condition, as shown in Figure 4-8. V_2O_5 acts as a much stronger catalyst than Fe_2O_3 and CuO over the tested temperature range, while Fe_2O_3 is slightly stronger than CuO. According to the investigation of Dunn *et al*. (1999) on the oxidation of SO_2 over different metal oxide catalysts, the turnover frequencies of sulfur dioxide oxidation (a number of SO_2 molecules oxidised per surface metal oxide site per second) for V_2O_5 is found higher than other metal oxides tested in their work. This observation of Dunn *et al*. (1999) could be an explanation for higher catalytic effect of V_2O_5 in this work. Kim and Choi, (1981) suggested that SO_2 appears to be adsorbed essentially on the O lattice of a-Fe_2O_3 as a molecular species, while O_2 is adsorbed on an O vacancy as an ionic species and the whole catalysis mechanism of Fe_2O_3 can be express as:

$$O_2(g) + e^- \rightleftharpoons O_2^-(ads) \quad (35)$$

$$O_2^-(ads) + e^- \rightleftharpoons 2O^-(ads) \quad (36)$$

$$SO_2(g) + O^{2-}(latt) \rightleftharpoons SO_3^-(ads) + e^- \quad (37)$$

$$SO_3^-(ads) + O^-(ads) \rightarrow SO_3 + O^{2-}(latt) \quad (38)$$

V_2O_5, as the widely used catalyst on SO_2 oxidation during the sulfuric acid manufacture process, has been extensively investigated on its catalysis mechanism (Dunn *et al*., 1999). The active site for the adsorption pathway of sulfur dioxide on the catalyst surface was used proposed which can be express as:

$$SO_2(g) + (V^{5+}) \quad \leftrightarrow \quad (V^{5+})SO_2(ads) \text{ or } (V^{3+})SO_3(ads) \qquad (39)$$

$$(V^{5+})SO_2(ads) \quad \text{or} \quad (V^{3+})SO_3(ads) \quad \rightarrow SO_3(g) + (V^{3+}) \qquad (40)$$

$$O_2 \quad \leftrightarrow \quad 2\,O - (ads) \qquad (41)$$

$$O^-(ads) + (V^{3+}) \quad \rightarrow \quad (V^{5+}) \qquad (42)$$

CuO has also been confirmed as a catalyst in SO_2 oxidation (Macken *et al*., 2000);(Tseng *et al*., 2003).

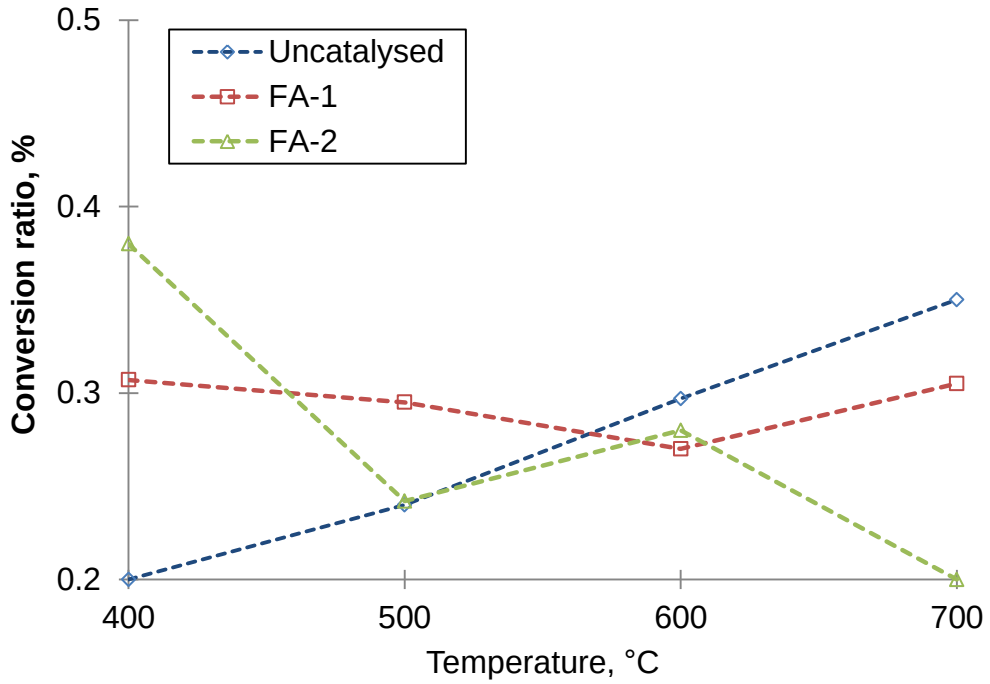

Figure 4-7 Effect of fly ash on the SO_3 formation under oxy-fuel condition in fixed bed rig (O_2 concentration: 6%, H_2O concentration: 10%; CO_2 balance)

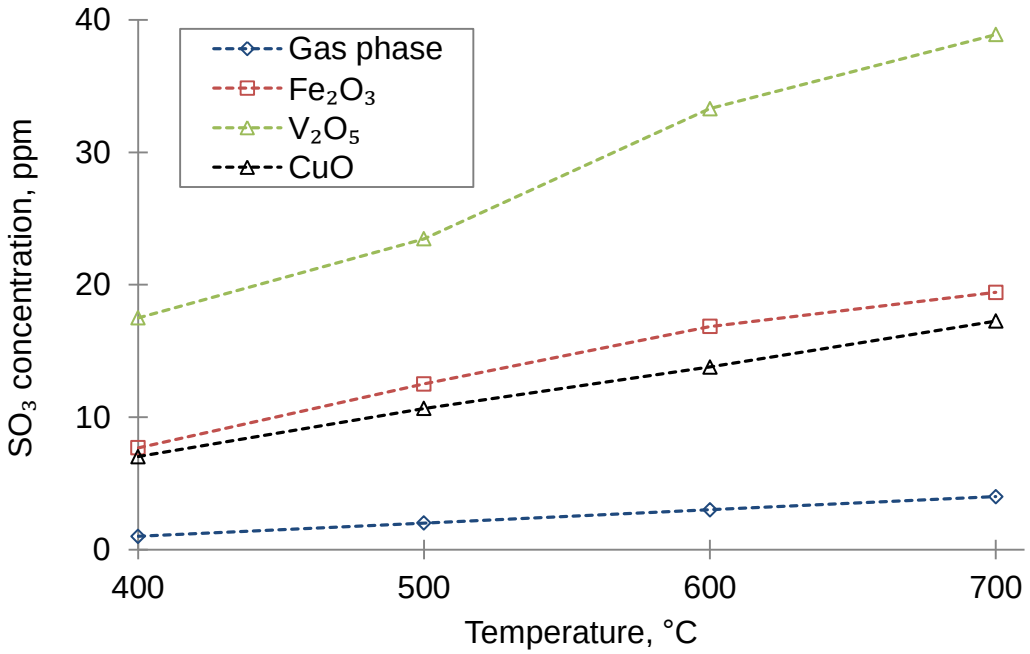

(a)

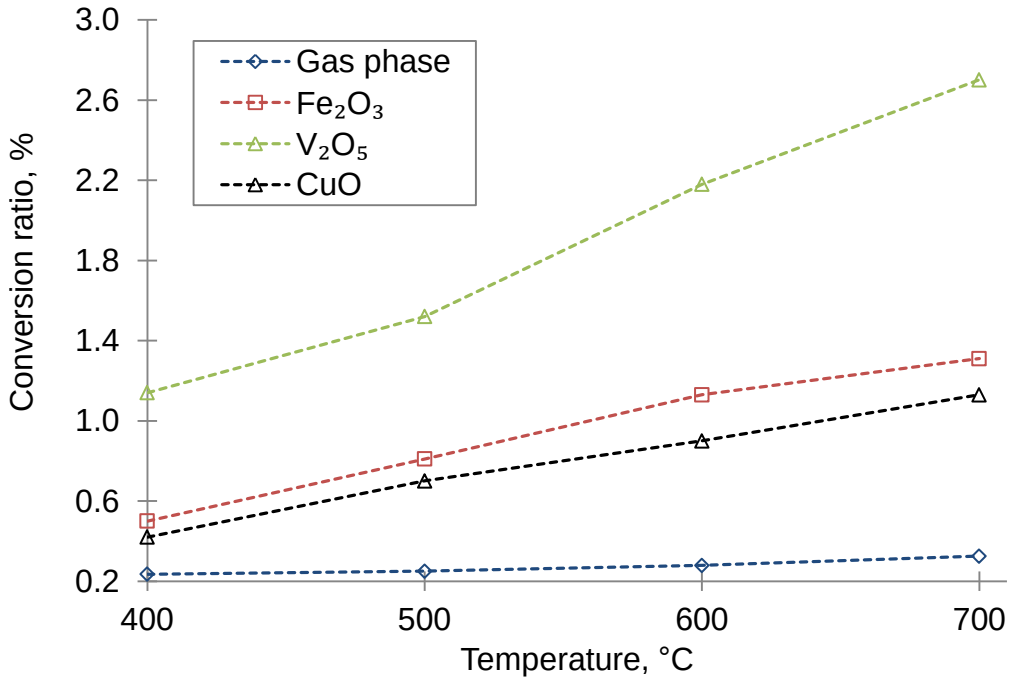

(b)

Figure 4-8 Effect of metal oxides on the SO_3 formation under oxy-fuel condition in fixed bed rig (O_2-6%, H_2O-10%; bal- CO_2)

The effects of the fly ash on SO_3 formation at different temperature under oxy-fuel condition are shown in Figure 4-7. At 400^{o}C, Fly ash-1 and Fly ash-2 both exhibit catalysis effects on the SO_3 formation, and Fly ash 2 has a larger catalytic effect than Fly ash-1 at 400°C. This is probably because the Fe_2O_3 content in ash 2 is higher than in Fly ash-1. At 500^{o}C, the two fly ashes still catalyse SO_3 formation even though the catalysis effect for ash 2 is minor.

With a further increase of the temperature to 600°C, SO_2 conversion ratios with fly ash are even less than those via gas phase reaction, indicating no catalysis takes place or the catalytic effect is dominated by other effects. At the highest temperature 700°C, the conversion ratios with the two fly ashes are both much lower than that from the gas phase. The conversion ratio with fly ash 2 is the lowest, which indicates the alkali and alkaline earth metal oxides like CaO can absorb the SO_3 and causes the SO_3 in the gas phase to decrease. This is in agreement with experience that the sulfur retention rate by CaO increases as the temperature increases. The results are different from the previous conclusion by Belo *et al*., (2014), which may be due to the large difference between the compositions of the fly ashes. The materials used in their study contain only a small amount of alkali and alkaline earth metal oxide, so any retention effect is insignificant. However, in our study, both fly ashes have relatively high CaO content, which will retain SO_3 rather than catalyse its formation (Marrier and Dibbst, 1974). Overall, the effect of fly ash on SO_3 formation seems to be largely decided by the ash composition.

4.2.2 Catalysed SO_3 tests in a bubbling fluidised bed

Catalytic effect of fly ashes on SO_3 formation were demonstrated from the uncatalysed SO_3 data, see Figure 4-9 and Figure 4-10. Figure 4-9 (a, b) shows experimental results with 1000 and 4000 ppm of SO_2 concentrations at 400°C. A stronger catalytic effects was seen with Fly ash-4 forming roughly 10 ppm under both air and oxy-fuel environments. A weaker, but still noticeable effect of oxy-fuel environment was observed for Fly ash-3 and Fly ash-4 at 400°C, see Figure 4-9(a). Higher SO_3 in the oxy-fuel tests can be explained by the increased concentrations of O_2 and H_2O that follow secondary SO_3 formation

route as in accordance with the reactions (6) and (7). Similar results were seen by Fleig *et al.* (2011); Belo *et al*., (2014). The reason for the lower SO_3 formation with Fly ash-3 FA could be due to the adsorption of sulfur by alkaline metal oxide compounds such as CaO and MgO. This agrees with conclusions of Marrier and Dibbst, (1974) and Cao *et al*., (2010).

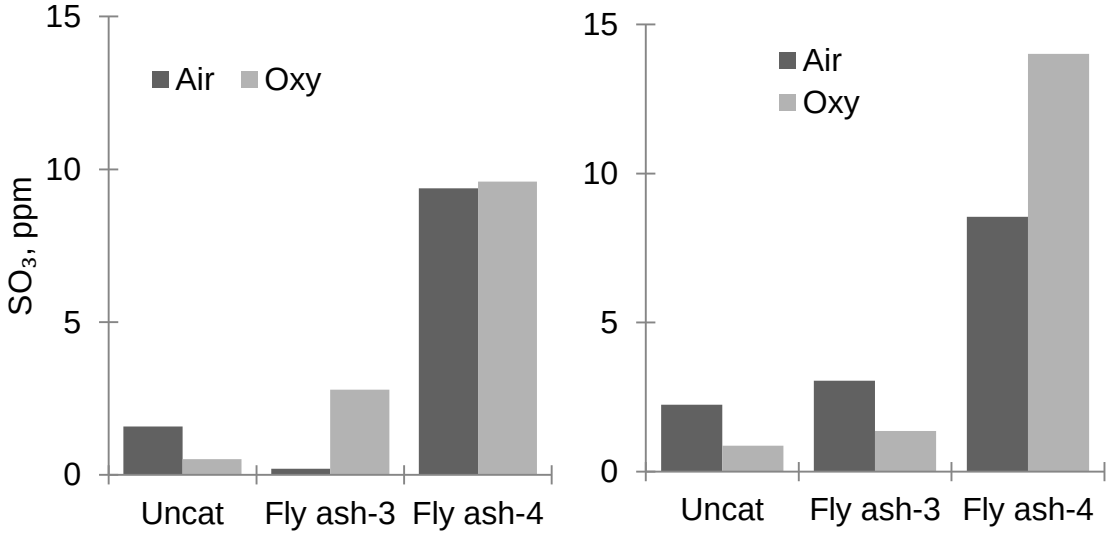

(a) SO_2-1000 ppm (b) SO_2-4000 ppm

Figure 4-9 Catalytic effect of FA on SO_3 formation at 400°C in BFB rig

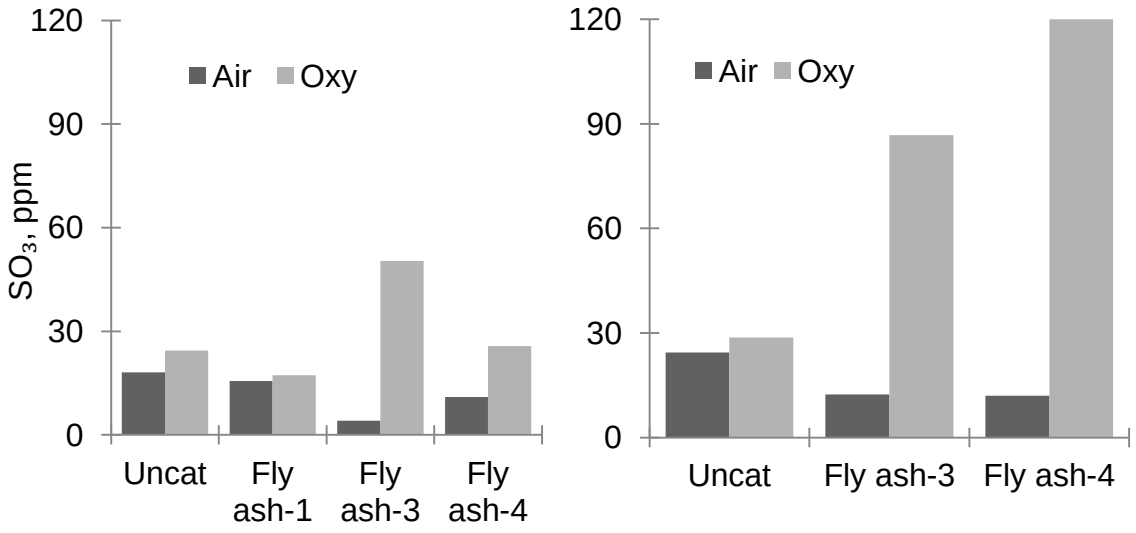

(a) SO_2-1000 ppm (b) SO_2-4000 ppm

Figure 4-10 Catalytic effect of FA on SO_3 formation at 950°C in BFB rig

Similarly, lower SO_3 concentrations was also noted by Ahn *et al*., (2011), in a pilot-scale 1.5 MW oxy-PC unit when PRB coal was used with high CaO content. At tests with 4000 ppm, 9 to 14 ppm of SO_3 concentration was detected for Fly ash-3 and Fly ash-4 under air and oxy environments, as shown in Figure 4-9(b). The increase of SO_2 concentrations from 1000 ppm to 4000 ppm had a minor effect in the presence of Fly ash-3 ash under both test environments. Lower SO_3 concentrations under oxy-fuel environment could be due to the slow reaction kinetics. The difference between air and oxy-fuel cases was roughly 1.5 to 2 ppm. Previous investigations of Belo *et al*., (2014) and Duan *et al*., (2015), have indicated negligible SO_3 concentrations at temperatures of 400°C and below.

Catalysed SO_3 formation data at 950°C were presented in Figure 4-10 (a, b). The effect of an oxy-fuel environment was more pronounced at 950°C than at 400°C. The results revealed that higher SO_3 were formed under oxy-fuel environments compare to air environments. It should be noted that higher concentration of SO_3 was observed under oxy-fuel tests for Fly ash-3 see Figure 4-10 (a). In contrast to air combustion environment, slightly higher than SO_3 concentration is observed in oxy-fuel environment which is still agrees with the previous studies. Higher SO_3 concentration could also occur due to the temperature drop of the exit gas in the exhaust section resulting reaction of SO_2 and steam to form sulfuric acid in the sampling glass. However, this value corresponds to the SO_3/SO_2 conversation of 5% which found to be similar to the thermodynamic equilibrium value of 5%. It is evident from these results that the increased O_2 and H_2O concentrations under oxy-fuel conditions favour the formation of SO_3.This is in agreement with the results of Belo *et al*., (2014), Ahn *et al*., (2011) and Eddings *et al*., (2010). In addition, it could be noted from Figure 4.10 (a) that alkaline compounds adsorbed most SO_2 and SO_3 concentrations under air environment. Similarly, lower SO_3 concentration was observed in 4000 ppm tests, see Figure 4.10 (b). The justification of this reaction between alkaline metal compounds (CaO and MgO) in Fly ash-3 and sulfur could be seen from Figure 4-11 (a). A decrease of CaO and MgO are observed before and after the tests at 950°C.

As expected, higher SO_3 concentrations were seen under oxy tests than in air tests, see Figure 4-10 (b). Higher SO_3 could be due to the steam, O_2 and CO_2 concentrations that favour SO_3 formation. Furthermore, the third body efficiency in reactions (1) and (2) are higher for CO_2 than N_2 (Fleig *et al*., 2013). Another reason for lower SO_3 under air tests could be caused by an unburnt carbon compound in the Fly ash-4 and Fly ash-1. As noted by Marrier and Dibbst, (1974), unburnt carbon in the ash leads to lower formation of SO_3 as available O_2 reacts mainly with carbon at high temperatures. To support this hypothesis, it should be noted that the stoichiometric estimation of these test conditions shows that roughly 20% of O_2 was reacted with carbon in the tests with Fly ash-1. This value was 4% for Fly ash-3 and 9% for Fly ash-4. The level of unburnt carbon in the ashes is shown in the TGA analysis in Figure 3-11. In addition to that, the absence of SO_3 was noted during the coal gasification tests conducted by Roy *et al*. (2014) in a small-scale FB reactor. In their work, Victorian brown coal was investigated under pyrolysis, oxy-fuel combustion and gasification processes. The authors have noted 10% sulfur conversion to SO_3 during the oxy-fuel tests, while no SO_3 was observed during pyrolysis and gasification tests.

Figure 4-11 (a, b, c) provides the chemical composition of bed materials determined by XRF analysis. Only, five metal oxides compounds such as CaO, MgO, Al_2O_3, Fe_2O_3 and SO_3 were selected to compare initial and final states. Final states of the fly ashes illustrated in Figure 4-11 (a, b, c) are from high temperature tests. CaO in the Fly ash-3 reduced from 25% to an average value of 8%, while MgO has dropped from 9 to 2%. These trends for Fly ash-4 and Fly ash-1 ashes were only 2% for CaO and 1% for MgO, respectively. The reason for the decrease of CaO and MgO was due to its reaction with SO_2. This reaction result in the SO_2 capture as discussed earlier in section 2.5.2. As noted in the literature, CaO and MgO adsorb SO_2 concentration by forming $CaSO_4$ and $MgSO_4$ in the presence of O_2. This behaviour of SO_2 capture was seen in separate tests where SO_2 concentration was monitored after feeding each fly ash into the BFB rig, see Appendix F. Significant reduction of metal oxides such as Fe_2O_3 and Al_2O_3, were detected with Fly ash-4 and Fly ash-3. This reduction

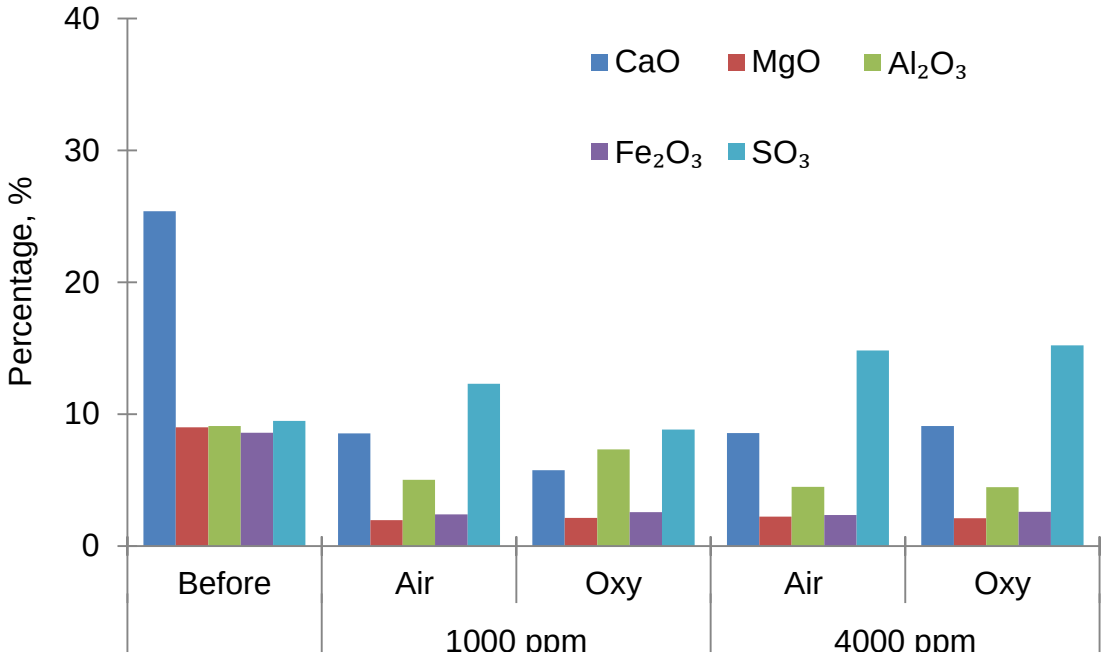

(a) Fly ash-3

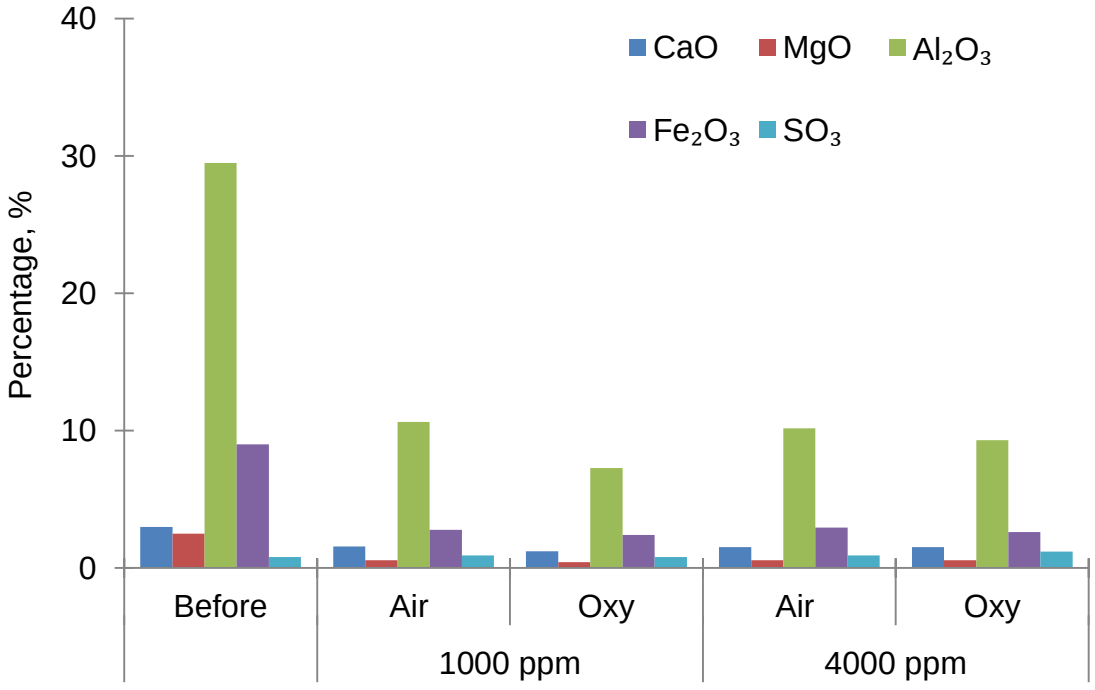

(a) Fly ash-4

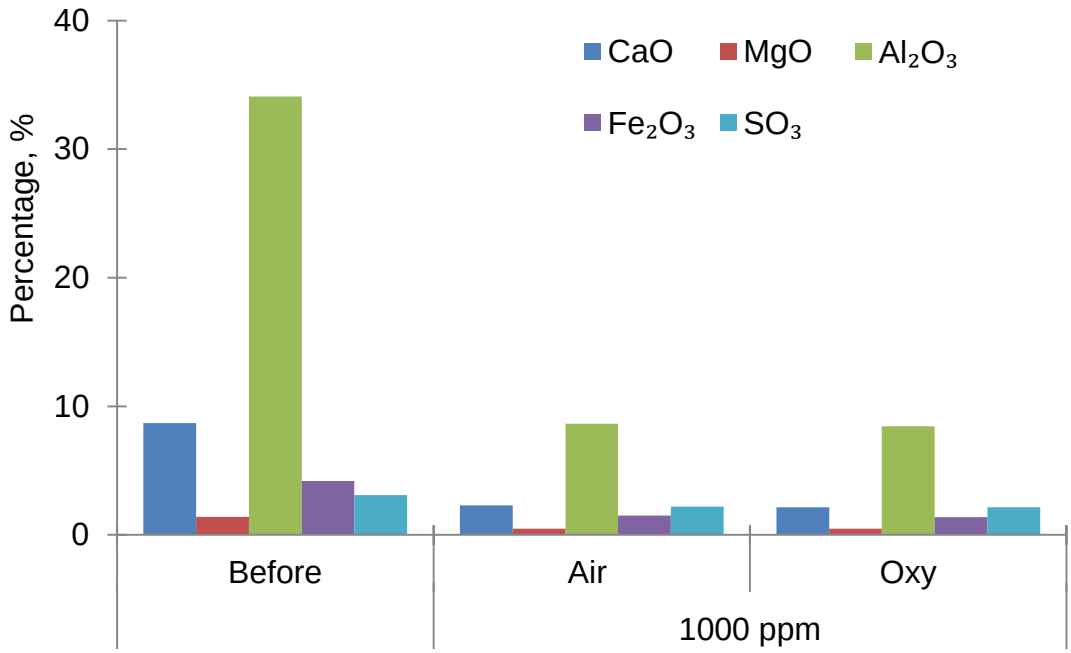

(c) Fly ash-1

Figure 4-11 Change of metal oxides in the fly ashes (before and after tests at 950°C) in BFB rig

of catalytic metal oxides is also associated with the oxidation of SO_2. The reaction mechanisms of SO_2 oxidation on Fe_2O_3 catalyst is provided in reactions (39–43). Full compounds on XRF analysis of bed material and fly ash during the tests are provided in Appendix D. Based on these XRF analyses, it could be concluded that fly ash with higher alkaline metal oxide CaO content could absorb SO_3, while higher Fe_2O_3 and Al_2O_3 favours the formation of SO_3.

4.2.3 SO_3 tests in a 50 kW oxy-CFB unit

Concentrations of SO_3 and the gases during pilot oxy-fuel CFB combustion with a wet RFG are shown in Figure 4-12. The overall oxygen concentration during oxy-fuel combustion was kept at around 23.4% to maintain a similar bed temperature and a similar exit oxygen concentration to those in air combustion. SO_2 concentration is observed to be higher during oxy-fuel combustion (Ca/S molar ratio = 4) than that in air combustion (Ca/S molar ratio = 2.5) due to the accumulation by gas recycle, even though more limestone has been injected

into the furnace during oxy-fuel operation. Due to the amount of the flue gas during oxy-fuel combustion being only about one fourth of that during air combustion higher limestone injection can largely decrease the total SO_2 emission amount rather than decrease the SO_2 concentration in the flue gas under oxy-fuel combustion (Duan *et al*., 2014). Consequently, SO_3 concentration during oxy-fuel combustion was 7.9 ppm, about 4.5 times that in air combustion. Furthermore, H_2O concentration in the flue gas during oxy-fuel combustion was 17.4% compared with 7.1% in air combustion, which also favours the SO_2 conversion to SO_3 under oxy-fuel combustion. For the fly ash, it has been found (Duan *et al*. 2011) calcium presents more likely in the form of $CaCO_3$ rather than CaO due to the higher partial pressure of CO_2 under oxy-fuel CFB combustion. The absorption reaction between CaO and SO_3 is faster than that between $CaCO_3$ and SO_3 (Anthony and Granatstein, 2001). The combined influence of these factors causes a higher SO_3 concentration during oxy-fuel CFB combustion. This result is also in agreement with the results from fixed bed rig, which confirm that SO_3 during oxy-fuel CFB combustion is mainly formed via the reactions (6) and (7). The higher SO_2 and H_2O concentration together with the low retention ability of fly ash in the flue gas enhances the SO_3 formation.

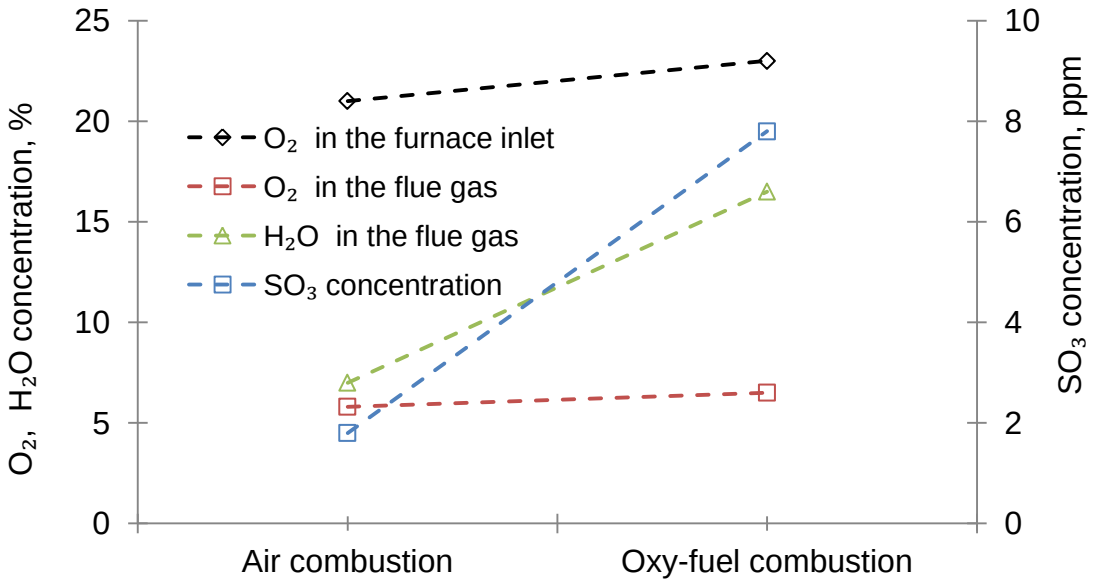

Figure 4-12 SO_3 concentration during oxy-fuel CFB pilot test

5 SUMMARY OF THE RESULTS

The experimental results of SO_3 formation are presented from three different rigs. The work also includes the characterisation of bed material for metal oxides and fly ashes that served as catalysts. Experiments were done separately for uncatalysed and catalysed SO_3 formation in fixed bed and bubbling fluidised bed rigs. For validation purpose of an experimental data, the thermodynamic equilibrium curves of SO_2 to SO_3 conversion were plotted. It is seen that the experimental results have not exceed the thermodynamic equilibrium. This means that the data obtained during the tests are reliable. The thermodynamic equilibrium curves of this work were also validated with the results of literature.

During uncatalysed tests, following parameters as O_2, SO_2, H_2O concentrations and reactor temperature were changed to investigate its effect on SO_3 formation. Uncatalysed SO_3 formation tests have demonstrated presentable results to the data available in the literature. In the fixed bed tests, the increase of temperature in the reactor has shown a clear effect on SO_3 concentration. In addition, the increase of H_2O in the mixture gas has also increased SO_3 concentration. As discussed in 2.5.1, this increase occurs due to the formation of OH radicals, which favours the secondary formation of SO_3. Replacing the N_2 to CO_2 at the temperature below 700°C has showed a negligible difference. This is explained by third-body effect. It is found that the third body effect of CO_2 at temperatures lower than 700°C is low and CO_2 mainly serves as an inert gas. SO_3 concentration has also increased notably with an increase of O_2 and SO_2 concentrations in both bench scale tests. In the bubbling fluidised bed, significant increase of SO_3 concentration was noted at higher temperatures than at lower temperature tests.

In catalysed tests, metal oxides such as Fe_2O_3, V_2O_5 and CuO could play a catalytic effect on the SO_3 formation under both air and oxy-fuel condition. However, catalytic or adsorption effect of fly ash compounds depends on the metal oxides and alkaline earth metal oxide compounds. Higher percentage of metal oxides and lower percentage of alkaline metal oxides in the fly ash tend to

increase the catalytic effect of SO_2 to SO_3. A reverse effect could be expected if a higher percentage of alkaline metal oxides is exists in the fly ash. This was noted with Canadian FA tests that had a higher percentage of alkaline metal oxides in BFB tests. When British FA is employed with higher metal oxide compounds, the higher SO_3 formation was observed at 950°C. In addition, fly ash with unburnt carbon content has led to a lower formation of SO_3. This could be explained by the fact that O_2 in the mixture mainly reacts with carbon in fly ash and only remained O_2 will react to SO_2 to form SO_3.

During the bituminous coal combustion in a pilot-scale oxy-CFB unit, a notable increase of SO_3 is observed. SO_3 concentration was 4.5 higher in oxy-fuel combustion than in air combustion environment. The results observed during the pilot-scale tests are in good agreement with data available in the literature.

5.1 The applicability of the results

Preventing the formation of SO_3 and its conversion to sulfuric acid is a long term technical challenge for engineers to design combustion systems. The findings of this work could support boiler industry to develop a better concept for oxy-fired fluidised combustion process and also controlling the flue gas temperature. The results of this work could be beneficial for existing power plants with fluidised bed technology, particularly where coals with high sulfur content are utilised.

In regard to the SO_3 sampling methods, the developed controlled condensation method in this work has shown a reliable method which could be adopted for the field applications. SO_3 concentration observed in this work provides a good prediction in regards to the SO_2 concentration in the flue gas. The effect of flue gas recirculation is another important part for controlling the formation of SO_3. Therefore, special measures should be given to the impurities in the recycled flue gas, including the flue gas recirculation condition (dry and wet FGR). Results with the fly ash provided a good understanding of the SO_3 formation. Catalytic effect or sulfur retention depends on the metal composition of the fly ash. Higher alkalinity content in the ash could capture most SO_3 formed in the combustion process, while metal oxides could increase SO_3 concentration significantly.

6 FINAL CONCLUSIONS AND FUTURE WORK

6.1 Conclusions

In this thesis, the formation of SO_3 is investigated under air and oxy-fuel combustion environments. SO_3 measurements were conducted in a number of rigs including a fixed bed, bubbling fluidised bed and pilot-scale 50 kW pilot-scale oxy-CFB units. Homogeneous SO_3 formation was performed in the bench-scale rigs and compared with heterogeneous tests in which different types of fly ashes and metal oxides were added as catalysts. In a pilot-scale unit, SO_3 concentration was measured under real coal combustion environment, under air and oxy-fuel environments. The controlled condensation method was developed method for SO_3 concentration and employed in all tests.

1. The following conclusions can be withdrawn from literature review:
    - Wet RFG results in the higher SO_3 concentration than in dry RFG. An increased amount of H_2O promotes SO_3 formation due to the production of OH radicals. This in turn promotes the secondary formation of SO_3. However, when H_2O concentration higher than 15% in the system strongly inhibits SO_3 formation. This was more pronounced in actual PC experiments rather than simulated flue gas experiments;
    - Higher and rapid conversion of S to SO_3 occurs near the burnout region where oxygen is found in excess amount. In this region, gas-phase homogeneous formation is found more dominant to promote the formation of SO_3;
    - The presence of reducing gases as NO, CO is likely to enhance SO_3 formation; however, their effect appear to be small compare to other factors such as combustion temperature, excess O_2 and presence of catalysis;
    - SO_3 formation is enhanced due to the metal compounds in fly ash. Among the chemical compounds that exist in the fly ashes Fe_2O_3 and V_2O_5 appear to catalyse SO_3 formation strongly.
    - It should be noted that, all the current post combustion SO_3 measurements still have technical challenges as SO_3 is a very labile

molecule. Thus some of SO_3 will be lost when it reaches sampling point. At present, the CCM method remains as the most used and reliable technique to quantify SO_3 concentrations, while other methods such as salt method and calcium oxalate with glass beads need to be improved.

2. Experimental results in a fixed reactor have showed an increasing trend of SO_3 concentrations under increasing bed temperature from 400 to 700°C. A notable effect of SO_2 and H_2O concentrations on SO_3 formation were observed during the homogeneous tests. The increase of H_2O in the flue gas resulted to a higher concentration of SO_3 which agrees with the literature findings. In the heterogeneous tests, where different the metal oxides and fly ashes were tested V_2O_5 has showed a strong catalytic effect.
3. In the pilot-scale oxy-CFB units, SO_3 concentration was 4.5 times higher under oxy fuel combustion than in the air combustion environment.
4. Bubbling fluidised bed tests have showed a strong effect of bed temperature on SO_3 formation. This was more pronounced in oxy-fuel flue gas composition. At temperature of 950°C, the reduction of metal oxides before and after the tests supports the hypothesis that the formation or absorption of SO_3 strongly depends on Fe_2O_3, Al_2O_3, and alkaline compounds CaO, MgO. It is also noted that the presence of unburnt carbon in the fly ash lowers the formation of SO_3. The SO_3 concentration was several times higher than in a pilot-scale oxy-fuel test with a wet RFG.

6.2 Future work

A significant amount of effort has been made to evaluate SO_3 concentrations at the laboratory scale as well as at commercial scale units. However, oxy-fuel combustion still requires more attention in terms of better understanding SO_3 formation mechanisms. At this point, the majority of SO_3 measurements have conducted in conventional PC and gas-fired combustion systems, while there only a few results available for oxy-fired FB combustors and pilot-scale studies are still sparse. More research should concentrate on the effect of FGR and catalysed SO_3 formation degree. Uncatalysed and catalysed SO_3 formation both

depend on reducing gases such as (NO, CO) and their effects may be different in oxy-fuel combustion and hence more experiments are needed on SO_3 formation with different types of coals. Development of pressurised FBC systems would also require SO_3 investigations as the effect of pressure was not well studied experimentally.

In the case of analytical methods, all the current post combustion SO_3 measurements still have technical challenges associated with them because SO_3 is a very labile molecule. It is revealed that some of SO_3 will be lost when it reaches sampling point. At present, the CCM method remains as the most used and reliable technique to quantify SO_3 concentrations, while other methods such as salt method or calcium oxalate with glass beads need to be improved.

REFERENCES

Abele, A.R., Kindt, G.S., Clark, W.D., Payne, R. and Chen, S.L. (1987) 'An experimental program to test the feasibility of obtaining normal performance from combustors using oxygen and recycled gas instead of air', Report: ANL/CNSV-TM-204, Argonne National Laboratory, Argonne, IL.

Ahn, J., Okerlund, R., Fry, A. and Eddings, E.G. (2011) 'Sulfur trioxide formation during oxy-coal combustion', *International Journal of Greenhouse Gas Control*, 5S pp. S127-S135.

Aimard, N., Prebende, C., Cieutat, D., Molinero, I.S. and Tsiava, R. (2008) 'The CO_2 Pilot at Lacq', *Proceedings of the 3rd Workshop IEAGHG International Oxy-Combustion Network*. Yokohama, 5-6 March 2008.

Andersson, K. and Johnsson, F. (2006) 'Process evaluation of an 865 MWe lignite fired O_2/CO_2 power plant', *Energy Conversion and Management,* 47(18–19), pp. 3487–3498.

Anheden, M., Rydberg, S. and Yan, J. (2008) 'Consideration for removal of non-CO_2 components from CO_2 rich flue gas of oxy-fuel combustion', *Proceedings of 3rd Workshop IEAGHG International Oxy-Combustion Network*. Yokohama, 5-6 March 2008.

Anthony, E.J. (2013) 'Oxyfuel CFBC Status and anticipated development' *Greenhouse Gases: Science and Technology*, 3 (2), 166–123. doi: 10.1002/ghg.1324.

Anthony, E.J. and Granatstein, D.L. (2001) 'Sulfation phenomena in fluidized bed combustion systems', *Progress in Energy and Combustion Science*. Doi: 10.1016/S0360-1285(00)00021-6.

Armitage, J.W. and Cullis, C.F. (1971) 'Studies of the reaction between nitrogen dioxide and sulfur dioxide', *Combustion and Flame,* 16(2), pp.125–130.

Aspelund, A. and Jordal, K. (2007) 'Gas conditioning-the interface between CO_2 capture and transport', *International Journal of Greenhouse Gas Control,* 1(3), pp. 343–354. doi: 10.1016/S1750-5836(07)00040-0.

Attar, A. (1978) 'Chemistry, Thermodynamics and kinetics of reactions of sulphur in coal-gas reactions: A review', *Fuel,* 57(4), pp. 201–212. doi: 10.1016/0016-2361(78)90117-5.

Barret R.E., Hummell, J.D. and William, T.R. (1966) 'Formation of SO_3 in a Noncatalytic Combustor. Journal of Engineering for Power', *Transactions of the ASME*, 88, pp. 165–172.

Bayless, D.J., Jewmaidang, J., Tanneer, S. and Birru, R. (2000) 'Kinetics of low-temperature homogeneous SO_3 formation for use in flue gas conditioning for improved electrostatic precipitator performance', *Proceedings of the Combustion Institute*, 28, pp. 2499–2505.

Belo, L.P., Elliott, L.K., Stanger, R.J., Spörl, R., Shah, K.V., Maier, J. and Wall, T.F. (2014) 'Laboratory investigations on the differences in the homogeneous and catalytic conversions with fly ash of SO_2 to SO_3 from air and oxy-fuel PF combustion', *Presented In: Impacts of Fuel Quality on Power Production,* Utah, 1–30.

Belo, L.P., Elliott, L.K., Stanger, R.J., Spörl, R., Shah, K.V., Maier, J. and Wall, T.F. (2014) 'High-Temperature Conversion of SO_2 to SO_3: Homogeneous experiments and catalytic effect of fly ash from air and oxy-fuel firing', *Energy & Fuels*, 28, pp. 7243–7251. doi: 10.1021/ef5020346.

Blitz, M.A., Hughes, K.J. and Pilling, M.J. (2003) 'Determination of the high-pressure limiting rate coefficient and the enthalpy of reaction for OH + SO_2', *Journal of Physical Chemistry A*, 107(12), pp. 1971–1978.

Boot-Handford, M.E., Abanades, J.C., Anthony, E.J., Blunt, M.J., Brandani, S., Dowell, N.M., Fernández, J.R., Ferrari, M.C., Gross, R., Hallett, J.P., Haszeldine, R.S., Heptonstall, P., Lyngfelt, A., Makuch, Z., Mangano, E., Porter, R.T.J., Pourkashanian, M., Rochelle, G.T., Shah, N., Yao, J.G. and Fennell, P.S. (2014) 'Carbon capture and storage update', *Energy & Environmental Science*, 7(1), pp. 130-189. doi: 10.1039/c3ee42350f.

Brix, J., Navascués, L.G., Nielsen, J.B., Bonnek, P.L., Larsen, H.E., Clausen, S., Glarborg, P. and Jensen, A.D. (2013) 'Oxy-fuel combustion of millimeter-sized coal char: particle temperatures and NO formation', *Fuel,* 106, pp.72–78. doi: 10.1016/j.fuel.2013.01.017.

Bryers, R.W. (1996) 'Fireside slagging, fouling, and high-temperature corrosion of heat-transfer surface due to impurities in steam-raising fuels'. *Progress in Energy and Combustion Science*, 22, pp. 29–120.

Buhre, B.J.P., Elliott, L.K., Sheng, C.D., Gupta, R.P. and Wall, T.F. (2005) 'Oxy-fuel combustion technology for coal-fired power generation', *Progress in Energy and Combustion Science,* 31(4), pp. 283–307. doi:10.1016/j.pecs.2005.07.001.

Burdett, N.A., Gliddon, B.J., Hotchkiss, R.C. and Squires, R.T. (1983) 'SO_3 in coal-fired fluidized bed combustors', *Journal of the Institute of Energy*, 56, pp.119–124.

Burdett, N.A., Langdon, W.E., and Squires R.T. (1984) 'Rate of the coefficients for the reaction SO_2 + O_2 = SO_3 +O', *Journal of the Institute of the Energy* 57, pp.373–376.

Burnol, A., Thinon, I., Ruffine, L. and Herri. J.M. (2015) 'Influence of impurities (nitrogen and methane) on the CO_2 storage capacity as sediment-hosted gas hydrates - Application in the area of the Celtic Sea and the Bay of Biscay', *International Journal of Greenhouse Gas Control*', 35, pp.96–109. doi:10.1016/j.ijggc.2015.01.018.

Cao, Y., Zhou, H., Jiang, W., Chen, C.W. and Pan, W.P. (2010) 'Studies of the fate of sulfur trioxide in coal-fired utility boilers based on modified selected condensation method', *Environmental Science and Technology*, 44, pp. 3429–3434.

Chamberlain, D.S., Reeder, T., Stimpson, C. K. and Tree D. R. (2013) 'A comparison of sulfur and chlorine gas species in pulverized-coal, air- and oxy-combustion', *Combustion and Flame*, 160, pp. 2529–2539.

Chang, C.C. (1978) 'Infrared Studies of SO_2 on ɣ-Alumina' *Journal of catalysis*, 53, pp. 374–385.

Colin, D. (2011) 'Impact of oxyfuel operation on corrosion in coal fired boilers based on experience with E-ON's $1MW_{th}$ combustion test facility', *Presented in the IEAGHG Special Workshop on Oxyfuel Combustion,* London, January 25. Available at: http://ieaghg.org/docs/General_Docs/TSB_Oxyfuel/01%20-%20Colin%20Davis.pdf. (Accessed: 03.10.2015).

Colorado State University. (2016) '*Chemical Equilibrium Calculation*', Available at: http://navier.engr.colostate.edu/~dandy/code/code-4/index.html. (Accessed: 18 April 2016).

Cooper, D. (1995) '*Optimisation of a NaCl Adsorbent Tube Method for SO3 Measurements in Combustion Flue Gases*', Report B-1177, Swedish Environmental Research Institute (IVL) Gothenburg. (Received by personal communication).

Cooper, D. and Andersson, C. (1997) '*Determination of SO_3 in flue gases using the NaCl method - a comparison with other techniques'*, Report U3-507 och F6-636, Varmeforsk, Stockholm.

Corley, T. L. and Wendt, J.O.L. (1984) 'Postflame behavior of nitrogenous species in the presence of fuel sulfur: II. Rich, CH_4/He/O_2 Flames', *Combustion and Flame*, 58, pp. 141–152. doi: 10.1016/0010-2180(84)90089-0.

Couling, D. (2011) 'Impact of oxyfuel operation on emissions and ash properties based on E.ON's 1MW CTF', In: *the IEAGHG Special Workshop on Oxyfuel Combustion*, January.

Croiset, E. and Thambimuthu, K.V. (2001) 'NOx and SO_2 emissions from O_2/CO_2 recycle coal combustion', *Fuel*, 80(14), pp. 2117–2121. doi: 10.1016/S0016-2361(00)00197-6.

Croiset, E., Heurtebise, C., Rouan, J.P. and Richard, J.R. (1998) 'Influence of pressure on the heterogeneous formation and destruction of nitrogen oxides during char combustion', *Combustion and Flame,* 112, pp. 33–44.

Cullis, C.F. and Mulcahy, M.F.R. (1972) 'The kinetics of combustion of gaseous sulphur compounds' *Combustion and Flame,* 18(2), pp. 225–292. doi: 10.1016/S0010-2180(72)80139-1.

Cutler, A.J.B. and Raask, E. (1984) 'External corrosion in coal-fired boilers: assessment from laboratory data', *Corrosion Science*, 21(12), pp.789–800. doi: 10.1017/CBO9781107415324.004.

Czakiert, T., Bis, Z., Muskala, W. and Nowak, W. (2006) 'Fuel Conversion from oxy-fuel combustion in a circulating fluidized bed', *Fuel Processing Technology*, 87(6), pp. 531–38. doi: 10.1016/j.fuproc.2005.12.003.

Czakiert, T., Sztekler, K., Karski, S., Markiewicz, D., Nowak, W. (2010) 'Oxy-fuel circulating fluidized bed combustion in a small pilot-scale test rig', *Fuel Processing Technology*, 91(11), pp. 1617–1623. doi:10.1016/j.fuproc.2010.06.010.

de Diego, L.F., de las Obras-Loscertales, M., Rufas, A., García-Labiano, F., Gayán, P. and Abad, A. (2013) 'Pollutant emissions in a bubbling fluidized bed combustor working in oxy-fuel operating conditions: effect of flue gas recirculation', *Applied Energy,* 102, pp. 860–867.

Dellinger, B., Grotecioss, G., Fortune, C.R., Cheney, J.L. and Homolya, J.B. (1980) 'Sulfur dioxide oxidation and plume formation at cement kilns', *Environmental Science and Technology,*14(10), pp. 1244–1249.

Dene, C. and Himes, R. (2004) 'Continuous Measurement Technologies for SO_3 and H_2SO_4 in Coal-Fired Power Plants', *Technical report EPRI (Electric Power Research Institute),* Palo Alto, 2004. 1009812.

Dennis, J.S. and Hayhurst, A.N. (1988) 'The formation of SO_3 in a fiuidized bed', *Combustion and Flame*, 72, pp. 241–258.

Dhungel, B., Ellul, C., Gibson, J.R. and Fitzgerald, F.D. (2011) 'SO_3 control in oxyfuel applications', Presented in IEAGHG Special Workshop on Oxyfuel Combustion, London, 25-26 January. Available at: http://www.ieaghg.org/docs/General_Docs/TSB_Oxyfuel/01%20%20Bhupesh%20Dhungel.pdf. (Accessed: 24 February 2016).

Dillon, D.J., White, V., Allam, R.J., Wall, R.A. and Gibbins, J. (2005) 'Oxy Combustion Processes for CO_2 Capture from Power Plant, *IEA Greenhouse Gas R&D Programme*, Report number: 2005/9, July 2005.

Duan, L., Duan, Y., Sarbassov, Y., Li, Y. and Anthony, E.J. (2015) 'SO_3 formation under Oxy-CFB Combustion Conditions', *International Journal of Greenhouse Gas Control*, 43, pp.172–178. doi.10.1016/j.ijggc.2015.10.028.

Duan, L., Sun, H., Zhao, C., Zhou, W. and Chen, X. (2014) 'Coal combustion characteristics on an oxy-fuel circulating fluidized bed combustor with warm flue gas recycle', *Fuel*, 127, pp.47-51. doi: 10.1016/j.fuel.2013.06.016.

Duan, L., Sun, H., Zhao, C., Zhou, W. and Chen, X. (2014) 'Coal combustion characteristics on an oxy-fuel circulating fluidized bed combustor with warm flue gas recycle', *Fuel*, 127, pp. 47–51.

Duan, L., Zhao, C., Zhou, W., Qu, C. and Chen, X. (2011) 'Effects of operation parameters on NO emission in an oxy-fired CFB combustor', *Fuel Processing Technology*, 92(3), 379–384. doi: 10.1016/j.fuproc.2010.09.031.

Duan, L., Zhao, C., Zhou, W., Qu, C. and Chen, X. (2011) 'O_2/CO_2 coal combustion characteristics in a 50kW_{th} Circulating Fluidized Bed', *International Journal of Greenhouse Gas Control,* 5(4), pp. 770–776.

Duan, L., Zhou, W., Li H., Chen, X. and Zhao, C. (2011) 'Sulfur fate during bituminous coal combustion in an oxy-fired circulating fluidized bed combustor', *Korean Journal of Chemical Engineering*, 28(9), pp. 1952–1955.

Dunn J. P., Koppula, P.R., Stenger, H.G. and Wachs, I.E. (1998) 'Oxidation of sulfur dioxide to sulfur trioxide over supported vanadia catalysts', *Applied catalysis B: Environmental,* 19(2), pp. 103–117.

Dunn J. P., Stenger, H.G. and Wachs, I.E. (1999) 'Oxidation of SO_2 over supported metal oxide catalysts', *Journal of catalysis*, 181, pp. 233–243.

Durie R.A., Matthews, C.J. and Smith, M.Y. (1970) 'The catalytic formation of sulfur trioxide in fuel-rich propane-air flames'. *Combustion and Flame*, 15, pp. 159–165.

Eddings, E.G., Wang, L. and Ahn, J. (2010) 'Bench-Scale Fluid Bed Experiments of SO_2/SO_3 Formation and Sulfur Capture in N_2/O_2 and CO_2/O_2 Environments', *In IEAGHG Special Workshop on Oxyfuel Combustion*, 25-26 January, London. doi: 10.1016/j.lwt.2010.11.034.

Edge, P., Gharebaghi, M., Irons, R., Porter, R.T.J., Pourkashanian, M., Smith, D., Stephenson, P. and Williams, A. (2011) 'Combustion modelling opportunities and challenges for oxy-coal carbon capture Technology. *Chemical Engineering Research and Design,* 89(9), pp. 1470–1493.

Eriksson, T., Sippu, O., Hotta, A., Fan, Z., Myöhänen, K., Hyppänen, T. and Pikkarainen, T. (2007) 'Oxyfuel CFB boiler as a route to near zero CO_2 emission coal firing'. Presented in: Power Generation Europe, June 26-28.

Fateev, A. and Clausen, S. (2011) 'Sulfur trioxide on-line measurement technique for power plants', Proceedings of the IEAGHG Special Workshop on Oxyfuel Combustion, January 25-26, London.

Fleig, D., Alzueta, M.U., Normann, F., Abián, M., Andersson, K. and Johnsson, F. (2013) 'Measurement and modeling of sulfur trioxide formation in a flow reactor under post-flame conditions', *Combustion and Flame*, 160, pp.1142–1151.

Fleig, D., Andersson, K., Johnsson, F. and Leckner, B. (2011) 'Conversion of Sulfur during Pulverized Oxy-Coal Combustion." *Energy and Fuels,* 25(2), pp. 647–655.

Fleig, D., Andersson, K., Normann, F., Johnsson, F. (2011) 'SO_3 formation under oxyfuel combustion conditions', *Industrial & Engineering Chemistry Research*, 50, pp. 8505–8514. doi: 10.1021/ie2005274.

Fleig, D., Andersson, Klas, and Johnsson, F. (2012) 'Influence of operating conditions on so3 formation during air and oxy-fuel combustion' *Industrial & Engineering Chemistry Research,* 51, pp. 9484–9491.
Fleig, D., Normann, F., Andersson, K., Johnsson, F. and Leckner, B. (2009) 'The fate of sulphur during oxy-fuel combustion of lignite' *Energy Procedia*, 1, pp. 383–390.

Fleig, D., Vainio, E., Andersson, K., Brink, A. Johnsson, F. and Hupa. M. (2012) 'Evaluation of SO_3 Measurement Techniques in Air and Oxy-Fuel Combustion', *Energy & Fuels*, 26, pp. 5537–5549. doi: 10.1021/ef301127x.

Flint, D. and Lindsay, A.W. (1951) 'Catalytic oxidation of sulphur dioxide on heated quartz surfaces', *Fuel*, 30, pp. 288-288.

Galloway, B.D., Sasmaz, E. and Padak, B. (2015) 'Binding of SO_3 to fly ash components: CaO, MgO, Na_2O and K_2O', *Fuel*, 145, pp. 79–83. doi: 10.1016/j.fuel.2014.12.046.

Giménez-López, J., Martinez, M., Millera, A., Bilbao, R. and Alzueta, M.U. (2011) 'SO_2 effects on CO oxidation in a CO_2 atmosphere, characteristic of oxy-fuel conditions', *Combustion and Flame*, 158(1), pp. 48–56.

Glarborg, P. (1996) 'Impact of SO_2 and NO on CO oxidation under post-flame conditions', *International Journal of Chemical Kinetics'*, 28(10), pp. 773–790.

Glarborg, P. (2007) 'Hidden interactions-Trace species governing combustion and emissions', *Proceedings of the Combustion Institute*, 31, pp. 77–98.

Glarborg, P. and Bentzen, L.L.B. (2007) 'Chemical effects of a high CO_2 concentration in oxy-fuel combustion of methane', *Energy & Fuels*, 22, pp. 291–296. doi:10.1021/ef7005854.

Glarborg, P., Alzueta, M.U., Dam-Johansen, K. and Miller. J.A. (1998) 'Kinetic modeling of hydrocarbon nitric oxide interactions in a flow reactor', *Combustion and Flame,* 115, pp. 1–27.

Glarborg, P., Kubel, Dorte., Dam-Johansen, K., Giang, H.M. and Bozzelli, J.W. (1996) 'Impact of SO_2 and NO on CO oxidation under post-flame conditions' *International Journal of Chemical Kinetics*, 28(10), pp. 773–790.

Glassman, I. and Yetter, R.A. (2008) '*Combustion',* Fourth Edition, Elsevier. pp. 441-443.

Gómez, M., Fernández, A., Llavona, I., Kuivalainen, R. (2014) 'Experiences in sulphur capture in a 30 MW_{th} Circulating fluidized bed boiler under oxy-combustion conditions', *Applied Thermal Engineering*, 65, pp. 617–622.

Günther, C., Weng, M., Kather, A. (2013) 'Restrictions and limitations for the design of a steam generator for a coal-fired oxyfuel power plant with circulating fluidised bed combustion', *Energy Procedia*, 37, pp. 1312–1321.doi:10.1016/j.egypro.2013.06.006.

Harb, J.N. and Smith, E.E. (1990) 'Fireside corrosion in PC-fired boilers', *Progress in Energy and Combustion Science*, 16, pp. 169–190.

Hecht, S, E., Shaddix, C.R., Geier, M., Molina, A. and Haynes, B.S. (2012) 'Effect of CO_2 and steam gasification reactions on the oxy-combustion of pulverized coal char', *Combustion and Flame*, 159(11), pp. 3437–3447.

Himes, R. (2006) 'Continuous Measurement of SO_3 in a Coal-Fired Power Plant', Technical update, EPRI (Electric Power Research Institute), Palo Alto, CA. 1010375.

Hindiyarti, L., Glarborg, P. and Marshall, P. (2007) 'Reactions of SO_3 with the O/H radical pool under combustion conditions', *Journal of Physical Chemistry A*, 111(19), pp. 3984–3991.

Hofbauer, G., Beisheim, T., Dieter, H. and Scheffknecht, G. (2014) 'Experiences from oxy-fuel combustion of bituminous coal in a 150 kW_{th} circulating fluidized bed pilot facility', Energy Procedia, 51, pp. 24–30. doi:10.1016/j.egypro.2014.07.003.

Hu, Y. and Yan, J. (2012) Characterization of flue gas in oxy-coal combustion processes for CO_2 capture', *Applied Energy*, 90(1) pp.113–121. doi:10.1016/j.apenergy.2011.03.005.

Ibanez, J.G., Batten, C.F., and Wentworth, W.E. (2008) 'Simultaneous determination of $SO_{3(g)}$ and $SO_{2(g)}$ in a flowing gas', *Industrial & Engineering Chemistry Research*, 47(7), pp. 2449–2454. doi:10.1021/ie0715198.

Intergovernmental Panel on Climate Change (IPCC) (2005), 'Special report on Carbon dioxide capture and storage', *Cambridge University Press*, Cambridge, UK, and New York, NY, USA.

International Energy Agency (IEA), (2012) 'Energy Technology Perspectives. Available at: http://www.iea.org/etp/. (Accessed: 06 January 2015).

International Energy Agency (IEA), (2014) 'CO_2 emissions from fuel combustion highlights', 2014 edition/IEA statistics. Available at: https://www.iea.org/publications/freepublications/publication/CO2EmissionsFromFuelCombustionHighlights2015.pdf. (Accessed: 24 May 2016)

International Energy Agency (IEA), (2015) 'Tracking clean energy progress 2015, Energy technology perspectives 2015 Excerpt IEA Input to the Clean Energy Ministerial', Available at: https://www.iea.org/etp/tracking2015/. (Accessed: 03 June 2016)

International Energy Agency Greenhouse Gas Emissions (IEAGHG) (2011) 'Effects of impurities on geological storage of CO_2'. Available at: http://ieaghg.org/docs/General_Docs/Reports/2011-04.pdf. (Accessed: 26 April 2016).

Jackson, P.J., Hilton, D.A. and Buddery, J.H. (1981) 'Continuous measurement of sulphuric acid vapour in combustion gases using a portable automatic monitor', *Journal of the Institute of Energy*, 124.

Jaworowski, R.J., and Mack, S.S. (1979) 'Evaluation of the air pollution control association', *Journal of the Air Pollution Control Association*, 29(1), pp. 43–46. doi: 10.1080/00022470.1979.10470750.

Jia, L., Tan, Y., McCalden, D., Wu, Y., He, I., Symonds, R. and Anthony, E.J. (2012) 'Commisioning of a 0.8 MW_{th} CFBC for oxy-fuel combustion', *International Journal of Greenhouse Gas Control*, 7, pp. 240-243. doi: 10.1016/j.ijggc.2011.10.009.

Jia, L., Tan, Y., Wu, Y. and Anthony, E.J. (2011) 'Oxy-fuel tests and results using a pilot-scale circulating fluidized bed', *In 2nd Oxyfuel Combustion Conference.* 12-16 September, Australia.

Jiao, F., Chen, J., Zhang, L., Wei, Y., Ninomiya, Y., Bhattacharya, S. and Yao, Y.H. (2011) 'Ash partitioning during the oxy-fuel combustion of lignite and its dependence on the recirculation of flue gas impurities (H_2O, HCl and SO_2)', *Fuel*, 90(6), pp. 2207–2216.

John, D. (2007) 'Performance and costs of power plants with capture and storage of CO_2', *Energy*, 32(7), pp. 1163–1176. doi: 10.1016/j.energy.2006.07.039.

Jordal, K., Anheden, M., Yan, J. and Strömberg, L. (2004) 'Oxyfuel combustion for coal-fired power generation with CO_2 capture - opportunities and challenges', In: *The 7th International Conference on Greenhouse Gas Control Technologies* (GHGT-7), Vancouver, 5-9 September.

Jurado N., Darabkhani H.G., Anthony E.J. and Oakey. J.E. (2014) 'Oxy-combustion studies into the co –firing of coal and biomass blends: effects on heat transfer, gas and ash compositions', *Energy Procedia,* pp. 440–452.

Kather, A. and Günter S. (2009) 'The oxycoal process with cryogenic oxygen supply." *Naturwissenschaften*, 96(9), pp. 993–1010. doi: 10.1007/s00114-009-0557-2.

Kelman, F.N. (1952) 'Direct method determination of sulfuric acid in solution with sulfuric gases and air', *Zavodskaya Lab*, 11, pp. 1316–1318 (in Russian).

Kenney, J.R., Clark, M.M., Levasseur, A A., Kang, S.G. (2011) 'SO_3 emissions from a tangentially-fired pilot scale boiler operating under oxy-combustion conditions', *In IEAGHG Special Workshop on Oxyfuel Combustion*, 25-26 January 2011 London. Available at: http://www.ieaghg.org/docs/General_Docs/TSB_Oxyfuel/03%20-%20James%20Kenney.pdf.

Kiga, T., Takano, S., Kimura, N., Omata, K., Okawa, M., Mori, T., Kato, M. (1997) 'Characteristics of pulverized-coal combustion in the system of oxygen recycled flue gas combustion', *Energy Conversion and Management*, 38, pp. S129–S134.

Kim K.H and Choi J.H. (1981) 'Kinetics and mechanism of the oxidation of sulfur dioxide on α-$Fe_2O_{3'}$, *Journal of Physical Chemistry*, 85, pp. 2247–2450.

Kühnemuth, D., Normann, F., Andersson, K., Johnsson, F. (2014) 'On the carbon monoxide formation in oxy-fuel combustion - Contribution by homogenous and heterogeneous reactions', *International Journal of Greenhouse Gas Control*, 25: 33-41. doi:10.1016/j.ijggc.2014.02.014.

Kuivalainen, R., Eriksson, T., Hotta, A., Sacristän, AS-B., Jubitero, J.M. and Ballesteros, J.C. (2010) 'Development and Demonstration of oxy-fuel CFB technology', In: *The International technical conference on coal utilization and fuel systems*, Clearwater, FL, 6-10 June.

Kunii, D. and Levenspiel, O. (1991). *Fluidization Engineering*. second ed. Butterworth Heinemann, Stoneham.

Li, G.D., Li, S.Q, Dong, M., Yao, Q., Guo, C.Y. and Axelbaum, R.L. (2013) 'Comparison of particulate formation and ash deposition under oxy-fuel and conventional pulverized coal combustions', *Fuel*, 106, 544–551. doi: 10.1016/j.fuel.2014.11.067.

Li, H., Yan, J., Yan, J. and Anheden, M. (2009) 'Impurity impacts on the purification process in oxy-fuel combustion based co_2 capture and storage system', *Applied Energy*, 86(2), pp. 202–213. doi: 10.1016/j.apenergy.2008.05.006.

Li, S., Li, W., Xu, M., Wang, X., Li, H. and Lu, Q. (2015) 'The experimental study on nitrogen oxides and SO_2 emission for oxy-fuel circulation fluidized bed combustion with high oxygen concentration', *Fuel*, 146, pp. 81–87. doi:10.1016/j.fuel.2014.12.089.

Linak, W.P. and Wendt, J.O.L. (1994) 'Trace metal transformation mechanisms during coal combustion' *Fuel Processing Technology*, 39(1–3), pp. 173–198. doi: 10.1016/0378-3820(94)90179-1.

Liu, H. and Shao, Y. (2010) 'Predictions of the impurities in the CO_2 stream of an oxy-coal combustion plant', *Applied Energy*, 87(10), pp. 3162–3170. doi: 10.1016/j.apenergy.2010.04.014.

Lupiáñez, C., Guedea, I., Bolea, I., Díez, L.I. and Romeo, L.M. (2013) 'Experimental study of SO_2 and NO_x emissions in fluidized bed oxy-fuel

combustion', *Fuel Processing Technology*, 106, pp. 587–594. doi: 10.1016/j.fuproc.2012.09.030.

Lupiáñez, C., Scala, F., Salatino, P., Romeo, L.M. and Díez, L.I. (2011) 'Primary fragmentation of limestone under oxy-firing conditions in a bubbling fluidized bed', *Fuel Processing Technology*, 92(8), pp. 1449–1456. doi: 10.1016/j.fuproc.2011.03.005.

Lupion, M., Alvarez, I., Otero, P., Kuivalainen, R., Lantto, J., Hotta, A. and Hack, H. (2013) '30 MW_{th} CIUDEN Oxy-CFB Boiler - First Experiences', *Energy Procedia*, 37, pp. 6179–6188. doi: 10.1016/j.egypro.2013.06.547.

MacDowell, N., Florin, N., Buchard, A., Hallett, J., Galindo, A., Jackson, G., Adjiman, C.S., Williams, C.K., Shah, N. and Fennell, P. (2010). 'An overview of CO_2 capture technologies' *Energy & Environmental Science*, 3(11) pp. 16451669. doi: 10.1039/c004106h.

Macken, C., Hodnett, B.K. and Paparatto, G. (2000) 'Testing of the CuO/Al_2O_3 catalyst-sorbent in extended operation for the simultaneous removal of NO_x and SO_2 from flue gases' *Industrial & Engineering Chemistry Research*, 39, pp. 3868–3874. doi: 10.1021/ie000342d.

Maddalone, R.F., Newton, S.F., Rhudy R.G. and Statnick R.M. (1979) 'Laboratory and Field Evaluation of the Controlled Condensation System for $S0_3$ Measurements in Flue Gas Streams', *Journal of the Air Pollution Control Association*, 29, pp. 626–631.

Marier, P. and Dibbst, H.P. (1974) 'The catalytic conversion of SO_2 to SO_3 by fly ash and capture of SO_2 and SO_3 by CaO and MgO', *Thermochimica Acta*. 8, pp.155–165.

Markewitz, P., Kuckshinrichs, W., Leitner, W., Linssen, J., Zapp, P., Bongartz, R., Schreiber, A. and Müller, T. E. (2012) 'Worldwide innovations in the development of carbon capture technologies and the utilization of CO_2', *Energy & Environmental Science*, 5(6), pp. 7281-7305. doi: 10.1039/c2ee03403d.

Merryman, E.L. and Levy, A. (1979) 'Enhanced SO_3 emissions from staged combustion', *Proceedings of the Seventeenth Symposium (International) on Combustion*, The combustion Institute, Pittsburgh PA, 1979, pp. 727–736.

Miccio, F., Löffler, G., Wargadalam, V.J. and Winter, F. (2001) 'The Influence of SO_2 level and operating conditions on NO_x and N_2O emissions during fluidized bed combustion of coals', *Fuel,* 80, pp. 1555–1566.

Mitsui, Y., Imada, N., Kikkawa, H. and Katagawa, A. (2011) 'Study of Hg and SO_3 behavior in flue gas of oxy-fuel combustion system', *International Journal of Greenhouse Gas Control*, 5S, pp.143–150. doi: 10.1016/j.ijggc.2011.05.017.

Molburg, J.C., Doctor, R.D., Brockmeier, N.F. and Plasynski. S. (2001) 'CO_2 capture from PC Boilers with O_2-firing. *In: 18th Annual International Pittsburgh Coal Conference*, December 4-7, Newcastle, New South Wales, Australia.

Monckert P., Dhungel, B., Kull, R. and Maier, J. (2008) 'Impact of combustion conditions on emission formation (SO_2, NO_x) and fly ash. In: *The 3rd Workshop IEAGHG International Oxy-Combustion Network*, 5-6 March.

Moser, R.E. (2006) 'Benefits of effective SO_3 removal in coal-fired power plants: beyond opacity control', In: *Power Plant Air Pollutant Control, Mega Symposium*.

Mulcahy, J.R. and Steven, J.C.W. (1966) 'The kinetics of reaction between oxygen atoms and sulfur dioxide: an investigation by electron spin resonance spectrometry' *The Journal of Physical Chemistry*, 363, pp. 2124–2131.

Mulcahy, M.F.R., Steven, J.R., Ward, J.C. and Williams, D.J. (1969) 'Kinetics of interaction of oxygen atoms with sulfur oxides', *Symposium (International) on Combustion*, 12(1), pp. 323–330.

Müller, M., Schnell, U., Grathwohl, S., Scheffknecht, G. and Maier, J. (2012) 'Evaluation of oxy-coal combustion modelling at semi-industrial scale', *In Energy Procedia*, 23, pp. 197–206. doi: 10.1016/j.egypro.2012.06.054.

Naidoo, J., Goumri, A., and Marshall, P. (2005) 'A kinetic study of the reaction of atomic oxygen with SO_2', *Proceedings of the Combustion Institute*, 30(1), pp. 1219–1225. doi: 10.1016/j.proci.2004.08.214.

Nakayama, S. and Noguchi, Y. (1992) 'Pulverized coal combustion in O_2/CO_2 mixtures on a power plant for CO_2 recovery', *Energy Conversion and Management*, 33(5), pp. 379–386.

NCASI Southern Regional Center. (1996) '*Method 8a-Determination of Sulfuric Acid Vapor or Mist and Sulfur Dioxide Emissions From Kraft Recovery Furnaces*', December.

Ndibe, C., Spörl, R., Maier, J. and Scheffknecht, G. (2013) 'Experimental study of NO and NO2 formation in a PF oxy-fuel firing system', *Fuel*, 107(2), pp. 749–756. doi: 10.1016/j.fuel.2013.01.055.

Nielsen M.T. (2003) 'On the relative importance of SO_2 oxidation to high dust SCR DeNO$_x$ units. In: *DOE/NETL 2003 Conference on Selective Catalytic*

Reduction (SRC) and Selective Non-Catalytic Reduction (SNCR) for NOx Control, pp. 1-12.

Normann, F., Andersson, K., Leckner, B. and Johnsson, F. (2009) 'Emission control of nitrogen oxides in the oxy-fuel process', *Progress in Energy and Combustion Science*, 35(5), pp. 385–397. doi:10.1016/j.pecs.2009.04.002.

Obras-Loscertales, M.De., Mendiara, T., Rufas, A., de Diego, L.F., Gayán, P., Abad, A. and Adánez, J. (2015) 'NO and N_2O emissions in oxy-fuel combustion of coal in a bubbling fluidized bed combustor', *Fuel*, 150, pp. 146–153. doi: 10.1016/j.fuel.2015.02.023.

Pentol, SO_3 Monitor, How much SO_3 do you generate? Available at: http://www.pentol.pl/dokumenty/Pentol_SO3_Monitor_address.pdf. (Accessed: 20 September 2015).

Peterson, J. and Jones, A.F. (1994) 'SO_3 Mitigation Guide, *Final Report EPRI (Electric Power Research Institute)* Palo Alto, CA: TR-104424. Research project 2250-03.

Raask, E. (1982) 'Sulphate capture in ash and boiler deposits in relation to SO_2 emission', *Progress in Energy and Combustion Science,* 8, pp. 261–276.

Rasmussen, L.C., Glarborg, P. and Marshall, P. (2007) 'Mechanisms of radical removal by SO_2', *Proceedings of the Combustion Institute*, 31, pp. 339–347. doi:10.1016/j.proci.2006.07.249.

Reid W.T. (1971) 'External corrosion and deposits: boilers and gas turbines', Elsevier, New York.

Richard, F., Yan, J., Stark, F. and Priesnitz, S. (2011) 'Flue gas desulphurization for hot recycle Oxyfuel combustion: Experiences from the 30 MW_{th} Oxyfuel pilot plant in Schwarze Pumpe', *International Journal of Greenhouse Gas Control*, 5S pp. S210–S223. doi:10.1016/j.ijggc.2011.05.027.

Roy, B., Chen, L. and Bhattacharya, S. (2014) 'Nitrogen oxides, sulfur trioxide, and mercury emissions during oxy-fuel fluidized bed combustion of victorian brown coal', *Environmental Science and Technology*, 48(24), pp. 14844–14850. doi: 10.1021/es504667r.

Schafer, S. and Bonn, B. (2000) 'Hydrolysis of HCN as an important step in nitrogen oxide formation in fluidised combustion. Part I: Homogeneous reactions', *Fuel*, 79, pp. 1641–1646.

Schneider, D.R. and Bogdan, Z. (2003) 'Modelling of SO_3 formation in the flame of a heavy-oil fired furnace', *Chemical and Biochemical Engineering Quarterly*, 17(3), pp. 175–181.

Seddighi K.,S., Pallarès, D., Normann, F. and Johnsson, F. (2013). 'Carbon Monoxide Formation during Oxy-fuel-Fired Fluidized-Bed Combustion', *Energy & Fuels*, 27(4), pp. 2275–2282. doi: 10.1021/ef3021393.

Seddighi, K.S., Pallares, D., Normann, F. and Johnsson, F. (2013) 'Progress of combustion in an oxy-fuel circulating fluidized-bed furnace: measurements and modeling in a 4 MW', *Energy & Fuels*, 27, pp. 6222–6230.

Seddighi, S., Pallarès, D., Normann, F. and Johnsson, F. (2015) 'International Journal of Greenhouse Gas Control Heat transfer in a 4 – MW th circulating fluidized bed furnace operated under oxy-fired and air-fired conditions : Modeling and measurements'. *International Journal of Greenhouse Gas Control*, 37, pp. 264–273. doi: 10.1016/j.ijggc.2015.03.032.

Shaddix, C. R. and Molina, A. (2011) 'Fundamental investigation of NO_x formation during oxy-fuel combustion of pulverized coal', *Proceedings of the Combustion Institute*, 33(2), pp. 1723–1730. doi: 10.1016/j.proci.2010.07.072.

Sheng, C. and Li, Y. (2008) 'Experimental study of ash formation during pulverized coal combustion in O_2/CO_2 mixtures', *Fuel*, 87, pp. 1297–1305. doi: 10.1016/j.fuel.2007.07.023.

Sheng, C., Li, Y., Liu, X., Yao, H. and Xu, M. (2007) 'Ash particle formation during O_2/CO_2 combustion of pulverized coals', *Fuel Processing Technology*, 88, pp. 1021–1028. doi: 10.1016/j.fuproc.2007.06.009.

Spero, C., Yamada, T., Sturm, E., and McGregor, D. (2008) 'Callide oxyfuel project. Technical evaluation of oxy-combustion and CO_2 capture system', *Proceedings of the 3rd Workshop IEAGHG International Oxy-Combustion Network*, Yokohama, 5-6 March, 2008.

Spörl, R., Belo, L., Shah, K., Stanger, R., Giniyatullin, R., Maier, J., Wall, T. and Scheffknecht, G. (2014) 'Mercury emissions and removal by ash in coal-fired oxy-fuel combustion', *Energy & Fuels*, 28, pp. 123–135.

Spörl, R., Belo, L., Shah, K., Stanger, R., Giniyatullin, R., Maier, J., Wall,-T. and Scheffknecht, G. (2014) 'SO_3 emissions and removal by ash in coal-fired oxy-fuel combustion', *Energy and Fuels*, 28, pp. 5296–5306. doi: 10.1021/ef4014604.

Spörl, R., Maier, J. and Scheffknecht, G. (2011) 'Experiences and Results of SO_3 Measurements Performed under Oxy-Coal Fired Conditions', In: *IEAGHG Special Workshop on Oxyfuel Combustion*. 25-26 January.

Spörl, R., Maier, J., Belo, L., Shah, K., Stanger, R., Wall, T. and Scheffknecht G. (2014) 'Mercury and SO_3 Emissions in Oxy-Fuel Combustion', *Energy Procedia*, pp. 386–402.

Srivastava, R.K., Miller, C.A., Erickson, C. and Jambhekar, R. (2004) 'Emissions of Sulfur Trioxide from Coal-Fired Power Plants', *Journal of Air and Waste Management Association*, 54, pp. 750–762.

Stadler, H., Christ, D., Habermehl, M., Heil, P., Kellermann, A., Ohliger, A., Toporov, D. and Kneer, R. (2011) 'Experimental investigation of NOx emissions in oxycoal combustion', *Fuel*, 90(4), pp. 1604–1611. doi: 10.1016/j.fuel.2010.11.026.

Stanger, R., Wall, T., Stanger, R. and Wall, T. (2011) 'Sulphur impacts during pulverised coal combustion in oxy-fuel technology for carbon capture and storage', *Progress in Energy and Combustion Science*, 37(1), pp. 69–88. doi: 10.1016/j.pecs.2010.04.001.

Stewart, M.C., Symonds, R.T., Manovic, V., Macchi, A. and Anthony, E.J. (2012) 'Effects of steam on the sulfation of limestone and NO_x formation in an air- and oxy-fired pilot-scale circulating fluidized bed combustor', *Fuel*, 92(1), pp. 107–115. doi: 10.1016/j.fuel.2011.06.054.

Strömberg, L., Lindgren, G., Jacoby, J., Giering, R. and Anheden, M. (2009) 'Energy Procedia Update on Vattenfall's 30 MW_{th} Oxyfuel Pilot Plant in Schwarze Pumpe', *Energy Procedia*, 1(1), pp. 581–589. doi: 10.1016/j.egypro.2009.01.077.

Stuart, D.D. (2010) 'Acid Dewpoint Temperature Measurement and Its Use in Estimating Sulfur Trioxide Concentration. *In Analysis Division Symposium*, pp. 1–12. Available at: http://www.ametekpi.com/download/Sulfur-Trioxide-Concentrations.pdf.

Suraniti, S.L. Nsakala, N.Y. and Darling, S.L. (2009) 'Alstom oxyfuel CFB boilers: A promising option for CO_2 capture', *Energy Procedia*, 1(1), pp. 543–548. doi: 10.1016/j.egypro.2009.01.072.

Suriyawong, A., Gamble, M., Lee, M.H., Axelbaum, R.L., Biswas, P. (2006) 'Submicrometer particle formation and mercury speciation under O_2/CO_2 coal combustion', *Energy & Fuels*, 20(6), pp. 2357–2363. doi: 10.1021/ef060178s.

Svachula, J., Alemany, L.J., Ferlazzo, N. and Tronconi E. (1993) 'Oxidation of SO_2 to SO_3 over honeycomb DeNoxing catalysts', *Industrial & Engineering Chemistry Research*, 32, pp. 826–834.

Talman, S. (2015) ‘Subsurface geochemical fate and effects of impurities contained in a CO_2 stream injected into a deep saline aquifer: What is known’, *International Journal of Greenhouse Gas Control*, 40, pp. 267–291. doi:10.1016/j.ijggc.2015.04.019.

Tan, Y., Croiset, E., Douglas, M.A. and Thambimuthu, K.V. (2006) ‘Combustion characteristics of coal in a mixture of oxygen and recycled flue gas’, *Fuel*, 85, pp. 507–512. doi: 10.1016/j.fuel.2005.08.010.

Tan, Y., Croiset, E., Douglas, M.A. and Thambimuthu, K.V. (2006) ‘Combustion characteristics of coal in a mixture of oxygen and recycled flue gas’, *Fuel,* 85, pp. 507–512. doi: 10/1016/j.fuel.2005.08.010.

Taylor, H.D. (1951) ‘The condensation of sulphuric acid on cooled surfaces exposed to hot gases containing sulphur trioxide’, *Transactions of the Faraday Society*, 47(1114), pp. 1114. doi: 10.1039/tf9514701114.

Thibault J.D., Steward F.R. and Ruthven D.M. (1982) ‘The kinetics of absorption of SO_3 in calcium and magnesium oxides’. *The Canadian Journal of Chemical Engineering*, 60, pp. 796–801.

Toftegaard M.B., Brix, J., Jensen, P.A., Glarborg, P. and Jensen A.D. (2010) ‘Oxy-fuel combustion of solid fuels’, *Progress in Energy and Combustion Science*, 36(5), pp. 581–625. doi: 10.1016/j.pecs.2010.02.001.

Tommy L., Jorgensen, H. and Livbjerg, P.G. (2007) ‘Homogeneous and heterogeneously catalyzed oxidation of SO_2’, *Chemical Engineering Science*, 62, pp. 4496–4499.

Tronconi, E., Cavanna, A., Orsenigo, C. and Forzatti, P. (1999) ‘Transient Kinetics of SO_2 Oxidation Over SCR-DeNOx Monolith Catalysts’, *Industrial & Engineering Chemistry Research*, 38, pp. 2593–2598.

Tseng, H., Wey, M. and Fu, C. (2003) ‘Carbon materials as catalyst supports for SO_2 oxidation : catalytic activity of CuO – AC’, *Carbon*, 41, pp. 139–149.

Urbanek, A. and Trela, M. (1980) ‘Catalytic Oxidation of Sulfur Dioxide’, *Catalysis Reviews: Science and Engineering*, 21(1), pp. 73–133.

Vainio, E., Fleig, D., Brink, A., Andersson, K., Johnsson, F. and Hupa, M. (2013) ‘Experimental Evaluation and Field Application of a Salt Method for SO3 Measurement in Flue Gases’, *Energy & Fuels*. doi: 10.1021/ef400271t.

Verhoff, F.H. and Banchero, J.T. (1974) ‘Predicting dew points of flue gases’, *Chemical Engineering Progress*, 70(8), pp. 71–72.

Wall, T., Liu, Y. and Bhattacharya, S. (2012) 'A scoping study on oxy-CFB technology as an alternative carbon capture option for Australian black and brown coals', ANLEC R&D, ACT 2600, *Global CCS Institute*, Australia. Available at: http://www.globalccsinstitute.com/sites/www.globalccsinstitute.com/files/publications/33801/scoping-study-oxy-cfb-technology-alternative-carbon-capture-option-australian-black-and-brown-coals.pdf. (Accessed: 15.09.2015)

Wall, T., Liu, Y., Spero, C., Elliott, L., Khare, S., Rathnam, R., Farida Z.,Behdad M.,Bart, B.,Changdong, S.,Raj, G.,Toshihiko Y.,Keiji, M. and Yu, J. (2009) 'An overview on oxyfuel coal combustion—State of the art research and technology development', *Chemical Engineering Research and Design*, 87(8), pp. 1003–1016. doi: 10.1016/j.cherd.2009.02.005.

Wall, T., Stanger, R. and Santos, S. (2011) 'Demonstrations of coal-fired oxy-fuel technology for carbon capture and storage and issues with commercial deployment', *International Journal of Greenhouse Gas Control*, 5, S5–S15. doi: 10.1016/j.ijggc.2011.03.014.

Wall, T.F. (2007) 'Combustion processes for carbon capture', *Proceedings of the Combustion Institute*, 31 I, pp. 31–47. doi: 10.1016/j.proci.2006.08.123.

Walsh, P.M., Mormile, D.J. and Piper, B. F. (1972) 'Sulfur trioxide formation in the presence of residual oil ash deposits in a electric utility boiler', *American Chemical Society, Division of Fuel Chemistry, Preprints*, 38, pp. 294–300.

Wang, C., Du, Y. and Che, D. (2015) 'Study on N_2O reduction with synthetic coal char and high concentration CO during oxy-fuel combustion'. *Proceedings of the Combustion Institute*, 35, pp. 2323–2330. doi: 10.1016/j.proci.2014.07.018.

Wendt, J.O.L. and Ekmann, J.M. (1975) 'Effect of fuel sulfur species on nitrogen oxide emissions from premixed flames', *Combustion and Flame*, 25(3), pp. 355–360. doi: 10.1016/0010-2180(75)90107-8.

Wendt, J.O.L. and Sternling, C.V. (1973) 'Catalysis of SO_2 oxidation by nitrogen oxides', *Combustion and Flame*, 21(3), pp. 387–390. doi:10.1016/S0010-2180(73)80062-8.

Wendt, J.O.L. Corley, T.L. and Wootan, E.C. (1983) 'Postflame behavior of nitrogenous species in the presence of fuel sulfur I. Rich, Moist CO/Ar/O_2 flames', *Combustion and Flame*, 49, pp. 261–274.

Wheeldon, J. (2007) 'Review of CO_2-Capture Development Activities for Coal-Fired Power Generation Plants' *Technical report EPRI (Electric Power Research Institute)*, Palo Alto, CA: 2007. 1012239.

White, V., Torrente-Murciano, L., Sturgeon, D. and Chadwick, D. (2010) 'Purification of oxyfuel-derived CO_2', *International Journal of Greenhouse Gas Control*, 4(2), pp. 137–142. doi: 10.1016/j.ijggc.2009.07.004.

Wine, P.H., Thompston, A.R., Ravishankara, A.R., Semmes, D.H., Gump, C.A., Torabi, A. and Nikovich, J.M. (1984) 'Kinetics of the reaction OH + SO_2 + M = $HOSO_2$ + M. Temperature and Pressure Dependence in the Falloff Region', *Journal of Physical Chemistry*, 88, pp. 2095–2104. doi: 10.1017/CBO9781107415324.004.

Wu, Y., Wang, C., Tan, Y., Jia, L. and Anthony, E. J. (2011) 'Characterization of ashes from a 100kWth pilot-scale circulating fluidized bed with oxy-fuel combustion', *Applied Energy*, 88(9), pp. 2940–2948. doi: 10.1016/j.apenergy.2011.03.007.

X. Wang, X. Liu, D. Li, Y. Zhang, M. X., Wang, X., Liu, X., Li, D., Zhang, Y. and Xu, M. (2015) 'Effect of steam and sulfur dioxide on sulfur trioxide formation during oxy-fuel combustion', *International Journal of Greenhouse Gas Control*, 4, pp. 1–9. doi: 10.1016/j.ijggc.2015.10.002.

Yilmaz, A., Hindiyarti, L., Jensen, A. D., Glarborg, P., and Marshall, P. (2006) 'Thermal Dissociation of SO_3 at 1000 - 1400 K', *Journal of Physical Chemistry A*, 110, pp. 6654–6659.

Yoshiie, R., Hikosaka, N., Nunome, Y., Ueki, Y. and Naruse, I. (2015) 'Effects of flue gas re-circulation and nitrogen contents in coal on NOx emissions under oxy-fuel coal combustion', *Fuel Processing Technology*, 136, pp. 106–111.

Yu, D., Morris, W. J., Erickson, R., Wendt, J.O.L., Fry, A. and Senior, C.L. (2011) 'Ash and deposit formation from oxy-coal combustion in a 100 kW test furnace', *International Journal of Greenhouse Gas Control*, 5, pp. S159–S167. doi: 10.1016/j.ijggc.2011.04.003.

Zachariah, M.R. and Smith, O.I. (1987). 'Experimental and numerical studies of sulfur chemistry in $H_2/O_2/SO_2$ flames', *Combustion and Flame*, 69(2), pp. 125–139. doi.org/10.1016/0010-2180(87)90026-5.

Zanganeh, K.E. and Shafeen, A. (2007) 'A novel process integration, optimization and design approach for large-scale implementation of oxy-fired coal power plants with CO_2 capture', *International Journal of Greenhouse Gas Control*, 1(1), pp. 47–54. doi: 10.1016/S1750-5836(07)00035-7.

ZareNezhad, B. (2009) 'New correlation predicts flue gas sulfuric acid dewpoints', *Oil & Gas Journal*.

Zhang, L., Jiao, F., Binner, E., Bhattacharya, S., Ninomiya, Y. and Li, C. (2011) 'Experimental investigation of the combustion of bituminous coal in air and O_2/CO_2 mixtures: 2. Variation of the transformation behaviour of mineral matter with bulk gas composition', *Fuel*, 90(4), pp. 1361–1369. doi: 10.1016/j.fuel.2011.01.012.

Zhang, X., Zhuang, G., Chen, J., Wang, Y., Wang, X., An, Z. and Zhang, P. (2006). 'Heterogeneous reactions of sulfur dioxide on typical mineral particles', *Journal of Physical Chemistry*, 110, pp. 12588–12596. doi: 10.1021/jp0617773.

Zheng, L. and Furimsky, E. (2003) 'Assessment of coal combustion in O_2+CO_2 by equilibrium calculations', *Fuel Processing Technology.* doi:10.1016/S0378-3820(02)00250-3.

Zygarlicke C.J., Stomberg, A.L., Folkedahl, B.C. and Strege, J.R. (2006) 'Alkali influences on sulfur capture for North Dakota lignite combustion', *Fuel Processing Technology*, 87, pp. 855–861.

APPENDICES

Appendix A Minimum fluidisation velocity

A.1 Experimental evaluation of minimum fluidisation velocity (Umf) under increasing and decreasing superficial gas velocities

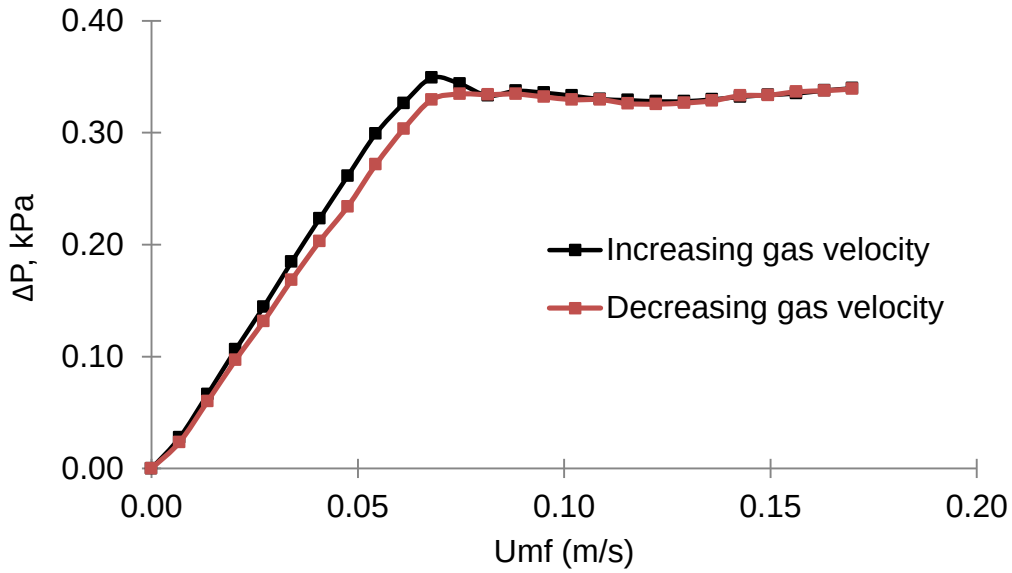

Figure A-1 Experimental validation of Umf (dp – 260 μm; bed material-20 g of silica sand)

Table A-1 Experimental spreadsheet on U_{mf}

		Increasing gas velocity				Decreasing gas velocity			
ΔP_{bed}, kPa	Velocity	Test1	Test2	Test3	Average	Test1	Test2	Test3	Average
0	0	0	0	0	0	0	0	0	0
6.28E-06	0.006794	32	24	27	0.027667	23	24	24	0.0235
1.26E-05	0.013588	74	62	63	0.066333	60	60	58	0.06
1.88E-05	0.020382	118	100	101	0.106333	97	97	92	0.097
2.51E-05	0.027176	160	136	137	0.144333	130	133	124	0.1315
3.14E-05	0.03397	203	175	176	0.184667	168	169	159	0.1685
3.77E-05	0.040764	245	212	213	0.223333	201	205	191	0.203
4.4E-05	0.047558	285	248	251	0.261333	235	233	221	0.234
5.03E-05	0.054352	328	284	285	0.299	268	275	251	0.2715
5.65E-05	0.061146	337	320	322	0.326333	304	303	279	0.3035
6.28E-05	0.067941	343	352	352	0.349	338	321	308	0.3295
6.91E-05	0.074735	339	335	357	0.343667	337	332	336	0.3345
7.54E-05	0.081529	337	330	332	0.333	335	333	343	0.334
8.17E-05	0.088323	338	334	340	0.337333	334	335	336	0.3345
8.79E-05	0.095117	337	332	338	0.335667	329	335	333	0.332
9.42E-05	0.101911	335	329	335	0.333	326	333	332	0.3295
1.01E-04	0.108705	333	324	333	0.33	327	332	332	0.3295
1.07E-04	0.115499	331	326	330	0.329	325	327	326	0.326
1.13E-04	0.122293	332	327	325	0.328	326	325	327	0.3255
1.19E-04	0.129087	330	327	327	0.328	327	326	327	0.3265
1.26E-04	0.135881	331	329	329	0.329667	330	327	329	0.3285
1.32E-04	0.142675	334	330	332	0.332	332	334	331	0.333
1.38E-04	0.149469	335	331	335	0.333667	334	333	334	0.3335
1.44E-04	0.156263	336	333	336	0.335	337	336	335	0.3365
1.51E-04	0.163057	339	337	337	0.337667	338	337	339	0.3375
1.57E-04	0.169851	340	338	341	0.339667	340	338	340	0.339

Appendix B Design of experiment

B.1 Design of experimental tests

Table B-1 Number of tests

Variables	Extended	Reduced
Flue gas environment for (Air, OXY)[ff]	4	4
Bed temperature level	2	2
Residence time	2	1
Bed material (Sand, Fly ash mixture)	2	2
Number of experiments:	**32**	**16**

[ff] Flue gas environment includes high and low SO_2 concentrations for air and oxy cases

Appendix C Calibration of mass flow controllers

C.1 Mass flow controller for nitrogen and carbon dioxide

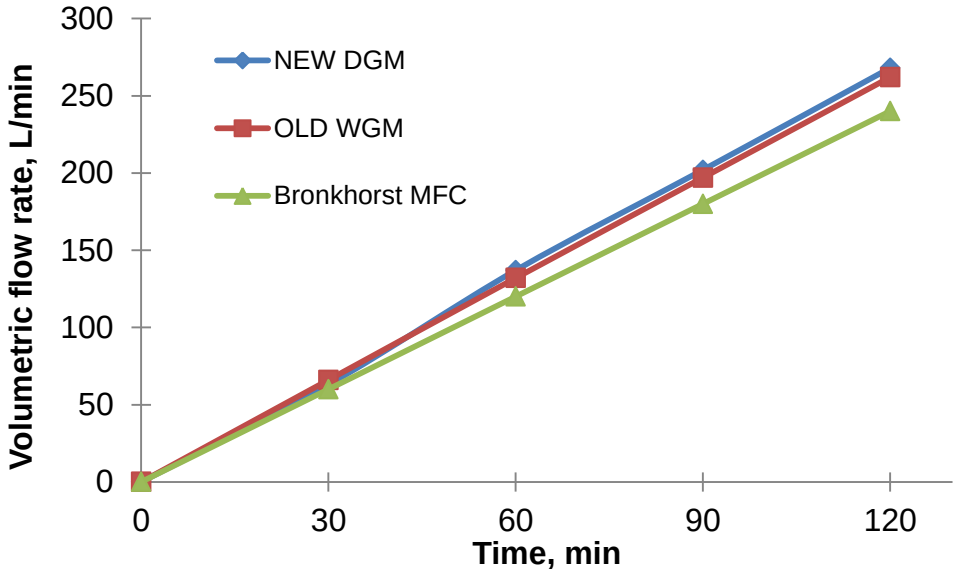

Figure C-1 Calibration of nitrogen MFC (2 l/min)

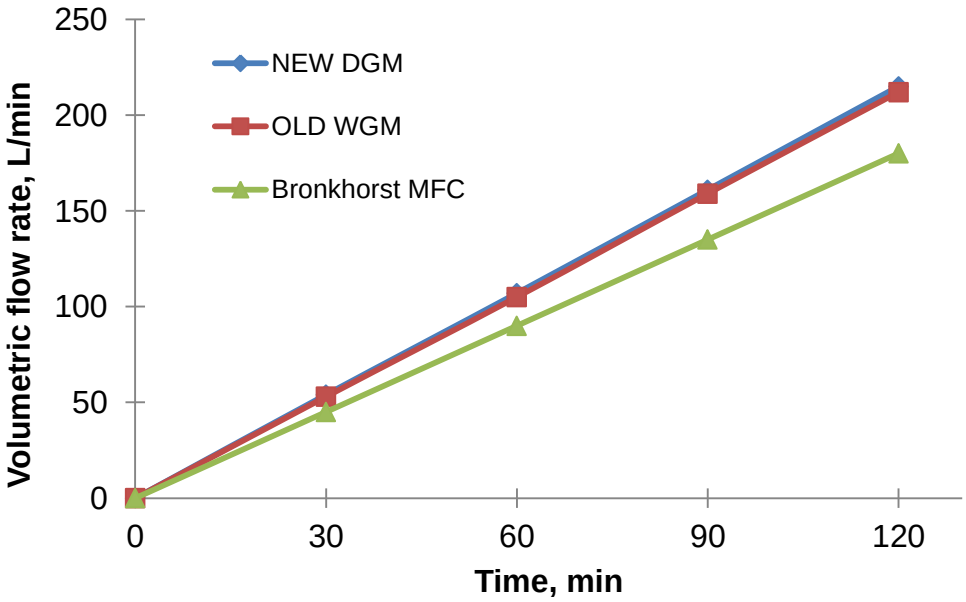

Figure C-2 Calibration of carbon dioxide MFC (1.5 l/min)

Since, the existing WGM was not calibrated for a long time, the recently

calibrated (2011) WGM were connected in series along with the old one. However, quite similar flow rate were measured via two WGMs. The difference between Bronkhorst WGM and MFC with nitrogen is 6 % and 12% for CO_2; Therefore, these values were taken into account during the tests in the bubbling fluidised bed rig.

C.2 Analysis of SO_2 concentration trapped by the impingers

In order to check the sulfur dioxide concentration in the third impinger, all three impingers were filled with 3% of hydrogen peroxide solution and conducted under the same test conditions. The mixture of gas was provided at room temperature through these impingers under 1000 and 4000 ppm of SO_2 concentrations. As a result, all sulfur in the exit gas is trapped in the first two impingers. Therefore, the third impinger was not required for analysis during the tests.

Table C- 1 Assessment of SO_2 concentration by impingers

Low and high sulfur	Impinger 1	Impinger 2	Impinger 3
SO_2-1050 ppm Total flow rate 2.45 L/min Mixture gas: $SO_2/O_2/CO_2$/Bal-N_2	97.7%	2.33%	0.00%
SO_2-4500 ppm Total flow rate 2.6 L/min Mixture gas: $SO_2/O_2/CO_2$/Bal-N_2	95.75%	4.25%	0.06%

Appendix D Fly ash composition

Table D-1 XRF analysis of bed materials after the tests at 950°C

Fly ash composition:	Fly ash-3				Fly ash-4				Fly ash-1	
	1000 ppm		4000 ppm		1000 ppm		4000 ppm		1000 ppm	
	Air	Oxy	Air	Oxy	Air	Oxy	Air	Oxy	Air	Oxy
Na_2O	0.14	0.249	0.123	0.152	0.273	0.193	0.246	0.181	0.237	0.281
MgO	1.97	2.14	2.22	2.11	0.573	0.436	0.566	0.568	0.479	0.466
Al_2O_3	5.01	7.33	4.49	4.47	10.64	7.29	10.18	9.32	8.66	8.46
SiO_2	68.69	71.78	66.5	65.29	81.38	86.18	81.77	82.91	83.33	83.9
P_2O_5	0.05	0.097	0.054	0.052	0.141	0.096	0.128	0.114	0.041	0.046
SO_3	12.31	8.84	14.82	15.22	0.908	0.799	0.911	1.2	2.21	2.15
K_2O	0.39	0.641	0.384	0.368	0.918	0.639	0.898	0.776	0.604	0.602
CaO	8.53	5.76	8.56	9.1	1.58	1.23	1.53	1.53	2.31	2.15
TiO_2	0.12	0.151	0.107	0.108	0.353	0.256	0.357	0.318	0.228	0.227
V_2O_5	0.00	0.0064	0.0055		0.0196	0.0141	0.0193	0.0159	0.0071	0.008
Cr_2O_3	0.08	0.091	0.082	0.132	0.066	0.086	0.058	0.086	0.066	0.06
MnO	0.07	0.049	0.074	0.076	0.044	0.0395	0.049	0.047	0.0215	0.0185
Fe_2O_3	2.39	2.57	2.34	2.59	2.78	2.4	2.95	2.62	1.51	1.38
CuO	0.01	0.056	0.0123	0.0131	0.0153	0.0147	0.0144	0.0101		

Table D- 2 XRF analysis of fly ashes after the tests at 950°C

Fly ash composition:	Fly ash-3				Fly ash-4				Fly ash-1	
	1000 ppm		4000 ppm		1000 ppm		4000 ppm		1000 ppm	
	Air	Oxy	Air	Oxy	Air	Oxy	Air	Oxy	Air	Oxy
Na_2O	0.15	0.19	0.20	0.14	0.65	0.66	0.20	0.76	0.22	0.33
MgO	1.42	1.57	1.52	1.04	1.44	1.53	0.48	1.59	1.36	1.29
Al_2O_3	11.42	8.64	15.15	5.8	24.79	24.37	8.90	27.31	19.28	21.45
SiO_2	49.24	51.58	38.16	68.17	51.03	53.97	73.66	51.42	52.77	52.68
P_2O_5	0.16	0.17	0.15	0.13	0.46	0.49	0.13	0.40	0.17	0.17
SO_3	8.11	4.99	15.15	5	4.42	2.74	3.59	3.5	3.05	3.49
K_2O	0.44	0.29	0.66	0.14	2.42	2.08	0.64	2.37	0.26	0.45
CaO	20.05	10.67	19.73	8.16	4.67	4.59	1.37	4.22	16.7	13.92
TiO_2	0.44	0.38	0.49	0.25	1.16	1.02	0.41	1.06	1.04	1.15
V_2O_5	0.03	0.06	0.02		0.08	0.07	0.034	0.06	0.04	0.05
Cr_2O_3	0.12	0.68	0.18	0.304	0.07	0.13	0.17	0.08	0.11	0.14
MnO	0.11	0.28	0.11	0.13	0.12	0.12	0.07	0.11	0.10	0.08
Fe_2O_3	8.06	18.89	8.11	9.59	7.93	7.35	5.84	6.58	4.21	4.22
CuO	0.02	0.62	0.02	0.06	0.04	0.08	0.05	0.03	0.017	0.019

Appendix E Illustration of glass condenser and sintered filter

E.1 Design of experimental tests

(a) (b)

Figure E-1 Clean glass condenser (a) and with condensed SO_3 (b)

Figure E-2 Sintered filter with fly ash

Appendix F Sulfur balance

F.1 SO_2 retention test and sulfur balance table

During the catalysed tests at 950°C, a lower SO_2 concentration was noted. This change of SO_2 concentration was detected using FTIR and later confirmed by titration method as noted in section 3.3. Therefore, to measure the amount of SO_2 captured by the fly ashes, a similar test procedure was performed as in SO_3 measurements. These tests were conducted in the presence of 10 g of each fly ashes. The exit gas was measured by the gas analyser to monitor SO_2 concentration. The only difference between SO_3 tests was that the flow rate of the gas through the rig was higher in the SO_2 tests since this was required by the gas analyser. Therefore, the volumetric flow rate of N_2 in the final mixture gas was increased two times. As a result, an increase of N_2 corresponded to the equivalent decrease of SO_2 to 500 ppm, O_2 to 3%, and H_2O to 3% concentrations through the reactor.

The effect of fly ashes on SO_2 concentrations are illustrated in Figure G-1 when 10 g of FA was added. SO_2 concentration increased suddenly for Fly ash 1 and 4, and then dropped gradually. Rapid increase of SO_2 concentration with Fly ash 1 and Fly ash 4 was due to the combustion process of an unburnt char in the ashes. This appears to have led to the oxidation of the sulfur left in the unburnt char. In comparison to Fly ash 1 and Fly ash 4, SO_2 concentration did not change when Fly ash 3 is added and but instead started to decrease suddenly. It appears that less SO_2 concentration is absorbed by Fly ash-1 and Fly ash 4 due to their low alkalinity content. The details of the ash composition can be found in Table 3-3. By contrast, Fly ash 4 with higher CaO and MgO contents absorbed all of the SO_2. Therefore, it can be concluded that alkaline content of fly ashes can absorb SO_2 concentration.

Following Table F-1 and F-2 give experimental data on the sulfur balance including SO_3, SO_2 in the exit gas and SO_2 sink to the ash.

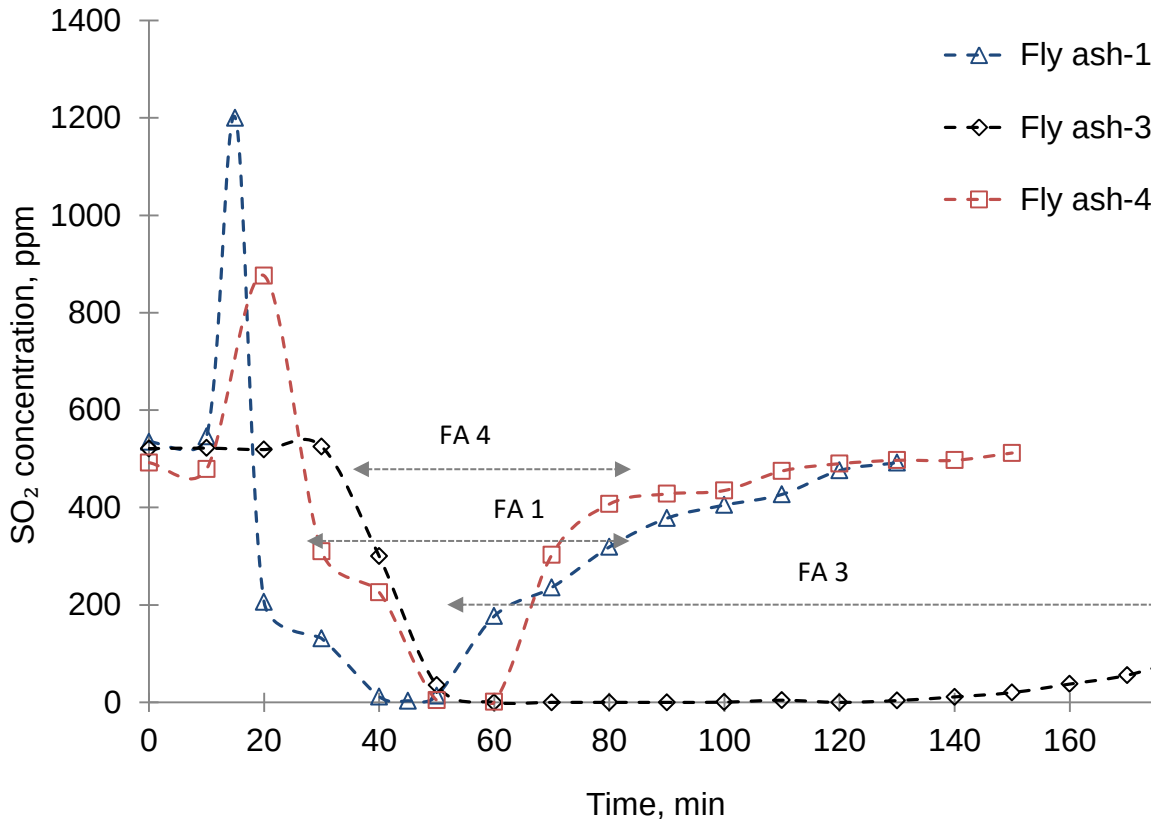

Figure F-1 SO_2 capture by fly ashes

Table F-1 Sulfur balance from bench-scale BFB tests (Uncatalysed tests at 950°C)

Test conditions	Mode	SO_3 (ppm)	SO_2 (ppm)	SO_3/SO_2, %	SO_2 sink (ppm)
SO_2-1000 ppm, O_2 - 4%, CO_2- 17%, H_2O - 6%, bal - N_2;	Air	18.15	965.55	1.88%	-
SO_2-4000 ppm, O_2 - 4%, CO_2- 17%, H_2O - 6%, Bal - N_2;	Air	81.32	3695.00	2.20%	-
SO_2-1000 ppm, O_2 - 5%, H_2O - 12%, CO_2- bal;	Oxy	24.4	973.3	2.51%	-
SO_2-4000 ppm, O_2 - 5%, H_2O - 11%, bal - CO_2;	Oxy	28.7	4185.9	0.69%	-

Table F-2 Sulfur balance from the bench-scale BFB (Catalysed tests at 950°C)

Test conditions	Mode	SO_3 (ppm)	SO_2 (ppm)	SO_3/SO_2, %	SO_2 sink (ppm)
Fly Ash-1 (Southeast FA)					
SO_2-1000 ppm, O_2 - 5%, H_2O - 11%, bal- CO_2;	Air	15.6	785	1.9%	215
SO_2-1000 ppm, O_2 - 4%, CO_2- 17%, H_2O - 6%, bal - N_2;	Air	17.3	762	2.2%	221
Fly Ash-3 (Canadian FA)					
SO_2-1000 ppm, O_2 - 4%, CO_2- 17%, H_2O - 6%, bal - N_2;	Air	4.1	353	0.46	647
SO_2-4000 ppm, O_2 - 4%, CO_2- 17%, H_2O - 6%, Bal - N_2;	Air	12.4	3383	0.31	617
SO_2-1000 ppm, O_2 - 5%, H_2O - 12%, CO_2- bal;	Oxy	50.4	409	5.04%	541
SO_2-4000 ppm, O_2 - 5%, H_2O - 11%, bal - CO_2;	Oxy	86.8	2909	2.17%	1004
Fly Ash-4 (British FA)					
SO_2-1000 ppm, O_2 - 4%, CO_2- 17%, H_2O - 6%, bal - N_2;	Air	11.0	922	1.2	78
SO_2-4000 ppm, O_2 - 4%, CO_2- 17%, H_2O - 6%, Bal - N_2;	Air	12.0	4177	0.3	-
SO_2-1000 ppm, O_2 - 5%, H_2O - 12%, CO_2- bal;	Oxy	25.7	1055	2.4	-
SO_2-4000 ppm, O_2 - 5%, H_2O - 11%, bal - CO_2;	Oxy	122	4117	2.9	-

Appendix G Coals analysis

G.1 High heating value (HHV) of South-East Indian coal

During the visit to an Indian Institute of Technology, low-rank bituminous coal from South-East part of India was analysed. This part employed bomb colorimeter and CHNS analyser. The results can be seen in Table G-1.

Table G-1 Ultimate, proximate analysis and HHV of coal

Proximate analysis	**Assam coal**
Moisture	2.18 %
Volatile matter	22.96 %
Fixed carbon	27.34 %
Ash	47.52 %
Ultimate analysis	
Carbon	38.94 %
Hydrogen	3.76 %
Nitrogen	0.99 %
Oxygen	54.74 %
Sulphur	1.71 %
HHV	13 500 kJ/kg

Appendix H Hydrodynamic experiments on a small-scale circulating fluidised bed reactor at elevated operating pressure, and under an O_2/CO_2 environment.

HYDRODYNAMIC EXPERIMENTS ON A SMALL-SCALE CIRCULATING FLUIDISED BED REACTOR AT ELEVATED OPERATING PRESSURE, AND UNDER AN O_2/CO_2 ENVIRONMENT.

Yerbol SARBASSOV*[a], Azd ZAYOUD[b], Pinakeswar MAHANTA[b], Sai GU[a], Panneerselvam RANGANATHAN[a] and Ujjwal K. SAHA[b]

[a]School of Energy, Environment and Agrifood, Cranfield University,Cranfield MK43OAL,United Kingdom

[b]Mechanical Engineering Department, Indian Institute of Technology Guwahati, Guwahati 781039, Assam, India

Pressurised circulating fluidised bed (CFB) technology is a potentially promising development for clean coal technologies. The current work explores the hydrodynamics of a small-scale circulating fluidised bed at elevated operating pressures ranging from 0.10 to 0.25 MPa. The initial experiments were performed at atmospheric pressure with air and O_2/CO_2 environments as the fluidisation gas to simulate the hydrodynamics in a CFB. A comparison between the effects of air and O_2/CO_2 mixtures on the hydrodynamics was outlined in this paper for particles of 160 μm diameter. A small but distinct effect on axial voidage was observed due to the change in gas density in the dense zone of the bed at lower gas velocity, while only minimal differences were noticed at higher gas velocities. The hydrodynamic parameters such as pressure drop and axial voidage profile along the height were reported at two different bed inventories (0.5 and 0.75 kg) for three mean particle sizes of 160, 302 and 427 μm and three superficial gas velocities. It was observed that the operating pressure had a significant effect on the hydrodynamic parameters of bed pressure drop and axial bed voidage profiles. The effect of solids loading resulted in an exponential change in pressure drop profile at atmospheric pressure as well as at elevated pressure. The experimental results on hydrodynamic parameters are in reasonable agreement with published observations in the literature.

Keywords: *circulating fluidised bed, pressurised circulating fluidised bed, pressure drop, axial voidage profile, O_2/CO_2 mixture*

1. Introduction

Currently, 40% of the world's electricity is generated by coal-fired power plants which consequently are a major contributor to climate change due to greenhouse gas emissions, mainly carbon dioxide [1]. Further research on development of clean coal technology and carbon capture and storage (CCS) technology is required to reduce emissions from heavy industry and power plants. Circulating fluidised bed (CFB) technologies, have been developed commercially over the past 50 years, and are utilised in clean coal technologies to produce electricity [2]. However, the technology is still evolving and it is possible to increase the energy efficiency of the CFB power plants. CFB technology has a number of advantages over pulverised coal boilers such as the ability to utilise low-rank coals, and provide a wider turndown capacity [3-5]. Nowak et al. [5] have outlined the advantages of CFB technologies

built in Poland between 1996 and 2003. Recently, CanmetENERGY has developed various oxy-fuel CFB reactors with capacity range of 0.1 MW to 0.8 MW [6-7]. Moreover, Foster Wheeler has commissioned and successfully tested a 30 MW oxy-fired CFB pilot-scale plant in Spain [8]. Most experimental research focuses on atmospheric CFB technologies. However, circulating fluidised bed technology at elevated operating pressure could prove to be an additional option to use in conjunction with clean coal technology. It was reported that overall combustion efficiency increases at elevated pressure, due to higher char burn-out rate and higher heat transfer [9-11]. Furthermore, building pressurised fluidised bed systems requires less space because of their compactness [9]. Taking into account the size advantages of pressurised fluidised beds over atmospheric fluidised beds, more research on new design configurations, such as the novel design tested by Wang et al. [12], are still desirable for efficient utilisation of certain coals. Gupta and Nag [11] have studied bed-to-wall heat transfer including hydrodynamic parameters such as voidage and suspension density in pressurised circulating fluidised beds (PCFBs). Silica sand was used with particle size of 260 μm and superficial gas velocity ranged between 0.25 m/s and 1.25 m/s. These authors have carried out experiments mostly in the bubbling fluidised bed regime rather than the fast fluidised or pneumatic transport regimes. Li et al. [13] also investigated minimum and terminal velocity of coal gasification materials under 2.5 MPa pressure. Results show that minimum fluidisation and terminal velocity decrease with pressure. The reported fundamental studies of fluidisation conducted in pressurised bubbling fluidised bed (PBFB) reactors are given in tab. 1.

In addition to the cold flow investigation in PCFB, some notable hot flow investigations have been found in the literature. Duan et al. [14] reported that higher operating pressure improves both heat transfer and carbon conversion than for atmospheric CFB reactors. MacNeil and Basu [15] investigated char combustion rate in a 5.5 kW PCFB reactor. The results show a large effect of pressure on combustion rate. Pressurised fluidised bed systems with combined cycle have been widely used in Japan, particularly for large-scale electricity generation [16]. Hong et al. [17] have investigated the feasibility of oxy-fuel combustion in a pressurised coal reactor by different simulation packages such as Thermoflex and Aspen plus. Their results show an increase of overall net efficiency by 3% at 1.0 MPa. Previously, a parametric study of a pressurised CFB reactor has been investigated by Kalita et al. [18-19] on the same unit. The tests have covered the hydrodynamics for blended inert particles and biomass under different weight proportions. It is important to notice that these studies were conducted with relatively higher parameters, where bed pressure increased from 0.3 to 0.5 MPa while superficial gas velocities through the unit were fixed at from 5 to 7 m/sec. Granted that a few experimental studies have been conducted on the hydrodynamics of circulating fluidised beds at elevated operating pressure; however, studies related to the cold flow hydrodynamics of CFB under oxy-fuel conditions at elevated pressure have not been reported in detail. Previously, Komorowski and Nowak have tested the effect of air and carbon dioxide as the fluidisation medium for glass beads under cold conditions [20]. Their results showed that the axial solids distribution was non-uniform at low superficial velocity and gradually tended to uniform with increasing superficial gas velocity to 1.25 m/s. Guedea et al. [21] investigated the influence of

Table 1 Fundamental pressurised fluidised bed studies

Authors	Bed material	d_p range (mm)	Pressure (kPa)	Findings
Llop *et al*. [22]	Silica sand	0.21-1.46;	1500	Prediction of bed expansion has been developed; bed expansion increases with pressure for both Geldart B and D particles.
Barreto *et al*. [23]	Silica-Alumina, zeolite	0.07-0.09	2000	Decrease of average particle size and bubble velocity observed. Bubble flow and hold up decreased with pressure; U_{mf} and U_{mb} increase with pressure.
Wiman *et al*. [24]	Sand	0.45-0.70	1600	Erosion rate and average heat transfer coefficient increased with pressure.
Olowson *et al*. [25-27]	Silica sand	0.31; 0.70; 0.98	1600	Minimum fluidisation velocity decreases with pressure increases. Dense phase voidage at U_{mf} does not change with pressure for small particles, while slight increase is observed for the larger particles.
Carsky *et al*. [28]	Sand	0.60	1300	Overall bubble size decreases up to 400 kPa, significant difference in bubble size for higher pressure was observed. Bubble frequency increases with excess velocity of air.
Sidorenko *et al*. [29]	Fluid catalytic cracking, sand	0.08	101-2100	No effect of pressure was observed for particles group Geldart A, while for Geldart B particle group, U_{mf} decreases slightly. Bed voidage at U_{mf} found independent of operating pressure.
Richtberg *et al*. [30]	Glass beads	0.08	100-500	Homogeneous fluidisation was obtained as result of bed pressure in PCFB.
Marzocchella *et al*. [31]	Glass beads	0.07-0.20	100-8000	Hydrodynamics at supercritical pressure with CO_2 ambient studied. Regions of homogeneous fluidisation broaden due to the density of carbon dioxide fluid; fluidisation was smoother under aggregative conditions.
Cao *et al*. [32]	Polystyrene beads	1.00	100-1100	Average bed voidage increases with pressure at same velocity.
Borodulya *et al*. [33-34]	Sand	0.13-1.22	8000	Heat transfer coefficient increases from the bed to the surface.

O_2/CO_2 mixtures on fluid dynamics in a bubbling fluidised bed (90 kW) at CIRCE, Spain. Experiments were conducted under ambient as well as high-temperature conditions. It was concluded that larger CO2 concentrations cause greater bed voidage and bed expansion. The current work studies the effect of operating pressure on hydrodynamic parameters such as bed pressure drop and voidage profiles. Furthermore, cold experiments were conducted with O2/CO2 mixtures at atmospheric pressure to simulate oxy-fired CFB hydrodynamics.

2. Experimental Setup and Methodology

Hydrodynamic experiments were conducted in a small-scale circulating fluidised bed setup is illustrated in fig.1. The CFB system consists of riser, solid separator cyclone, downcomer and auxiliaries such as air compressor and gas cylinders. The height of the CFB riser is 2000 mm with an inner diameter (ID) of 54 mm. Pressurised air was supplied by an air compressor connected to the bottom part of the riser. The height of the air plenum is 40 mm. The perforated distributor plate had an opening area of 17%. When an O2/CO2 mixture environment was used, the oxygen and carbon dioxide gases were provided by cylinders as seen in fig. 1. Before feeding gases to the reactor, both CO2 and O2 gases were well mixed in a static cyclone mix. The static mixer has a height of 200 mm and diameter of 60 mm. Silica sand of Geldart B group was used in the experiments with three mean particle diameters of 160, 302 and 427 μm. Sauter mean diameters (SMD) of the particles (dp) were determined from sieve analysis as noted by Olowson et al. [25]. The minimum fluidisation velocity (Umf) was determined from the Ergun equation. Experiments were conducted at four different operating pressures: 0.10, 0.15, 0.20 and 0.25 MPa. At each operating pressure, three superficial gas velocities were considered in terms of non-dimensional value Ugas/Ut as 25%, 50% and 75% of terminal velocity (Ut) depending on mean particle size. Actual values of superficial gas velocity are given in tab. 2.

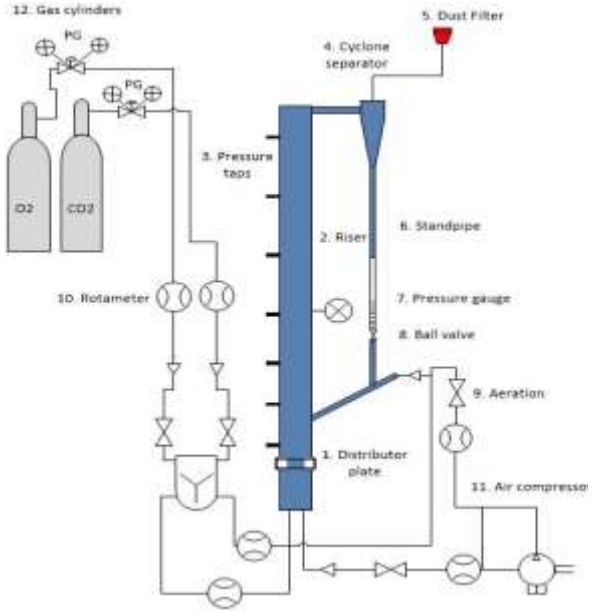

Figure 1. Circulating fluidised bed riser (air and O2/CO2 mode)

The terminal velocities of the mean particle sizes were determined following Kunii and Levenspiel [35]. The dimensionless values of particle size (d*) and gas velocity (U*) are approximated for the direct evaluation of the terminal velocity of particles. It should be noted that the gas viscosity is dependent on temperature and does not change significantly with bed pressure. With increase of gas density in the reactor due to the increasing bed pressure, the terminal velocity is expected to decrease, leading to a change of bed pressure drop. However, fixed terminal velocity values of atmospheric pressure are used for all conditions in these experiments. Experiments also included two bed inventory weights of 0.5 and 0.75 kg. The solid recirculation rate (Gs) was measured by a transparent high-pressure plastic tube in the return leg. The accumulated solids height was measured by transparent pipe. The pressure drop

Table 2 Calculated gas velocity (m/s) for each mean particle size

Mean particle size, μm	25%	50%	75%
160	1.1	1.3	1.5
302	2.1	2.5	2.9
427	2.7	3.3	3.8

along the riser was measured by a water column manometer which was fabricated with 11 reading taps. A high-pressure transparent plastic tube with ID of 10 mm was connected between pressure taps and a U-type water manometer. An extra wire mesh and cotton layer were fixed in all 11 taps to prevent escape of solid particles to the water manometer. For uncertainty analysis, each experiment was repeated three times and average data of these experiments were taken as representative. Pressure drop (ΔPbed) profiles were photographed three times by digital camera with 2 s intervals in order to catch ΔPbed fluctuation. Higher pressure fluctuation was observed in the dense zone of the riser than in the dilute zone. This occurs due to the coarse particles which were trapped in the freeboard. Similar pressure fluctuations in the dense zone were reported by Czakiert et al. [36].

3. Results and Discussion

3.1 Hydrodynamics at atmospheric pressure

3.1.1 Effect of superficial gas velocity on pressure drop

Superficial gas velocity ranges in this study were in the fast fluidised bed regime. Fig.2 illustrates the effect of superficial gas velocity on bed pressure drop (ΔP_{bed}), for smaller particle size of 160 μm at atmospheric pressure. The first two points in fig. 2 represent ΔP_{bed} through the distributor plate. Pressure drop increases with superficial gas velocity which agrees well with the literature [37]. It is also found that the increase of superficial gas velocity affects the axial particle holdup distribution due to increasing bed expansion. From fig. 2, it can be seen that the pressure drop along the bed remains constant for lower superficial velocities, whereas for higher gas velocity the pressure drop rises slightly along the bed height, and tends to reach a constant value. The higher pressure drop observed at the bottom of the bed may be due to the fact that the particles are being accelerated by the inlet gas velocity. The effect of solids loading on the pressure drop is also plotted in the same figure at a gas velocity of 1.1 m/s. It is also noticed that the pressure drop exponentially increases with bed height when the solid loading was increased to 0.75 kg. The exponential increase of pressure drop is more pronounced at the bottom of the bed and indicates the presence of a dense solid bed. This region is called the acceleration zone. Above this region, the pressure drop increases slightly with bed height. This

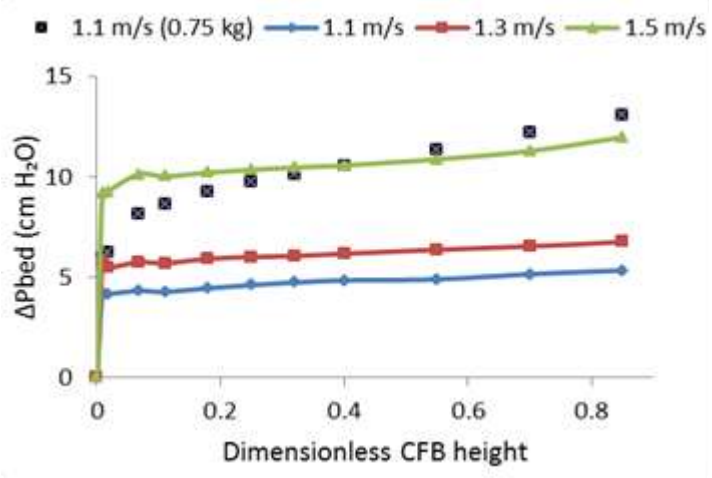

Figure 2. Effect of superficial gas velocity on ΔP_{bed} over the bed (d_p-160 μm, solids loading 0.5 kg)

suggests a fully accelerated particle flow in this region. This behaviour is also consistent with the literature [38].

3.1.2 Effect of superficial gas velocity on bed voidage

The effect of superficial gas velocity on bed voidage is illustrated in fig. 3(a-b). The voidage in the bed was determined using pressure drop calculations. It can be noticed from fig. 3(a) that voidage profiles increase with superficial gas velocity (1.1 – 1.5 m/s). Increase of superficial gas velocity raises the solids holdup capacity which tends to increase voidage, which agrees with other studies [39]. It is also found from fig. 3(a) that lower voidage at the bottom of the riser is observed for all gas velocities. This may be due to the fact that the bottom region of the riser is mainly affected by particle acceleration and gas distribution. Above this region, for all gas velocities, the voidage increases exponentially, approaching constant values near the riser exit. This exponential shape occurs when particles entering the bottom of the reactor are entrained by aeration [18]. It is clearly seen from fig. 3(a) that the developing flow region with low voidage occurs up to 0.2 m and a fully-developed region with relatively high voidage begins above 0.2 m. It is important to mention that the exponential shape of the axial profile varies with superficial gas velocity. Also, it is observed that the axial voidage profiles move in parallel from high voidage toward low voidage with decreasing gas velocity. The effect of particle size on the axial voidage profiles in the riser at lower gas velocities $U_{1g}=0.25U_t$ of 1.1, 2.1 and 2.7 m/s, respectively is shown in fig. 3(b). The results indicate that the increase of particle size had an obvious effect on voidage, resulting in a slight difference at the top of the riser, but significantly lower voidages at the bottom. It is also found that the voidage at the bottom of the riser is higher for the larger particle (427 μm) than for the smaller particle (160

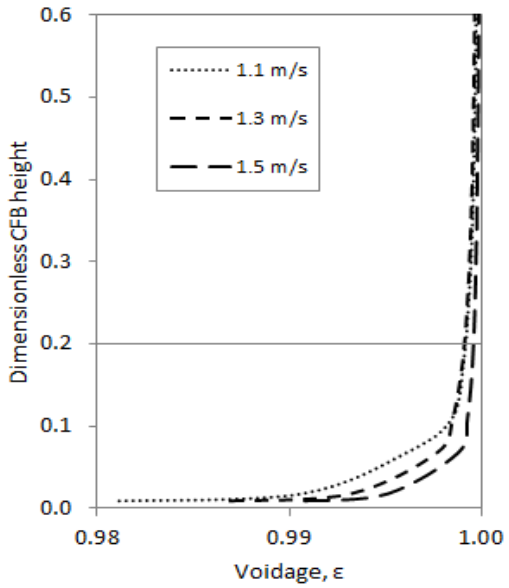

Figure 3a. Effect of superficial gas velocity on axial voidage profile (d_p-160 μm)

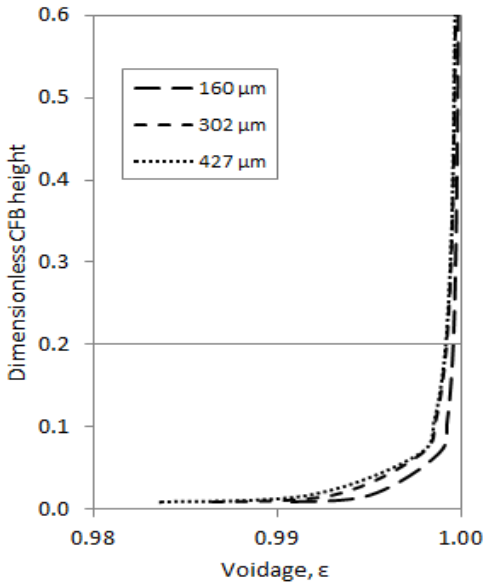

Figure 3b. Effect of particle size on axial voidage profile at lower gas velocity

μm). The voidage tends to distribute more at the riser bottom for the large particles in comparison to smaller particles. It has been shown that most particles are mainly found near the wall of the riser in the freeboard area (S. Mahmoudi, C. W. Chan, A. Brems, J. Seville, J. Baeyens 2012). Solid particles separated by the cyclone were injected into the riser with a small amount of aeration which diluted the particles near the wall. Due to the range of mean particle size distribution, the larger particles continue to remain in the dense zone at lower gas velocity, whereas the smaller particles are expected to be carried out to the top by gas velocity.

3.1.3 Effect of O_2/CO_2 mixture on bed voidage

Industrial-scale CFB reactors operate at temperatures between 800-900°C. The dynamic viscosity and density of gases change with operating temperature and pressure, respectively. The present case uses mixtures of CO_2 and O_2 gases to study the effect of density and viscosity on the cold flow hydrodynamics in the small-scale CFB riser. Only the smallest mean particle size of 160 μm with a solids loading of 0.5 kg was tested. Figure 4(a-b) represents the voidage profiles along the height of the bed for different fluidisation gases including O_2/CO_2 mixtures and air at superficial gas velocities 1.1 and 1.5 m/s (U_{1g} and U_{3g}). It is important to mention that the dynamic viscosity of gases does not change with pressure, while the density can be evaluated following by Li et al. [13]. Comparing O_2/CO_2 mixtures with air, the axial voidage profile shows a difference in both the dense and freeboard zones of the riser for the lower superficial gas velocity; *i.e.*, in the case of air, the axial profile of voidage is higher than that in O_2/CO_2. This behaviour may be due to the higher density of the O_2/CO_2 mixture compared to air. When superficial gas velocity increased to 1.5 m/s (U_{3g}), no difference in axial voidage was observed between O_2/CO_2 mixtures and air. Identical results were reported by Komorowski and Nowak [20]. These authors observed that a low superficial gas velocity of O_2/CO_2 mixture produced a large difference in suspension density profile compared to air, while at higher velocity, the profiles were similar. It can be concluded that in the fast fluidisation regime, the axial voidage profile of O_2/CO_2 mixture is similar to that for an air-fluidised CFB. In addition, similar heat transfer rates could be expected from identical voidage or suspension density profiles in air and O_2/CO_2 mixture gases. However, it should be noted that, for highly exothermic reactions such as occur in coal-fired CFB combustors, good temperature control can be achieved because of the intensive mixing and circulation rate. It is also important to highlight that CO_2 has higher heating capacity compared to nitrogen. For this reason, the combustion temperature in oxy-fired furnaces is moderated by flue gas recirculation [41].

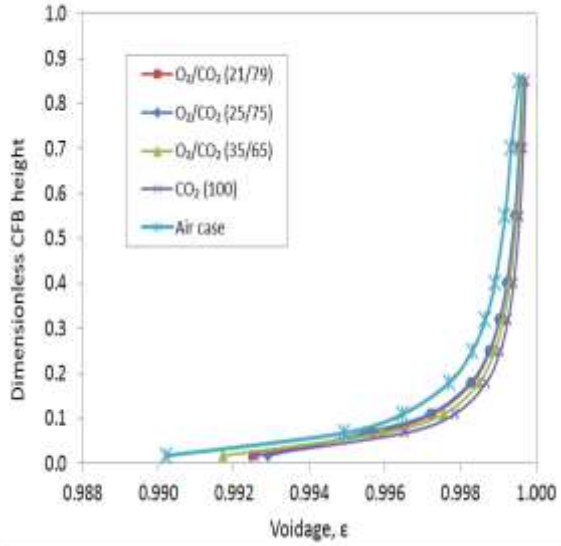

Figure 4a. Bed voidage vs O_2/CO_2 mixture (gas velocity 1.1 m/s, solids loading 0.5 kg)

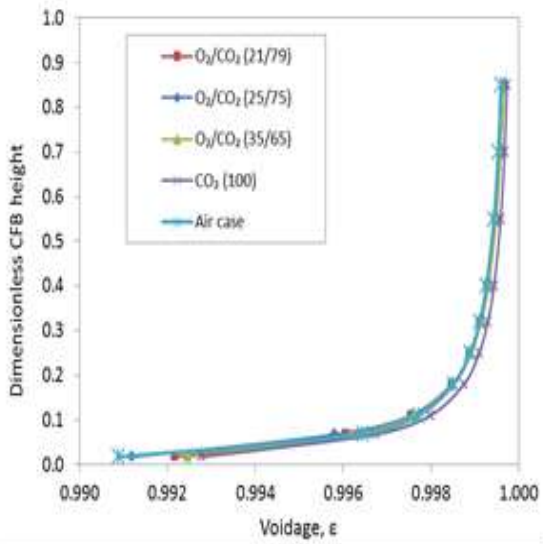

Figure 4b. Bed voidage vs O_2/CO_2 mixture (gas velocity 1.5 m/s, solids loading 0.5 kg)

3.2 Effect of operating pressure on hydrodynamic properties

3.2.1 Effect of operating pressure on pressure drop

Pressure drop (ΔP_{bed}) along the height of the riser was measured at different operating pressures from 0.10 to 0.25 MPa. Figure 5 illustrates pressure drop profiles along the bed riser at the lower superficial gas velocity of 2.1 m/s (U_{1g}) for the particle size of 302 μm. It can be seen from the fig. 5 that operating bed pressure has a clear effect on the bed pressure drop. The total pressure drop, ΔP_{bed} from 0.10 MPa (atmospheric pressure) to 0.25 MPa, increases from 10 cm H_2O to 15 cm H_2O, respectively. Small fluctuations were observed at 0.20 and 0.25 MPa in the acceleration zone due to the aeration of gas, while at the fully developed zone it increases exponentially over the bed height. As discussed by Yin *et al*. [40] the operating pressure conditions in the bed could lead to the decrease of superficial gas velocity in the reactor. This consequently results in a decrease of particle velocity. This means that more solid particles were found in the riser, leading to the higher pressure drop in the bed.

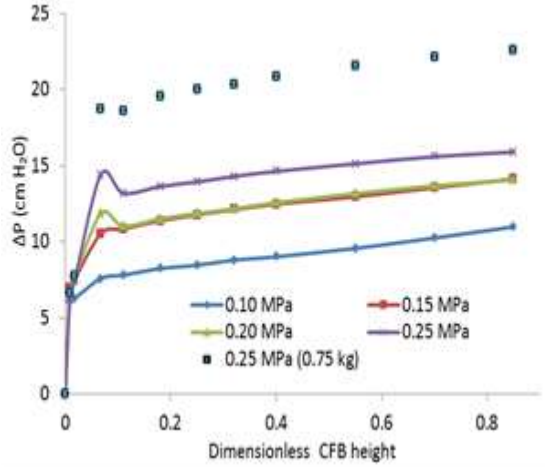

Figure 5. Effect of operating pressure on pressure drop at gas velocity 2.1 m/s (d_p - 302 µm, solids loading 0.5 kg)

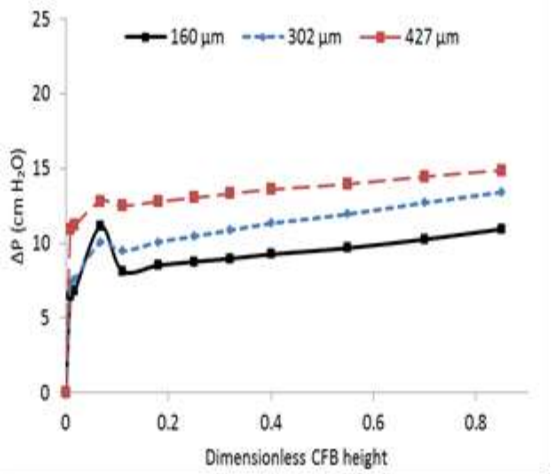

Figure 6. Effect of mean particle size on pressure drop at superficial gas velocity of 50% of U_t and bed pressure 0.20 MPa

Additionally, the effect of solids loading (0.75 kg) is also illustrated in fig. 5 at the operating pressure of 0.25 MPa, which shows higher pressure drop compared to the same case with bed inventory of 0.5 kg. This is due to the accumulation of additional bed material mass in the bed which leads to the further increase of bed pressure drop. Also it is found that the pressure drop gradually increases with the riser bed height. Similar observations were found by Richtberg *et al*. [30]. They observed an exponentially increasing trend at higher pressure (0.50 MPa) for bed pressure drop with glass beads. Figure 6 shows the effect of particle size of 160, 302 and 427 µm on pressure drop (ΔP_{bed}) for the operating pressure of 0.20 MPa, at the gas superficial velocity (U_{2g}=0.50U_t) of 1.3, 2.5 and 3.3 m/s, respectively. It can be noted from fig. 6 that the increase of particle size leads to increasing bed pressure drop. This could be due to the fact that smaller particles have less drag force compared to the larger particles. Also, it is found that for all particle sizes, the pressure drop increases exponentially with riser height. The effect of gas superficial velocity on pressure drop (ΔP_{bed}) at elevated pressure (0.20 MPa) for a particle size of 160 µm is shown in fig 7. It is found that the bed pressure increases with gas superficial velocity. This may be due to the fact that an increase in gas superficial velocity results in an increase of drag force on the particles, which leads to increasing solid particle distribution in the bed. As a result, higher bed pressure is generated for

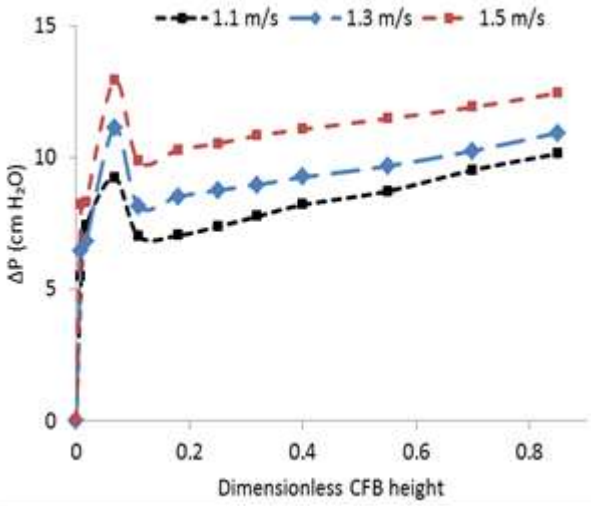

Figure 7. Effect of superficial gas velocity on pressure drop at operating pressure of 0.20 MPa

higher gas velocity at fixed operating pressure. It can also be seen from the fig.7 that the higher superficial gas velocity results in high fluctuations of pressure drop in the dense zone of the bed.

3.2.2 Effect of operating pressure on axial bed voidage

The voidage profiles of the riser are illustrated in fig. 8 for the superficial gas velocity of 2.1 m/s (U_{1g}) at different bed operating pressures (0.10 to 0.25 MPa). This plot is shown for the particle size of 302 µm. It can be seen that operating pressure in the bed decreases the voidage along the riser, particularly in the acceleration zone (dense zone). This could be due to the increase of bed pressure. The pressurised state of the bed leads to the decrease of gas velocity which results in particle accumulation in the bottom zone of the bed. Similar observations were made by Yin *et al*. [42]. Also it can be seen that the exponential shape of the

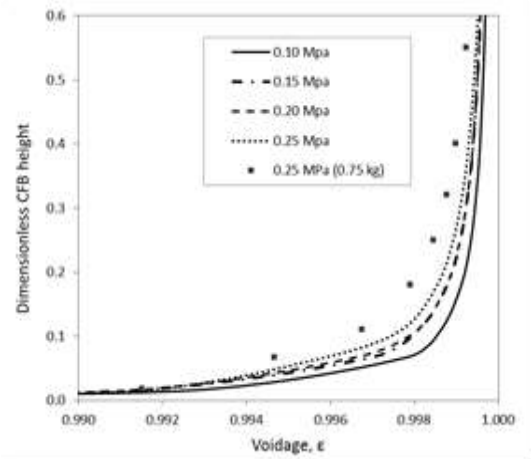

Figure 8. Voidage profile along the height for the fixed particle size (d_p - 302 µm, gas velocity-2.1 m/s, solids loading 0.5 kg)

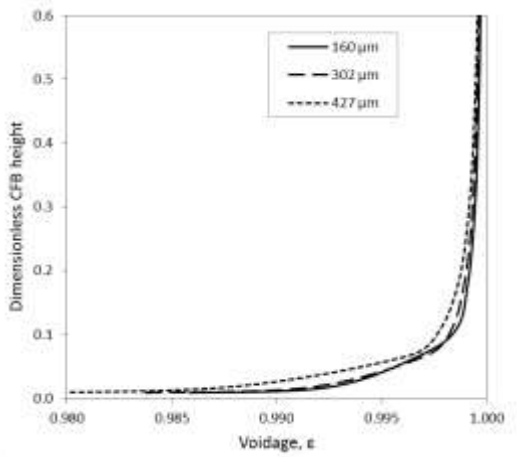

Figure 9. Effect of mean particle size on axial voidage (gas velocity 50% of U_t; bed pressure 0.20 MPa, solids loading 0.5 kg)

axial profile varies for different operating pressures and the developing flow region; *i.e*., the change from high to low voidage occurs mainly up to 0.5 m. The effect of higher solids loading (0.75 kg) is also included in fig. 8 to demonstrate its effect on the voidage profile in the riser. It can be seen from fig.8 that at the bottom of the riser, the voidage profiles show a similar trend, whereas higher voidage is observed above the dense zone of the riser for higher solid loading. The influence of mean particle size on the axial voidage profile at superficial gas velocity of 50% (U_t) is illustrated in fig. 9. As expected, the larger particle size develops higher voidage at the bottom dense zone of the riser

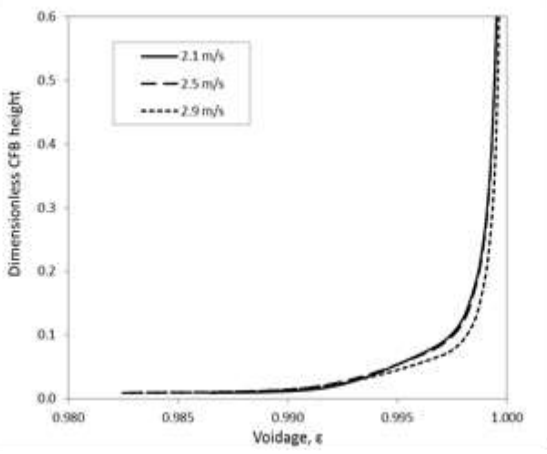

Figure 10. Axial voidage profile along the riser height at operating pressure 0.25 MPa (d_p-302 µm, superficial gas velocities – 2.1, 2.5, 2.9 m/s)

than does the smaller particle. It is also found that the voidage tends to distribute more at the riser bottom for large particles while for smaller particles, voidage is more or less uniform. The effect of superficial gas velocity on axial voidage is plotted in fig. 10, at the higher operating pressure of 0.25 MPa for particle size of 160 μm. It is found that the axial voidage profiles increase with increasing superficial gas velocity, similar to the atmospheric pressure case. This is due to the fact that the increase of superficial gas velocity causes the solids to distribute in the riser, which tends to increase the voidage in the bed. It is also found from the fig.10 that low voidages near the bottom of the riser are observed for higher gas velocity due to particle acceleration and gas distribution. Above this region, for all gas velocities, the voidage increases exponentially, eventually approaching a constant value near the riser exit. It is important to mention from the fig.10 that the developing flow region occurs up to about 0.35 m and a fully-developed region with relatively high voidage begins above 0.35 m height. These values are different from those found in the atmospheric pressure case.

4 Conclusions

A hydrodynamic cold flow study of silica sand was undertaken with air and O_2/CO_2 mixtures as the fluidisation medium at atmospheric pressure. Additionally, experiments were conducted with air at elevated operating pressure to investigate the pressure effect on hydrodynamic parameters. The increase of bed pressure drop (ΔP_{bed}) along the bed height is similar for all three superficial gas velocities. The effect of superficial gas velocity and particle size on axial bed voidage profiles shows an increasing trend as expected. These observations agree with previously reported studies. In the case of O_2/CO_2 mixtures, a notable effect of different O_2/CO_2 proportions on axial voidage was seen at the dense zone of the riser, compared to the voidage measured when air was used. However, with further increase of superficial gas velocity from 1.1 to 1.5 m/s, these differences in axial voidage disappeared. The overall pressure drop profile increases with operating bed pressure, which agrees well with the literature. Increased solids loading appear to increase hydrodynamic parameters. Also, increase of particle size and superficial gas velocity at elevated pressure resulted to increase of bed pressure drop and axial voidage profiles, respectively.

Overall, it can be concluded that operating pressure has a significant effect on hydrodynamic parameters in the cold flow environment. It should be mentioned that even at low operating pressure as mentioned in this work (0.25 MPa), the pressure drop increased from 10 to 15 (cm H_2O) and 22 (cm H_2O in) at increased solids loaded case. According to previous studies of hydrodynamics as presented in Table 2, more pronounced effect of hydrodynamic parameters could be expected with increase of operating bed pressure. In the case of cold flow hydrodynamics of O_2/CO_2 mixtures, it should be noted that at fast fluidized bed and pneumatic transport regimes, no significant differences are noted between O_2/CO_2 mixtures and air. Increasing interest in pressurized CFB over atmospheric CFB and change in size configuration should always lead to a detailed hydrodynamic investigation, particularly in cold flow environment.

Acknowledgements

The authors would like to acknowledge Project FP7 iComfluid (International collaboration on computational modelling of fluidised bed systems for clean energy technologies), No. 212261 for funding this work in the context of development of clean coal technologies in India.

References

[1] IEA, Key World Energy Statistics, 2012
[2] Basu, P., Combustion of coal in circulating fluidized-bed boilers: a review, Chem. Eng. Sci., 54 (1999), 22, pp. 5547–5557
[3] Beer, J.M., High efficiency electric power generation: The environmental role, Prog. Energy Combust. Sci., 33 (2007), pp. 107–134
[4] Grace, J.R., Avidan, A.A., Knowlton, T.M., Ed, Circulating Fluidized Beds, Blackie Academic & Professional., London, UK, 1997
[5] Nowak, W., Clean coal fluidized-bed technology in Poland, Appl. Energy., 74 (2003), pp. 405–413
[6] Anthony, E.J., Oxyfuel CFBC: status and anticipated development, Greenh. Gases Sci. Technol., 3 (2013), pp. 116–123
[7] Tan, Y., et al., Experiences and results on a 0.8MWth oxy-fuel operation pilot-scale circulating fluidized bed, Appl. Energy., 92 (2012), pp. 343–347
[8] Lupion, M., et al., 30 MWth CIUDEN Oxy-CFB Boiler - First Experiences, Energy Procedia, 37 (2013), pp. 6179–6188
[9] Niksa, S., et al., Coal conversion submodels for design applications at elevated pressures. Part I. devolatilization and char oxidation, Prog. Energy Combust. Sci., 29 (2003), 5, pp. 425–477
[10] Huang, Y., et al., Influences of coal type on the performance of a pressurised fluidised bed combustion power plant, Fuel., 79 (2000), pp. 1595–1601
[11] Gupta, A.V.S.S.K.S., Nag, P.K., Bed-to-wall heat transfer behaviour in a pressurized circulating fluidized bed, Int. J. Heat Mass Transf., 45 (2002), pp. 3429–3436
[12] Wang., A.T.L., et al., Hydrodynamic performance of a novel design on pressurized fluidized bed combustor, J. Energy Resour. Technol., 128 (2006), pp. 111–117
[13] Li, J., et al., Minimum and terminal velocity in fluidization of coal gasification materials and and coal blending of gasification under pressure, Fuel., 110 (2013), pp. 153–161
[14] Duan, F., et al., Dependence of bituminous coal gasification on pressure in a turbulent circulating fluidized bed, Asia-Pacific J. Chem. Eng., 7 (2012), pp. 822–827
[15] MacNeil, S., Basu, P., Effect of pressure on char combustion in a pressurized circulating fluidized bed boiler, Fuel., 77 (1998), 4, pp. 269–275
[16] Stubington, J.F., Wang, A.L.T., Unburnt carbon elutration from pressurised fluidised combustion of Australian black coals, Fuel., 79 (2000), pp. 1155–1160
[17] Hong, J., et al., Analysis of oxy-fuel combustion power cycle utilizing a pressurized coal combustor, Energy., 34 (2009), 9, pp. 1332–1340
[18] Kalita, P., et al., Parametric study on the hydrodynamics and heat transfer along the riser of a pressurized circulating fluidized bed unit, Exp. Therm. Fluid Sci., 44 (2013), pp. 620–630
[19] Kalita, P., et al., Effect of biomass blending on hydrodynamics and heat transfer behavior in a pressurized circulating fluidized bed unit, Int. J. Heat Mass Transf., 60 (2013), pp. 531–541
[20] Komorowski, M., Nowak, W.,Vertical solids distribution under air/carbon dioxide fluidization conditions in a circulating fluidized bed, Proceedings, 14th International Conference on Fluidization -From Fundamentals to Products, Noordwijkerhout, The

Netherlands, 2013
[21] Guedea, I., et al., Influence of O2/CO2 mixtures on the fluid-dynamics of an oxy-fired fluidized bed reactor, Chem. Eng. J., 178 (2011), pp. 129–137
[22] Llop, M.F., et al., Expansion of gas–solid fluidized beds at pressure and high temperature, Powder Technol.,107 (2000), pp. 212–225
[23] Barreto, G.F., et al., The effect of pressure on the flow of gas in fluidized beds of fine particles, Chem. Eng. Sci., 38 (1983), 12, pp. 1935–1945
[24] Wiman, J., Almstedt, A.E., Hydrodynamics, erosion and heat transfer in a pressurized fluidized: influence of pressure, fluidization velocity, particle size and tube bank geometry, Chem. Eng. Sci., 52 (1997), 16, pp. 2677–2695
[25] Olowson, P.A., Almstedt, A.E., Influence of pressure on the minimum fluidization velocity, Chem. Eng. Sci., 46 (1991), 2, pp. 637–640
[26] Olowson, P.A., Influence of pressure and fluidization velocity on the hydrodynamics of a fluidized bed containing horizontal tubes, Chem. Eng. Sci., 49 (1994), 15, pp. 2437–2446
[27] Olowson, P.A., Almstedt, A.E., Hydrodynamics of a bubbling fluidized bed: Influence of pressure and fluidization velocity in terms of of drag force, Chem. Eng. Sci., 47 (1992), 2, pp. 357–366
[28] Carsky, M., Hartman, M., The bubble frequency in a fluidized bed at elevated pressure, Powder Technol., 61 (1990), pp. 251–254
[29] Sidorenko, I., Rhodes, M.J., Influence of pressure on fluidization properties, Powder Technol., 141 (2004), pp. 137–154
[30] Richtberg, M., et al., Characterization of the flow patterns in a pressurized circulating fluidized bed, Powder Technol., 155 (2005), pp. 145–152
[31] Marzocchella, A., Salatino, P., Fluidization of solids with CO2 at pressures from ambient to supercritical, AIChE J., 46 (2000), 5, pp. 901–910
[32] Cao, J., et al., Simulation and experimental studies on fluidization properties in a pressurized jetting fluidized bed, Powder Technol., 183 (2008), pp. 127–132
[33] Borodulya, V.A., Heat transfer between a surface and a fluidized bed: consideration of pressure and temperature effects, Int. J. Heat Mass Transf., 34 (1991), 1, pp. 47–53
[34] Borodulya, V.A., et al., Heat transfer berween fluidized bed of large particles and horizontal tube bundles at high pressures, Int. J. Heat Mass Transf., 27 (1984), 8, pp. 1219–1225
[35] Kunii, D., Levenspiel, O., Fluidization Engineering, 2nd ed, Butterworth Heinemann., London, UK, 1991
[36] Czakiert, T., et al., Oxy-fuel circulating fluidized bed combustion in a small pilot-scale test rig, Fuel Process. Technol., 91 (2010),11, pp. 1617–1623
[37] Sanchez-Delgado, S., et al., On the minimum fluidization velocity in 2D fluidized beds, Powder Technol., 207 (2011), pp. 145-153.
[38] Chew, J.W., et al., Reverse core-annular flow of Geldart Group B particles in risers, Powder Technol., 221 (2012), pp. 1–12
[39] Das, M., et al., Axial voidage profiles and identification of flow regimes in the riser of a circulating fluidized bed, Chem. Eng. J., 145 (2008), 2, pp. 249–258
[40] Mahmoudi, S., et al., Solids flow diagram of a CFB riser using Geldart B-type powders, Particuology., 10 (2012), pp. 51–61
[41] Buhre, B.J.P., et al., Oxy-fuel combustion technology for coal-fired power generation, Prog. Energy Combust. Sci., 31 (2005), 4, pp. 283–307
[42] Yin, S., et al., Gas-solid flow behavior in a pressurized high-flux circulating fluidized bed riser, Chem. Eng. Commun., 201 (2014), pp. 352–366

Nomenclature

d_p	particle diameter [μm]	*Acronyms*	
T	temperature [K]	CFB	circulating fluidised bed
U_{gas}	superficial gas velocity [m/s]	PCFB	pressurised CFB

U_{mf}	minimum fluidisation velocity [m/s]	PFBC	pressurised FBC
U_t	terminal velocity [m/s]	OF	oxy fuel
G_s	solids recirculation rate [kg/m^2 –s]	ID	inner diameter
ΔP_{bed}	bed pressure drop [cmH_2O]	CCS	carbon capture and storage